Design and Implementation of a Wind Turbine Emulator with Extended Dynamic

Characteristics

Saeed Khedri

A Thesis

in

The Department

of

Electrical and Computer Engineering

Presented in Partial Fulfillment of the Requirements

for the Degree of Master of Applied Science at

Concordia University

Montréal, Québec, Canada

October 2008

Library and
Archives Canada

Published Heritage
Branch

395 Wellington Street
Ottawa ON K1A 0N4
Canada

Bibliothèque et
Archives Canada

Direction du
Patrimoine de l'édition

395, rue Wellington
Ottawa ON K1A 0N4
Canada

Canada

ABSTRACT

Design and Implementation of a Wind Turbine Emulator with Extended Dynamic
Characteristics

Saeed Khedri

The wind turbine emulator (WTE) is of concern due to the fact that the wind

energy conversion system (WECS) is a growing industry and needs further improvement.

It is a key component of a test bench which provides the opportunity to investigate the

effect of wind turbine parameters and characteristics on the system responses by

modeling the wind turbine and the drive train. Several WTEs have been proposed by the

researchers with different capabilities and degrees of complexity. The most important

factors which have significant impact on the dynamic behavior of the WECS, as

considered in the literature, are the wind turbine mass moment of inertia, system's natural

frequency, pulsating (oscillatory) torque, and damping constant. In general, at least the

effect of one of these facts was not included or not discussed in the reported WTEs.

This Thesis addresses this problem while considering on a simplified model of a

wind turbine which consists of a mass moment inertia (rotor and hub), a low speed side

flexible shaft, an ideal gearbox, a high speed side rigid shaft, and an electric generator.

The effect of the oscillatory torque is also considered in the model. The simulation results

indicate that the simplified model of the wind turbine and the drive train allow the

investigation of the above mentioned factors on the system responses. It also shows the

different ways of exciting the system's mechanical mode. A 2-hp experimental set-up is implemented and tested with a dynamometer as a mechanical load and also with a self-excited induction generator operating in the regulated and unregulated stand-alone mode. The experimental results agree with the simulation results.

ACKNOWLEDGMENTS

To my family

TABLE OF CONTENTS

LIST OF FIGURES

LIST OF TABLES

LIST OF ACRONYMS

AC   Alternating Current

ADC   Analogue to Digital Converter

BJT   Bipolar Junction Transistor

DAC   Digital to Analogue Converter

DC   Direct Current

DSP   Digital Signal Processor

emf   Electro-Motive Force

FFT   Fast Fourier Transform

hp   Horse Power

IGBT   Insulated-Gate Bipolar Transistor

KVL   Kirchhoff's Voltage Law

kW   Kilo Watt

MOSFET   Metal-Oxide-Semiconductor Field-Effect-Transistor

PI   Proportional Integral

PMDC   Permanent Magnet Direct Current

PMSG   Permanent Magnet Synchronous Generator

SCIG   Squirrel-Cage Induction Generator

VSI   Voltage Source Inverter

WECS   Wind Energy Conversion System

WRIG   Wound Rotor Induction Generator

WTE   Wind Turbine Emulator

LIST OF PRINCIPAL SYMBOLS

A	Wind Turbine Rotor Swept Area	(m^2)
B_{gen}	Generator Damping Constant	(Nms/rad)
B_{sh}	Shaft Damping Constant	(Nms/rad)
B_{wt}	Wind Turbine Damping Constant	(Nms/rad)
C	Capacitance	(F)
C_t	Wind Turbine Rotor Torque Coefficient	(-)
C_p	Wind Turbine Rotor Power Coefficient	(-)
e_b	PMDC Machine Back emf	(V)
f_n	Natural Frequency	(Hz)
G	Shear Modulus	(Pa)
J_{gen}	Generator Mass Moment of Inertia	(kgm^2)
J_{sh}	Shaft Polar Moment of Inertia	(m^4)
J_{wt}	Wind Turbine Mass Moment of Inertia	(kgm^2)
K_b	PMDC Machine Speed Constant	(Vs/rad)
K_{sh}	Shaft Torsional Spring Constant	(Nm/rad)
K_t	PMDC Machine Torque Constant	(m/A)
L	Inductance	(H)
L_a	PMDC Machine Armature Inductance	(H)
λ	Tip Speed Ratio	(-)
n	Gear Box Ratio	(-)
P_{dyn}	Dynamometer Power	(W)

P_{gen}	Generator Power (W)
P_{wt}	Wind Turbine Power (W)
R	Wind Turbine Rotor Radius (m)
R_a	PMDC Machine Armature Resistance (Ω)
R_r	Induction Machine Rotor Resistance (Ω)
R_s	Induction Machine Stator Resistance (Ω)
ρ	Air Density (kg/m^2)
τ_{hs}	High Speed Side Shaft Torque (Nm)
τ_{load}	Load Torque (Nm)
τ_{ls}	Low Speed Side Shaft Torque (Nm)
τ_{ref}	Refernce (High Speed Side Shaft) Torque (Nm)
τ_{wt_av}	Wind Turbine Rotor Average Torque (Nm)
θ_{sh}	Shaft Twist Angle (rad)
V_w	Wind Speed (m/s)
ω_{dyn}	Dynamometer Rotational Speed (rad/s)
ω_{gen}	Generator Rotational Speed (rad/s)
ω_{wt}	Wind Turbine Rotor Rotational Speed (rad/s)
ω_n	Natural Frequency (rad/s)
ζ	Second Order Low Pass Filter Damping Factor (-)
ζ_{sh}	Shaft Damping Ratio (-)

CHAPTER 1

INTRODUCTION

1.1 BACKGROUND

The interest for renewable sources of energy or in other words, green power, is drastically increasing worldwide. The main reasons are the green house effect and tendency towards less dependency on natural resources such as oil and coal. Researchers are working on renewable energy conversion systems to make them more cost effective, more environmentally friendly, and more reliable. The major renewable sources of energy can be listed as Biomass, Geothermal, Solar, and Wind [1].

Biomass is basically plant matter or any kind of biological material. It can be used for generating electricity with reduced greenhouse gas emissions in comparison with generating electricity using fossil fuel. Generating electricity by using biomass is called biomass power. Based on the method of using of biomass in generating electricity the technology can be categorized as: direct-firing, co-firing, gasification (high temperature environment with limited oxygen), pyrolysis (pyrolyzing biomass in the absence of oxygen), and anaerobic digestion (decomposing organic matter in a closed reactor without oxygen) [1].

Geothermal relates to the heat from the earth due to the hot water or stream in the earth. They can be accessed by drilling and be used for generating electricity instead of using fossil fuel. There are mainly three ways of using geothermal for producing electricity. They are dry steam, flash steam, and binary cycle. In dry steam, the steam is piped from the wells, which are dug to reach the hot water, to a power plant with steam

turbines. In flash steam, the very hot water rises through the well. Near the surface, as the pressure decreases, some of them turn to steam. The steam is separated from the water and used for turning the steam turbine. In the binary cycle, the heat of hot water is used to boil an organic compound (low boiling point) which will be used for turning a turbine [1].

Solar technologies concentrate on capturing energy from the sun. It is used for producing electricity in two general forms, concentrating solar power and solar cells (photovoltaic). The main types of concentrating solar power systems are: parabolic-trough (use of mirrors for concentrating solar energy on to the pipes with flowing oil which is used for boiling water), dish/engine (use of mirrors which concentrate the sun's energy on the fluid within the engine; expansion of the fluid produces mechanical power), and power tower (use of mirrors which concentrate the sun's energy on top of the tower, which heats the molten salt and its heat is used for boiling water). The solar cells (photovoltaic or PV) convert the sun's light directly into electricity. They can be used in arrays to form higher power electric generation [1].

A wind energy system is based on the capture of energy from moving air particles and its conversion into rotating (mechanical) power. There are different ways of capturing wind energy which are called wind turbines. The most popular one is horizontal axis wind turbine with 2 or 3 blades [1].

Each of above mentioned systems are a vast area and currently many researchers with the collaboration of industries and governments are working on them. Wind energy system is one of the fastest-growing renewable energy and the installed wind energy systems are increasing [1, 2].

In general, mechanical rotation which is created by capturing wind energy can be used in different ways. Wind-mills and wind-wheels are two types of WECS which have been used by mankind since long time ago for milling grains and pumping water, respectively [3].

The other way of using wind energy is to convert the captured energy into electricity. Environmental concerns and technological developments in the areas of power electronics, electric machines, and control have made possible the conversion of wind energy into electricity, in a cost-effective way. Nowadays, wind energy conversion systems (WECSs) — this terminology will be used for the systems which convert wind energy to electricity— are available in the capacity range of fraction of kW for residential application and hundreds of MW in the form of wind farms [3]. Thus, this Thesis focuses on WECSs and is organized in a way to highlight the important facts in this technology which will affect the quality of the generated electricity.

WECS as a new technology needs a great deal of research works. These can be split in mechanical and electrical research works to improve the performance of the systems such as efficiency, cost, and reliability. For these reasons it is necessary to investigate the effect of system parameters on its overall performance, to select suitable configuration for generating electricity, and to choose the most effective control strategy for a given system. Thus, the question is about the possible ways to perform the tests.

One option is to build the designed WECS and test different configurations and control techniques in generating electricity. This would be a good idea in a sense, that is, the researchers will be working on the real system. But there are few drawbacks which make it impossible for most researches. First, building the real system would be very

costly and time consuming. Second, once the system is built, varying each system parameter is impractical. Third, the system has to be tested in a field which in this case, there would be no control on wind speed and wind gusts since the wind speed variations is random. Therefore, it is not possible to study the impact of each system parameter individually.

The second option is to use the built system in a wind tunnel. This will solve the problem of non-controllable environment in the terms of having randomly variations on the wind speed, but it brings up other issues in addition to the first two issues that exist for the first option. The first issue is that, wind tunnel itself is costly. The second is due to the dimensions of the wind tunnel. This limits the size and capacity of the WECS which needs to be tested.

The third option [4] is to select and use a prime mover plus a flywheel, which represents the wind turbine mass moment of inertia, and the remaining parts such as shafts, gearbox, and the generator remain the same as the wind turbine which will be emulated. The main drawbacks of this type of wind turbine emulator (WTE) are briefly discussed below. First, the prime mover must be able to operate with high torque and low speed (this is true as the size of the wind turbine rotor increases). Second, since the major parts of the wind turbine are not modeled, it will not be easy to change the parameters to investigate their impacts on the system responses. The advantage of this WTE is that it provides a control over wind speed change, since it is modeled.

The last option, which is the aim of this Thesis, is to develop a simple model of the wind turbine rotor and the drive train and use it with the wind speed as the input reference for the torque developed by a wind turbine emulator. The idea is to simulate the

model of the wind turbine and control an electric motor as prime mover to follow the reference signals, for instance, torque created by the model. This can be done by using a real-time software as interface to communicate between the model and the system set-up. Since the wind turbine is modeled, the parameters can be set to different values to find out their impacts on the system outputs in transient and steady-state responses. Besides, since the wind speed is defined as an input within the model, it can be varied at will. Furthermore, as the prime mover runs a generator, the load at the output of the generator can be varied to study the impact of the load variations in the transient and steady-state responses.

1.2 WECSs

1.2.1 TERMINOLOGIES

In this section some basic terminologies of WECs are described which are useful in understanding WECSs technologies [3]. Fig. 1-1 depicts the general configuration of a WECS. It is generally called wind turbine. As it is shown, the main parts of a wind turbine are: Rotor (which includes the hub and the blades), nacelle (the compartment which usually contains the gearbox and the generator), and tower (which is the structure for supporting the whole system). Wind turbine types can be classified as: Horizontal axis (Up-wind and Down-wind), vertical axis (H-rotor, Darrieus-rotor, and Savonius-rotor), and wind energy concentrator (ducted rotor, turbine with a diffuser duct, vortex tower, delta wing vortex concentrator...). The most common type of wind turbines used in industry is horizontal axis with 2- blade or 3-blade rotor. In up-wind design, the rotor

is on the windward and in down-wind design; it is on the leeward of the tower. In up-wind
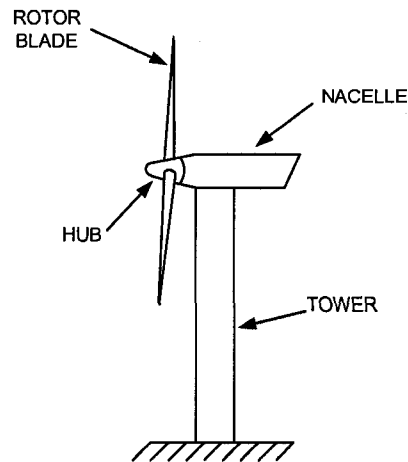
Fig. 1-1 A Typical horizontal axis wind turbine

design the nacelle has to have yaw mechanism to keep the rotor facing the wind direction

This mechanism may not be needed for downwind wind turbines by proper design of the

rotor and nacelle in such a way that the nacelle follows the wind passively. This is one of

the advantages of downwind design, but in practice it can be used for wind turbines up to

a certain capacity. Its other advantage is that it allows the use of more flexible blades,

which in turn will be lighter and help the structural dynamics of the wind turbine. The

disadvantage of down-wind designs is the pulsations in generated power, which happens

every time each rotor blade passes in front of the tower. This causes more fatigue load on

mechanical parts with respect to the up-wind design.

Since in WECSs, the rotor speed is usually lower than the required rotor speed at

the generator, a gearbox is used. *Low speed side* expression is used for the components

from the rotor to the gearbox. Similarly, *high speed side* expression is used for the

components from the gearbox to the generator. The other terminology is the blade pitch angle. It is related to the aerodynamics of blades and wind direction. The concept is that by changing the pitch angle the amount of power which is captured from wind can be controlled.

1.2.2 MAIN COMPONENTS

The main components of WECS which have significant impacts in the generated electricity are listed below.

Rotor: This mainly includes the hub and the blades. The main portion of total mass moment of inertia of wind turbines is due to the rotor as mentioned in the literature.

Drive train: It generally includes the low speed side shaft, gearbox, and the high speed side shaft.

Electric generator: The most popular electric generators in WECS industry are asynchronous and synchronous generators. The most common types of the generators are introduced in section 1.2.3.

Power electronics devices: This in general includes soft starters and different types of converters. Some of the configurations of the power electronics devices are introduced in section 1.2.3.

1.2.3 GENERAL CLASSIFICATION

With the ever-increasing advancement of power electronics different classifications of WECSs have been offered and tested by researchers and manufacturers

and there would be more to offer. WECSs can be classified based on the different concepts. Fig. 1-2 shows a general classification of WECSs. Each category is briefly described below.

Rotor speed concept [5]: It generally includes two types: Constant speed and variable speed. In the constant speed concept, the wind turbine the rotor rotates at constant speed independently of the load conditions. The wind speed determines how much power the wind turbine can produce. In the variable speed concept, as the wind speed changes the wind turbine rotor turns at different speed to produce its maximum or close to maximum power.
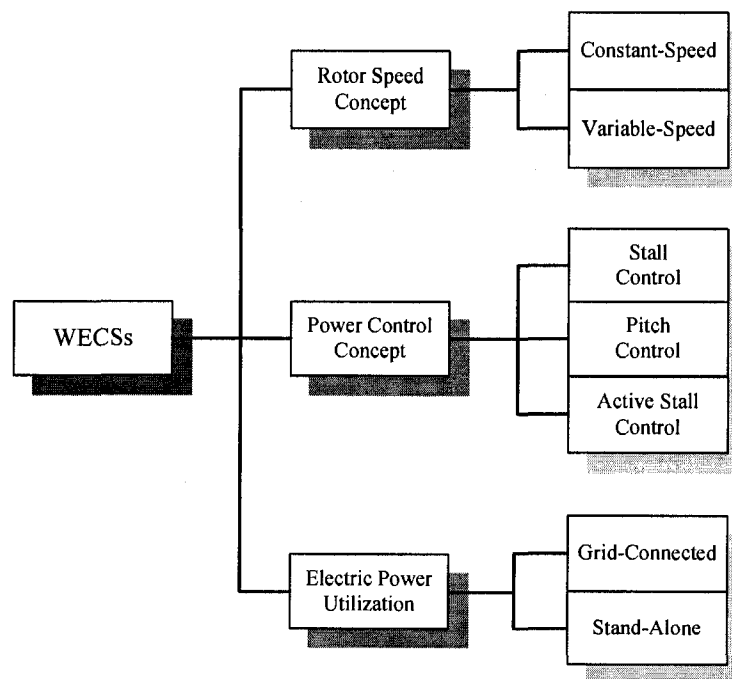
Fig. 1-2 General classification of WECSs

Power control concept [5]: It can be categorized in three general cases: Stall control, pitch control, and active stall control. In the stall (passive) control, the blades are aerodynamically designed in a manner that for the wind speeds higher than a certain

value the power captured by the blades reduces and for higher than another certain value

the blades captures no power (stall). In the pitch control concept, by pitching the blades

(turning them into or out of the wind) the amount of the power captured by the blades

will be controlled. In the active stall control, both concepts, which are stall and pitch

control, are used in the design of the wind turbine rotor.

Electric power utilization [3, 5]: This is categorized under grid-connected and

stand-alone configurations. Fig. 1-3 indicates 4 types of typical grid-connected wind

turbines which are currently in use.
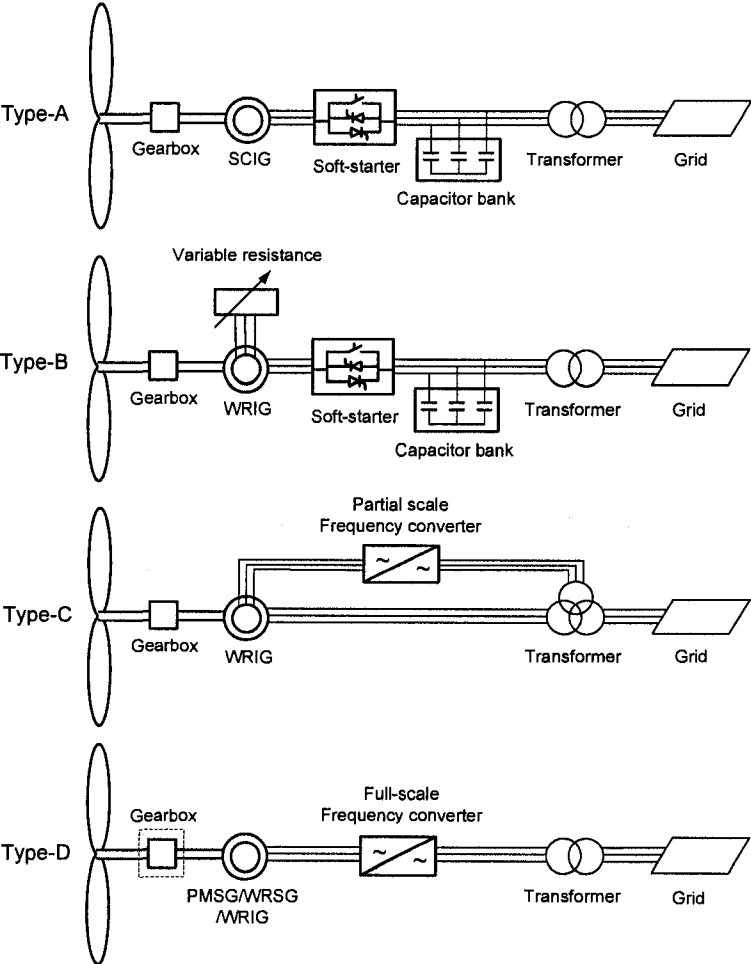
Fig. 1-3 Typical grid-connected WECSs configurations [5]

Type-A is a constant speed configuration. It is the most common and rugged configuration. A squirrel cage induction generator (SCIG) is used as the generator. Type-B is a limited variable speed configuration. The generator is a wound rotor induction generator (WRIG). The slip of induction generator is controlled by varying the variable resistor which is in series with rotor winding. Type-C is also a limited variable speed configuration. It includes a WRIG and a partial frequency converter. This is also called doubly fed induction generator (DFIG). The converter controls the speed (for a limited range) by controlling the rotor reactive power and also used for the smooth connection to the grid. Type-D is a variable speed configuration for a wide range by using a full-scale frequency converter. The generator types could be wound rotor synchronous generator (WRSG), WRIG, or permanent magnet synchronous generator (PMSG). In some cases the gearbox is eliminated by using a multi-pole generator [5].

In a stand-alone WECS, since wind is not available at all times, for continuous power generation, it has to be equipped with energy storage system and it may also be backed up, for instance, with diesel-engine electric power generation. There are different applications for stand-alone WECSs such as residential heating, pumping water, and desalination of sea water [3]. There are also different schemes and control strategies based on the type of the applications for stand-alone operation of WECSs in which power electronics converters play an important role. An available stand-alone scheme is introduced in Chapter 4.

1.3 THESIS SCOPE AND CONTRIBUTIONS

Different types of WTEs— in terms of types of prime movers, drive circuits, control strategies, needs for speed and torque measurement, and wind turbine parameters have been proposed in the literature [6-15]. A comparison of the proposed WTEs and also the implemented WTE in this Thesis is summarized in Table 1-1. Here are some more explanations on Table 1-1. In the Prime Mover Column, DC, SM, and IM stand for DC machine, Synchronous machine, and Induction machine, respectively. In the power electronics column, the numbers indicate the general type of converters used. Switch mode DC-DC converter (1), thyristor based converter (2), voltage source converter (3), 3-phase inverter (4), and frequency inverter (5). "NA" stands for "Not Available", which means that the information or results are not provided or concepts are not discussed in the reference document.

Table 1-1 Summary of comparison between proposed WTEs

Ref. No.	Prime Mover	Power Elect.	Speed Sensor	Torque Sensor	Turbine Inertia	Oscillatory Torque	Flexible Shaft	Shaft Damping	Natural Freq.
[6]	DC	1, 2	Y	N	0.1	Y	Y	N	Y
[7]	DC	2	Y	N	Y	Y	N	N	N
[8]	DC	2	Y	Y	Y	N	Y	Y	Y
[9]	DC	NA	Y	N	Y	N	Y	Y	NA
[10]	DC	2	Y	N	Y	Y	N	N	N
[11]	DC	2	Y	N	NA	N	N	N	N
[12]	DC	2	Y	N	Y	N	Y	Y	NA
[13]	SM	3	Y	Y	Y	Y	Y	Y	NA
[14]	IM	4	Y	Y	N	N	N	N	N
[15]	IM	5	Y	N	N	Y	N	N	N
Thesis	DC	1	Y	N	Y	Y	Y	Y	Y

In [6], the WTE has been tested with 2 types of converters for comparison, but in both cases the maximum wind turbine inertia was equal to 0.1 kgm^2. In [8], the values for system parameters such as wind turbine mass moment of inertia, shaft torsional spring and damping constants were not provided. In [13], a speed sensor is used but it is not mentioned if it is used for just monitoring purpose or used as part of control strategy.

In this Thesis, the proposed WTE consists of a model of the wind turbine, for generating the reference torque at the high speed side, a permanent magnet DC (PMDC) machine as prime mover and a switch-mode DC-DC converter with hysteresis current controller. The main concern in this research work is to show the effect of system parameters on the system responses. The proposed WTE is able to show the effect of the wind turbine mass moment of inertia on filtering of the wind speed variations and also torque pulsations. Effect of load variations on the system responses are verified by using a dynamometer in one case and an electric generator in another case. It also includes a flexible shaft in drive train which makes it possible to investigate the possibilities of mechanical resonance occurrence. In addition to these, two harmonics (1st and 3rd with respect to rotor speed) are added as torque pulsations to the average torque rotor, due to tower shadow effect and wind shear effect, and their effects are investigated.

The following are the main contributions of this Thesis:

1)   Modeling of WECSs and selection of parameters that would be used as an unregulated wind turbine as prime mover for stand-alone or grid-connected applications.

2)   Implementation of a 2-hp WTE. A PMDC machine is used as dynamometer. This allows imposing mechanical load on the prime mover without having an electric generator and variable electric load, to make the emulated wind turbine operates with

12

different loads. It also allows studying the impact of the wind speed variations, load variations and the wind turbine parameters on the system responses.

3) Applying the WTE prototype in a test bench for an available stand-alone electric generating set, consisting of voltage source inverter (VSI), SCIG, and PI controllers which were designed to regulate the generated voltage and frequency of a generator, connected to an unregulated prime mover. It provides a good opportunity to study the effect of wind turbine parameters, for instance, impact of the wind turbine mass moment of inertia on selection of PI controller gain coefficients.

1.4 THESIS OUTLINE

This Thesis is presented in 5 Chapters.

The first Chapter describes the WECS, its growth, and consequently the need for a WTE. It also briefly introduces the works that have been done and finally covers the scope and contribution of this Thesis.

The second Chapter presents the differential equations governing a WECS and a model to be simulated in MATLAB/Simulink. Simulation results are presented to indicate the effect of system parameters, individually and as a whole, wind speed variations and load variations on the system responses.

The third Chapter introduces the method of implementing a WTE. In this method, a permanent magnet DC machine (PMDC) is used as prime mover and another is used as dynamometer which behaves as a controllable mechanical load. The characteristics of the PMDC are presented. The controller and selection of the system parameters for experimental set-up are discussed. The real-time software dSPACE/ControlDesk and its

digital controller board (ds-1103) used for implementation of the WTE are briefly introduced. The experimental results are provided to show the system behavior and responses for different system parameters due to wind speed and load variations.

The fourth Chapter shows the application of the implemented WTE in Chapter three, where the dynamometer is replaced by a SCIG connected to variable electrical load. In this Chapter the characteristics of SCIG are described. The WTE set-up and the necessary rearrangements for applying it in an unregulated WECS are presented. Then, the available regulated electric generation set-up (as a stand-alone application of WECSs) for testing the implemented WTE is discussed. The experimental results are presented to show the effectiveness of the WTE in electric power generation applications.

The Fifth Chapter concludes the work and highlights the contribution of this Thesis. In the end, suggestions for future work are presented.

CHAPTER 2

MODELING AND SIMULATION OF A WIND TURBINE EMULATOR

2.1 INTRODUCTION

The first step in designing a wind turbine emulator (WTE) is the selection of its features which depend on the studies to be carried out with the WTE. For the analysis of the impact of load and wind speed variations in the steady state value of the shaft speed and consequently frequency of a stand-alone wind energy conversion system (WECS), the WTE could be simply a motor with a torque control loop. The reference torque varies with the shaft speed, wind speed and torque speed characteristics of the wind rotor. The WTE to be developed in this thesis is intended to be used in the study of the transient response of a WECS. A simplified system with the main elements of a stand-alone WECS is shown in Fig. 2.1. It includes the moment of inertia of the wind rotor, a flexible drive train with a gear box to increase the shaft speed, an electrical generator and a load. Such a system presents a natural mechanical (oscillatory) mode, usually lightly damped, that can be excited by variations in the wind speed, oscillatory component of the mechanical torque delivered by the wind rotor and also load variations. It will be used later in the power electronics laboratory to investigate how this mode impacts the system stability and power generation.

Section 2.2 describes how the wind and shaft speed and the characteristics of the wind rotor impact the torque developed by the wind rotor. Section 2.3 describes a simplified model for the drive train. Differential equations that represent the system are

derived in Section 2.4 and a number of simulations are carried out in section 2.5 with MATLAB/Simulink to verify if the selected simplified model allows the study of the mechanical modes of a WECS.
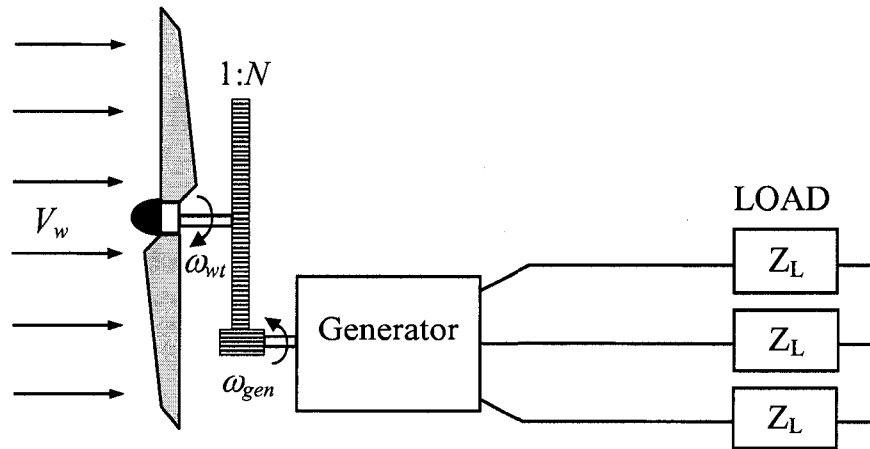
Fig. 2-1 Simplified schematic diagram of a stand-alone WECS

2.2 ROTOR (WIND WHEEL) [3]

The main mechanism of a wind turbine which captures energy from wind is called rotor or wind wheel. In the following sub-sections the theory of capturing energy from wind stream, torque-speed and power-speed characteristics of the rotor are presented.

2.2.1 POWER COEFFICIENT (C_P)

Power coefficient C_p is defined as the ratio of the mechanical power extracted by the rotor over the power contained in undisturbed air stream. Albert Betz calculated the maximum theoretical value of C_p based on the elementary momentum theory. This has

been expressed in [3]. A very brief explanation and conclusion of the discussion in [3], is presented below.

Fig. 2-2 shows the air flow at different stages of an ideal energy conversion system which is located at plane A'. The energy can be extracted from a free-stream air flow in the form of kinetic energy. Since the mass must remain unchanged, the velocity of air flow must be reduced after the energy converter. Therefore, by considering the fact that mass flow must remain unchanged, according to equation 2-1 the air flow must be widened in the presence of the energy converter as shown in Fig. 2-2.

$$\dot{m} = \rho V_w A \qquad\qquad (2\text{-}1)$$

Where $\dot{m}$ is mass flow in kg/s, ρ is the air density in kg/m^3, V_w is wind speed in m/s, and A is the area, which air passes through in m^2.
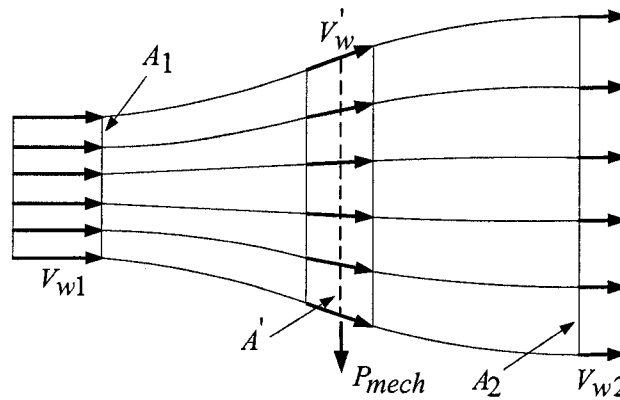
Fig. 2-2 Air flow conditions as a result of mechanical energy extraction from a free-stream air flow based on the elementary momentum theory [3].

The power coefficient is expressed as:

$$C_p = \frac{P_{mech}}{P_o} = \frac{1}{2}\left|1 - (\frac{V_{w2}}{V_{w1}})^2\right|\left|1 + \frac{V_{w2}}{V_{w1}}\right| \qquad\qquad (2\text{-}2)$$

Where P_{mech} is the extracted mechanical power by the converter in W, V_{w1} and V_{w2} are the undisturbed wind speeds before and after the converter in m/s, respectively, and P_o is the power , in W, contained in the undisturbed (in the absence of the converter) air at plane A' as given by:

$$P_o = \frac{1}{2} \rho V_{w1} A'$$ (2-3)

C_p in equation 2-2 is a function of $\frac{V_{w2}}{V_{w1}}$ which reaches its maximum value when $\frac{V_{w2}}{V_{w1}} = \frac{1}{3}$.

By inserting this value in the equation 2-2, $C_p = \frac{16}{27} = 0.593$. This, in fact, means that for even an ideal energy converter less than 60% of wind energy can be extracted by the converter.

2.2.2 TORQUE –SPEED AND POWER- SPEED CHARACTERISTICS

The performance of a specific wind turbine can be characterized by its rotor torque and power, versus speed curves. Power coefficient or torque coefficient, for any wind turbine, has to be known to allow the calculation of the power and torque captured and produced by its rotor. These two coefficients depend on the aerodynamic design of the rotor blades. They are functions of tip speed ratio which is [3]:

$$\lambda = \frac{Tangential\ Velocity\ of\ the\ Rotor\ Blade\ Tip}{Wind\ Speed} = \frac{R\omega_{wt}}{V_w}$$ (2-4)

Where R is the rotor radius in m, ω_{wt} is the rotor speed in rad/s, and V_w is the wind speed in m/s. Equations 2-5 and 2-6 express the power captured by the rotor and the average rotor torque, respectively [3].

18

$$P_{wt} = \frac{1}{2}\rho C_p(\lambda) V_w^3 A \qquad (2\text{-}5)$$

Where P_{wt} is the power captured by the rotor in W, $C_p(\lambda)$ is rotor power coefficient, ρ is the air density in kg/m^3, and A is the rotor swept area in m^2.

$$\tau_{wt\_av} = \frac{1}{2}\rho C_t(\lambda) V_w^2 AR \qquad (2\text{-}6)$$

Where τ_{wt_av} is in Nm $C_t(\lambda)$ is the rotor torque coefficient, and R is the rotor radius in m. Considering that, $P_{wt} = \tau_{wt}\,\omega_{wt}$ it results in the following relationship:

$$C_p(\lambda) = \lambda C_t(\lambda) \qquad (2\text{-}7)$$

From the above discussions, it is obvious that one needs to have either $C_t(\lambda)$ or $C_p(\lambda)$ curve, to be able to model a wind turbine. On the other hand, $C_t(\lambda)$ and $C_p(\lambda)$ curves for each wind turbine rotor design are different. The $C_t(\lambda)$ curve as presented in [6] for a 3-bladed, fixed pitch, small wind turbine is shown in Fig. 2-3. This curve will be used throughout this thesis for simulation and also experimental set-up.
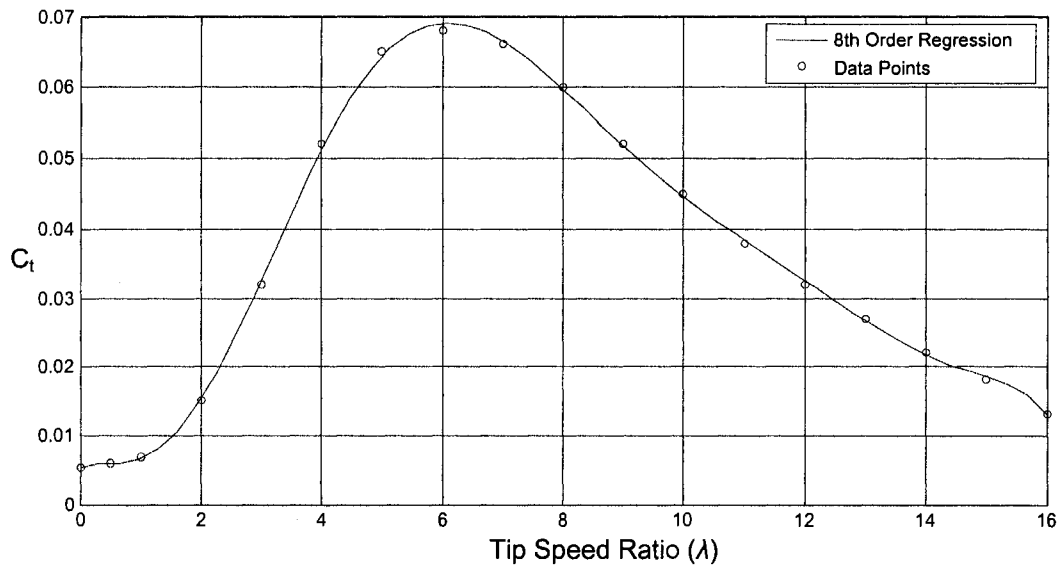
Fig. 2-3 Torque coefficient (C_t) versus tip speed ratio (λ) Curve [6]

The curve which is fitted to data points in Fig. 2-3 is an 8th order polynomial which is [6]:

$$C_t(\lambda) = 0.0056 + 2.871 \times 10^{-3}\lambda - 7.551 \times 10^{-3}\lambda^2 +$$

$$7.650 \times 10^{-3}\lambda^3 - 2.209 \times 10^{-3}\lambda^4 + 2.992 \times 10^{-4}\lambda^5$$

$$-2.140 \times 10^{-5}\lambda^6 + 7.848 \times 10^{-7}\lambda^7 - 1.166 \times 10^{-8}\lambda^8 \qquad (2\text{-}8)$$

On the other hand, equation 2-6 can be expressed in the form of:

$$\tau_{wt\_av} = \frac{1}{2}\rho\pi C_t(\lambda)V_w^2 R^3 \qquad (2\text{-}9)$$

By using equations 2-8 and 2-9, the torque-speed characteristic of the rotor is plotted as shown in Fig. 2-4. The value of air density is chosen $\rho = 1.224$ kg/m^3 as a typical value. In [16], the rotor radius and rotor rated speed, for a manufactured 1 kW wind turbine, are specified as 1.25 m and 490 RPM, respectively. Since the goal of this thesis is to implement a 2-hp WTE and the rated speed of the induction generator is 1800 RPM, therefore the gearbox ratio in the drive train is considered to be equal to $n = 4$. In this case the rated speed of the wind turbine rotor will be 450 RPM or about 47 rad/s which is less than the rotor rated speed of the 1 kW and can be an acceptable practical value. The radius of the wind turbine rotor is considered to be larger than 1.25 m. It is arbitrarily chosen as $R = 1.7$ m. These values are used for plotting of the curves in Fig. 2-4.

There is a maximum point associated with each curve for a given wind speed as marked and indicated in Fig. 2-4. It is worth noting that the points to the right of the maximum point on each curve are in the stable or operating region.

Another characteristic of the rotor is the power-speed characteristic shown in Fig.

2-5. This curve is obtained by applying torque equation of the rotor and using power and
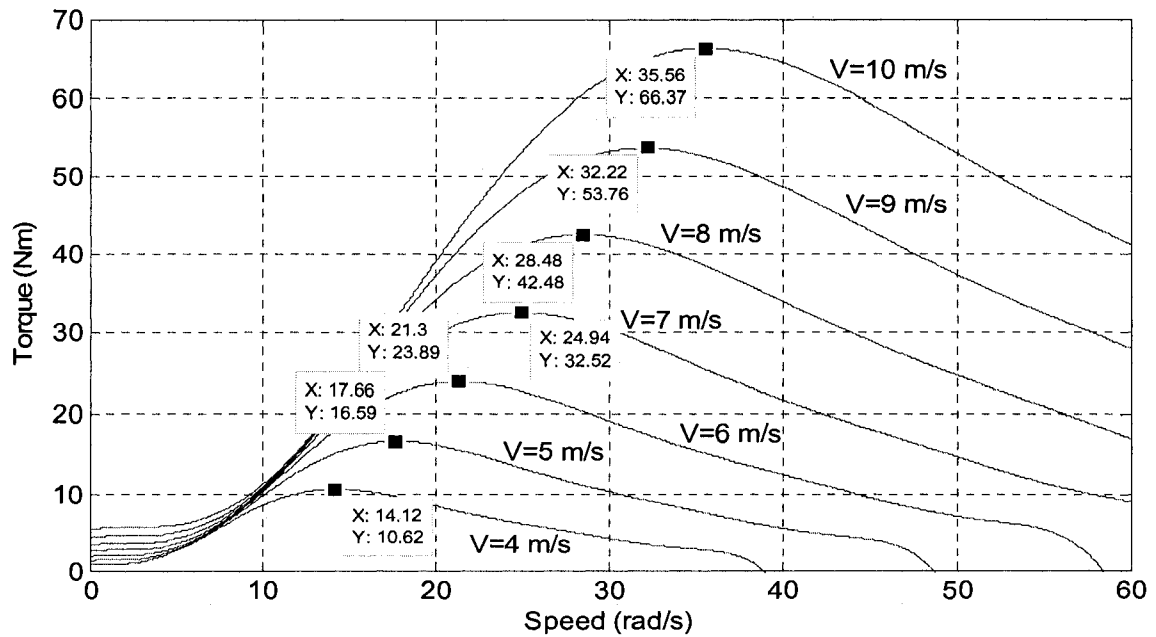
Fig. 2-4 Torque-speed characteristic of the rotor
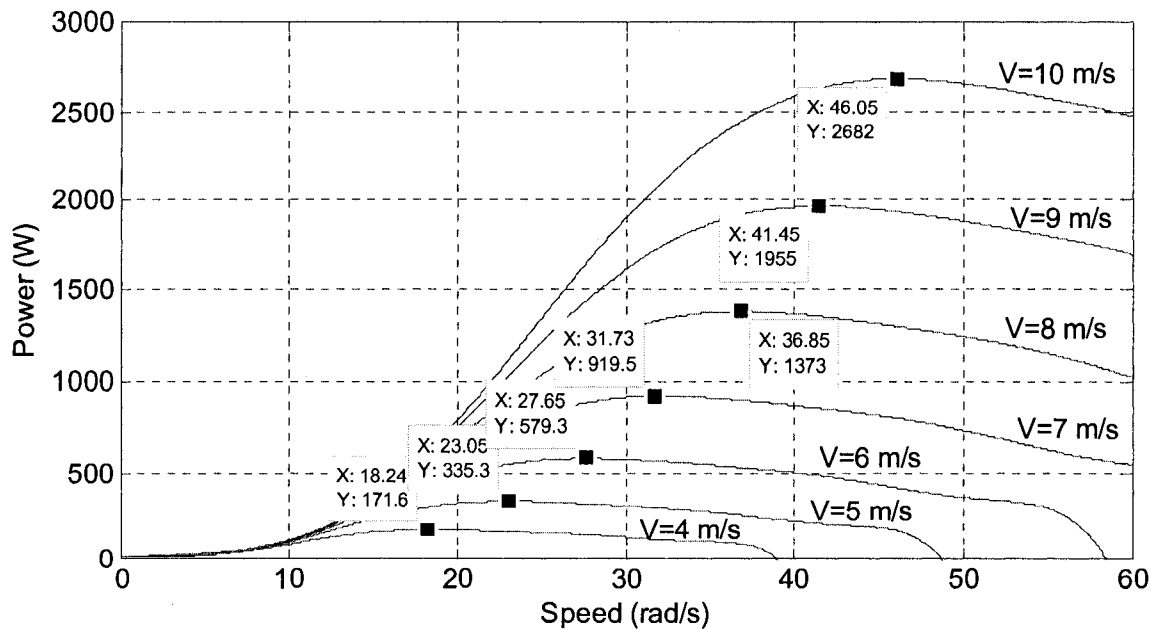
Fig. 2-5 Power-speed characteristic of the rotor

torque relationship which is $P_{wt} = \tau_{wt}\omega_{wt}$. The power-speed characteristic of the rotor shows that the converted power varies with the wind and shaft speeds. There is a maximum output power for each wind speed, which occurs at different shaft speeds. Besides, the maximum power increases as the wind speed increases. This reveals the fact that for maximum power tracking with varying wind speeds, the wind turbine must operate at variable speed. In other words, a control strategy must be applied in such a way that by varying the load at the generator output, it enforces the wind turbine to operate at the desired speed. By comparing Fig. 2-4 and Fig. 2-5 one can conclude that maximum power does not correspond to the maximum torque. In other words, for a certain wind speed, maximum power and maximum torque do not occur at the same rotor speed.

2.2.3 OSCILLATORY TORQUE

In reality the torque produced by the rotor is not constant, even though the wind speed is considered to be constant. The most important facts which create some pulsations on the produced torque are tower shadow and wind shear or gradient effects [3].

For down-wind wind turbines, the tower shadow effect is significant since the tower blocks the air flow. Thus, the wind speed behind the tower reduces significantly. The tower shadow effect for the down-wind wind turbines is also called tower dam effect in the literature. For up-wind wind turbines, the wind speed reduces in front of the tower. This happens because of the fact that air flow will be disturbed by the tower and its speed reduces comparing with the case when the air flow is undisturbed [3]. The effect of tower

22

shadow is highly reduced for the modern up-wind turbines by manufacturing slender towers [3].

However, for both types of wind turbines, every time a blade passes in front of the tower it faces lower wind speed comparing with the situations where the blade is in any other position. Therefore, whenever a blade is in front of the tower, it produces lower torque. The tower shadow effect on producing torque is shown in Fig. 2-6 as described and investigated in [17] for a 3-bladed wind turbine. As it is shown, there are 3 pulse-like torque reductions in one rotation of the rotor which can be considered as 3rd harmonic of the rotor speed. It should be noted that the plots in Fig. 2-6 are just indicative (also not to scale) and presented for better understanding of this discussion.

Wind shear or wind gradient effect is based on the fact that wind speed is higher at higher altitude. Because of the friction of the moving air particles with ground the air flow closer to ground will be slower than the air flow at higher altitude [3]. This means that each blade faces different wind speeds as it rotates even when there is no wind speed variations are considered. It is reported in [17] that the produced torque by each blade has a sinusoidal form as shown in Fig. 2-6(a). It should be noted that Fig. 2-6(a) shows the tower shadow effect and wind shear effect for each blade for one complete rotation of each blade.

Fig. 2-6(b) shows the total torque produced by all 3 blades, considering that the performances of the blades in producing torque are identical. In this case, as it is clear from the Fig. 2-6(b), the wind shear has no effect because of the symmetry of the 3-blade rotor [17]. But as it is discussed in [17], in practice, the performance of, for instance, one blade might be lower than the others due to manufacturing inaccuracy or by deformation

of the blade as the time passes (aging). In this case a 1st harmonic with its frequency equal to the frequency of the rotor speed should be added to the average torque produced by all three blades. Therefore, to include the pulsating (oscillatory) torque due to tower shadow effect (3rd harmonic) and wind shear effect when a blade has lower performance than the other two blades (1st harmonic) in the model, equation 2-10 [6] will be used.

$$\tau_{wt} = \tau_{wt\_av}[1 + A\sin(\omega_{wt}t) + B\sin(3\omega_{wt}t)] \tag{2-10}$$

Where ω_r is the rotor speed in (rad/s). It should be noted that $A=0.2$ and $B=0.4$ are specified as typical values in [6]. The same values of A and B are used in this Thesis whenever effect of wind turbine oscillatory torque is of concern.
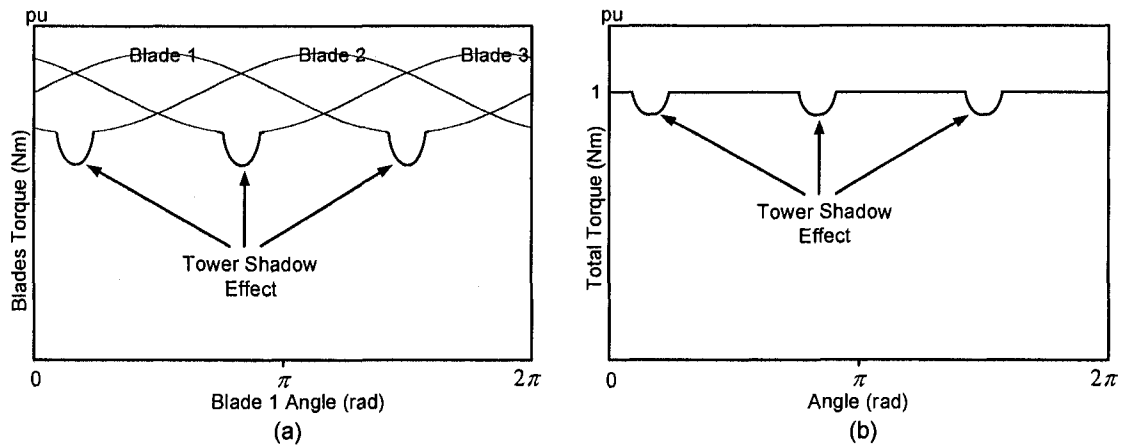
Fig. 2-6 Tower shadow and wind shear effects; (a) Produced torque by each blade; (b) Total produced torque when all blades have the same performance [17]

2.3 DRIVE TRAIN

The drive train is the mechanism which connects the rotor to the generator. In practice for large wind turbines it might include several shafts and gear boxes [3]. But in

this Thesis the drive train consists of two shafts and a gearbox, for two reasons. First, a small WTE is proposed. Second, the concept can be developed for more complicated drive trains. The shaft which connects the rotor to the gearbox (low speed side shaft) is considered to be flexible and the shaft which connects the gearbox to the generator (high speed side shaft) is considered to be rigid. These are acceptable assumptions since the low speed side shaft is longer than high speed side shaft and the amount of torque on the low speed side shaft is greater than the torque on the high speed side shaft by the factor of gear ratio [18]. The gearbox is considered to be ideal.

The effect of the drive train on the system differential equations is taken into consideration in section 2.4. The drive train can be simplified as a flexible shaft which is connected to a mass on each side. These are all energy storage elements where masses store energy in the form of kinetic energy due to their rotational speeds. The flexible shaft stores the energy in the form potential energy due to its twist. Transferring energy from the flexible shaft to each mass or vice versa will occur, whenever any of the inputs or outputs of the system varies. The combination of masses moment of inertias and the flexible shaft presents very low resistance to system inputs or outputs at certain frequencies. These frequencies are called natural frequencies which depend on the values of mass moment of inertias and the shaft torsional spring constant [19].

Thus, if any of the system's inputs or outputs presents a variation at or close to any of the natural frequencies, one should expect a large amount of energy transfer from one element to another. As it will be observed in the simulation results in this Chapter, excitation of the natural frequencies results in variation on the torque on the high speed side shaft. This might exceed the shaft and the generator capacities and result in

damaging the shaft or generator or both if it is not damped out. The flexible shaft damping plays an important role in suppressing those variations.

Therefore, in this section the drive train natural frequencies are investigated. Equations for calculating the shaft torsional spring constant and shaft damping constant are also presented.

2.3.1 NATURAL FREQUENCIES

Fig. 2-7(a) depicts the rotor and hub which represent about 90% of the wind turbine mass moment of inertia J_{wt}, on one side of the flexible shaft and the generator with the mass moment of inertia J_{gen}, on the other side of the shaft [20]. It is assumed that the masses moment of inertias of the shafts and the gear box in the drive train are lumped into the rotor's and the generator's masses moment of inertias. The gearbox is omitted from the drive train model in Fig. 2-7 by referring the generator mass moment of inertia to the low speed side. To do that, the generator moment of inertia is multiplied by n^2 where the gear ratio is assumed to be $n:1$ [18]. The shaft torsional spring constant is K_{sh}. In terms of system natural frequencies, the configuration in Fig. 2-7(a) has two degrees of freedom [19].

One mode corresponds to the case where the rotor and the generator start to oscillate around the flexible shaft if its modal natural frequency is excited. The other mode corresponds to the case where the generator rotates at the fixed speed. This might happen when the generator is connected to a strong grid, in this case, only the rotor starts to oscillate around the shaft if its modal natural frequency is excited. Fig. 2-7(b) indicates the equivalent model for the latter case just for the purpose of calculating the system

natural frequency for that mode. The configuration shown in Fig. 2-7 is called a 2-mass system in the literature.

The equations for calculating the modal natural frequencies of a 2-mass system were presented in the literature. But, because of significance of the method of deriving equations for calculating the natural frequencies of a mechanical system by an equivalent electrical circuit, it is briefly presented below. The method is called mesh analogy and it is expressed in [18].
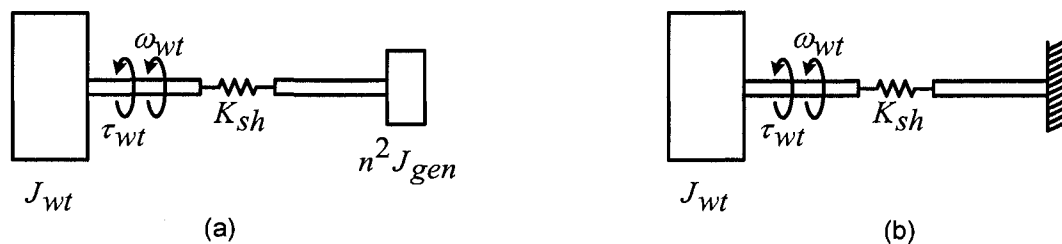
Fig. 2-7 A 2-mass system; (a) actual configuration; (b) equivalent configuration for calculating natural frequency when generator rotates at a constant speed.

In this method the torque is analogous to voltage, the mass moment of inertia is analogous to inductance, and the shaft torsional spring constant is analogous to inverse of capacitance. The equivalent circuit is shown in Fig. 2-8. To calculate the natural frequency of the circuit, Z_{eq} of the circuit needs to be derived. Thus, Z_{eq}, in Ω, can be expressed in frequency domain as:

$$Z_{eq} = j\omega L_1 + \cfrac{1}{j\omega C + \cfrac{1}{j\omega L_2}} = \frac{-j\omega^3 L_1 L_2 C + j\omega L_1 + j\omega L_2}{1 - \omega^2 L_2 C} \tag{2-11}$$

Where $\omega = 2\pi f$ in rad/s and f is voltage frequency in Hz. Equation 2-11 can be simplified as below:
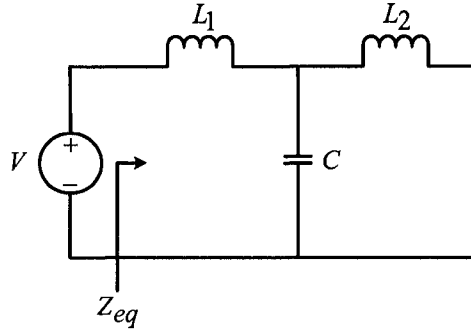
Fig. 2-8 Mesh analogy of Fig. 2-7(a)

$$Z_{eq} = \frac{j\omega(L_1 + L_2 - \omega^2 L_1 L_2 C)}{1 - \omega^2 L_2 C} \tag{2-12}$$

By equating the numerator of equation 2-12 to zero, the natural frequency of the circuit, in Hz, is:

$$f_n = \frac{1}{2\pi} \sqrt{\frac{1}{C}\left(\frac{1}{L_1} + \frac{1}{L_2}\right)} \tag{2-13}$$

Now, by referring to definition of mesh analogy and replace L_1, L_2, and C by J_{wt}, $n^2 J_{gen}$, and $1/K_{sh}$, respectively, one of the natural frequencies of the 2-mass system, in Hz, will be:

$$f_{n1} = \frac{1}{2\pi} \sqrt{K_{sh}\left(\frac{1}{J_{wt}} + \frac{1}{n^2 J_{gen}}\right)} \tag{2-14}$$

The other natural frequency of the 2-mass system, in Hz, can be obtained by removing L_2 from the circuit in Fig. 2-7 and setting the term $1/n^2 J_{gen}$ in equation 2-14 equal to zero. Thus, it will be:

$$f_{n2} = \frac{1}{2\pi} \sqrt{\frac{K_{sh}}{J_{wt}}} \tag{2-15}$$

28

Therefore, these frequencies should not be excited to avoid resonance effect during operation of wind turbines. It is also suggested, in the literature, to introduce additional damping (by special design) to suppress the amplitude of torque whenever the system's natural frequencies are excited.

2.3.2 SHAFT TORSIONAL SPRING AND DAMPING CONSTANTS

The following equations [19] are used for calculating torsional spring constant (K_{sh}) of a shaft with the dimensions which are shown in Fig. 2-9. Angle θ_{sh} is the shaft twist in rad.
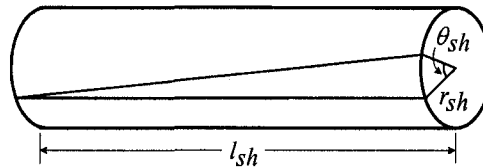
Fig. 2-9 Shaft with length l_{sh} and radius r_{sh} [19]

$$J_{sh} = \frac{\pi r_{sh}^4}{2} \qquad (2\text{-}16)$$

Where J_{sh} is the shaft polar moment of inertia in m^4 and r_{sh} is the shaft radius in m. Thus, K_{sh} in Nm/rad can be expressed as:

$$K_{sh} = \frac{J_{sh}G}{l_{sh}} \qquad (2\text{-}17)$$

Where G is the shear modulus of the material in N/m^{2}rad and l is the shaft length in m.

The flexible shaft damping constant can be generally calculated based on equation 2-18 which is related to a 2-mass system of Fig. 2-7(a) [21]:

$$B_{sh} = 2\xi_{sh} \sqrt{\dfrac{K_{sh}}{\dfrac{1}{J_{wt}} + \dfrac{1}{n^2 J_{gen}}}} \qquad (2\text{-}18)$$

Where B_{sh} is the shaft damping constant in Nms/rad, ξ_{sh} represents the damping ratio. It is experimentally determined to be in the range of 0.005 to 0.075 [21]. The damping ratio (ξ_{sh}) is 0.0175 for steel material [22]. This value will be used for calculating of shaft damping throughout this Thesis. Equation 2-18 reveals that the shaft damping constant not only depends on the material of the shaft but also on the shaft torsional spring constant and the masses moment of inertias on both sides.

2.4 WECS DIFFERENTIAL EQUATIONS AND BLOCK DIAGRAM

The WECS model is shown in Fig. 2-10. The model includes a wind turbine with the mass moment of inertia (J_{wt}) and friction damping (B_{wt}), low speed side shaft with the torsional spring constant (K_{sh}) and damping (B_{sh}), gear ratio (n_{ls}/n_{hs}), a rigid high speed side shaft, and electrical generator with the mass moment of inertia (J_{gen}) and friction damping (B_{gen}). The differential equations which describe the presented model are expressed in the following equations [6, 23].

$$J_{wt} \frac{d^2\theta_{wt}}{dt^2} = \tau_{wt} - B_{wt} \frac{d\theta_{wt}}{dt} - B_{sh} \left(\frac{d\theta_{wt}}{dt} - \frac{d\theta_{ls}}{dt} \right)$$
$$- K_{sh} (\theta_{wt} - \theta_{ls}) \qquad (2\text{-}19)$$
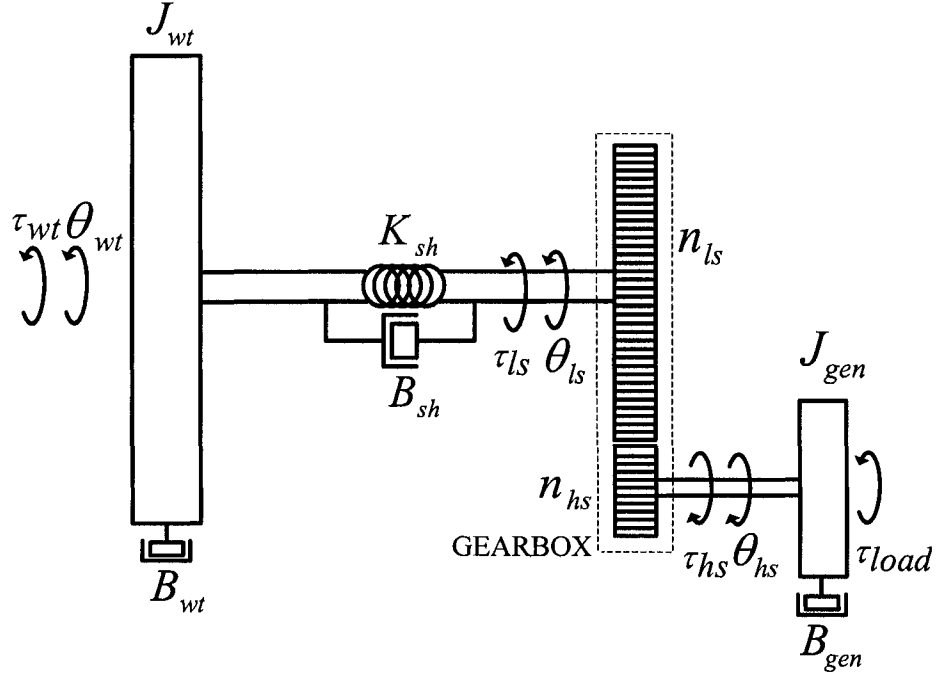
Fig. 2-10 WECS model [6]

Equation 2-19 is the differential equation which can be applied to the low speed side shaft. It includes the rotor, hub and the flexible shaft. The differential equation which represents the high speed side shaft is as follows:

$$J_{gen}\frac{d^2\theta_{hs}}{dt^2} = \tau_{hs} - B_{gen}\frac{d\theta_{hs}}{dt} - \tau_{load} \qquad (2\text{-}20)$$

The relationship between torques and positions on both sides of the gearbox are:

$$\frac{\tau_{ls}}{\tau_{hs}} = \frac{n_{ls}}{n_{hs}} = n \qquad , \qquad \frac{\theta_{ls}}{\theta_{hs}} = \frac{n_{hs}}{n_{ls}} = \frac{1}{n} \qquad (2\text{-}21)$$

Considering the above mentioned equations, the block diagram of the model of Fig. 2-10 is built as indicated in Fig. 2-11, which shows that τ_{wt} is a function of V_w and ω_{wt}. It also shows that the load is a function of wind turbine rotor speed. The load function is defined in section 2.5.1.

31
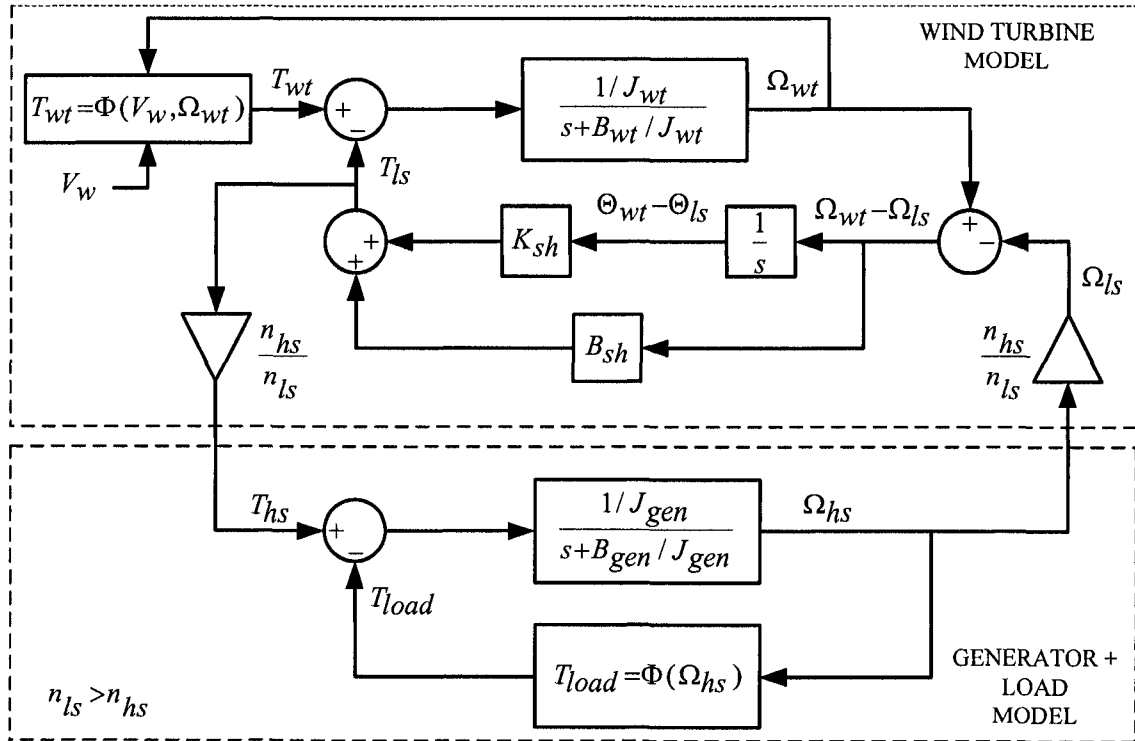
Fig. 2-11 Block diagram of WECS model [6, 23]

2.5 SIMULATION OF WECS

2.5.1 MATLAB/SIMULINK MODEL

Fig. 2-12 shows the developed MATLAB/Simulink model of the WECS under consideration. The "WT Torque Calculation" sub-system is developed according to equations 2-4, 2-8, and 2-9. The "Generating Oscillatory Torque" sub-system is developed based on equation 2-10. The "drive Train Model" sub-system is developed based on the block diagram of Fig. 2-11. The mechanical model of the generator in the "Generator and load Model" sub-system is the same as the generator model in Fig. 2-11.
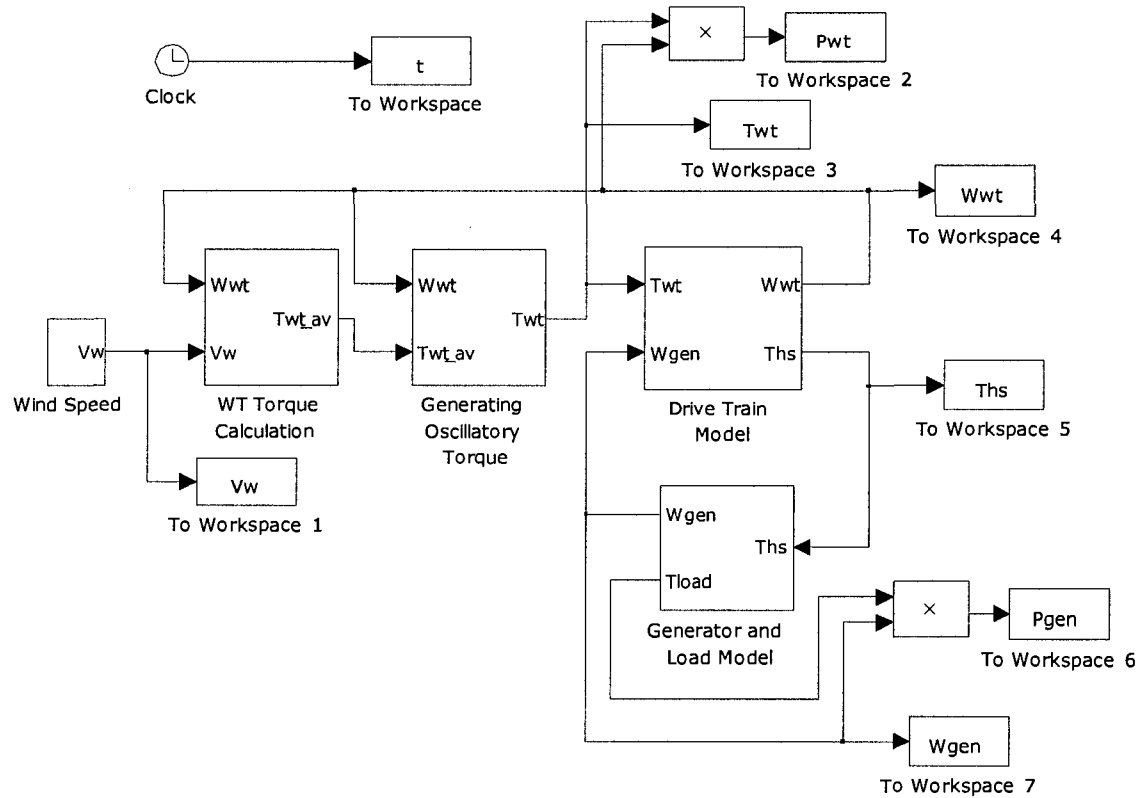
Fig. 2-12 MATLAB/Simulink model of WECS

The load model is defined as:

$$\tau_{load} = a + b\omega^2_{gen} \tag{2-22}$$

Where τ_{load} is in Nm, a is in Nm, b is in Nms^2/rad^2, and ω_{gen} is in rad/s. This load typically represents the torque-speed characteristics of the mechanical loads such as fans and centrifugal pumps as mentioned in the text books.

2.5.2 PARAMETERS SELECTION

In this section the parameters which are used for simulations are chosen. In this Thesis, a small wind turbine with the rating of 2 hp is emulated, as will be described in

Chapters 3 and 4. Because of lack of enough information for small wind turbines some parameters are selected arbitrarily. The wind turbine rotor radius, $R = 1.7$ m, and gear box ratio, $n = 4$, are selected as discussed in section 2.2.2. The wind turbine mass moment of inertia and friction coefficient are considered to be $J_{wt} = 3$ kgm^2, and $Bwt = 0.1$ Nms/rad, respectively. A procedure of calculating the wind speed at which the wind turbine produces 2 hp on the generator shaft, for the selected wind turbine parameters, is provided in Appendix A.

The generator mass moment of inertia and friction coefficient are considered as $J_{gen} = 0.0203$ kgm^2 and $B_{gen} = 0.003075$ Nms/rad, respectively. These values are estimated values of total masses moment of inertias of two PMDC machines (one as prime mover and the other one as dynamometer) used as wind turbine emulator discussed in Chapter 3. In this case, it will be easier to compare the simulation results in this chapter and experimental results which will be presented in Chapter 3.

Based on equation 2-22, the load coefficient is defined as $a = 0$ Nm and $b = 182 \times 10^{-6}$ Nms^2/rad^2. It should be noted that the load coefficient will be changed for different case studies.

Referring to equations 2-16 and 2-17, with $r_{sh} = 0.009$ m and $l_{sh} = 0.5$ m, and assuming that the shaft is made of steel with shear modulus $G = 83 \times 10^9$ Pa, shaft torsional constant can be calculated as $K_{sh} = 1710.80$ Nm/rad.

According to equation 2-18, the shaft damping constant can be calculated as $B_{sh} = 0.7837$ Nms/rad.

2.5.3 SIMULATION RESULTS

Simulation results are provided for six different cases which include the steady-state and transient responses. The parameters for the simulation results are the same as parameters provided in Table 2-1, unless otherwise stated.

Table 2-1 Parameters used for simulation results

Wind Turbine, Generator, and Mechanical Load Parameters			
Wind Turbine		Generator and Mechanical Load Constants	
J_{wt} (kgm^2)	3	J_{gen} (kgm^2)	0.0203
B_{wt} (Nms/rad)	0.1	B_{gen} (Nms/rad)	0.0030725
K_{sh} (Nm/rad)	1710.8	a (Nm)	0
B_{sh} (Nms/rad)	0.7837	b (Nms^2/rad^2)	0.000182
n	4		

Case 1) This case highlights the effect of the wind turbine mass moment of inertia on filtering of the oscillatory torque as far as generator torque and speed are concerned. The results for this case are shown in Fig. 2-13. The results are taken in steady-state. The wind speed is constant at $V_w = 8.25$ m/s. The responses are shown for wind turbines with mass moment of inertia (J_{wt}) equal to 1 and 10 kgm^2. According to equation 2-18, the shaft damping (B_{sh}) are 0.7168 and 0.8120 Nms/rad, respectively.

The results show that for the wind turbine with higher mass moment of inertia the variations on the wind turbine rotor speed, high speed side torque (generator shaft), and generator speed are lower than the wind turbine with lower mass moment of inertia. Higher mass moment of inertia can be achieved by fabricating larger and heavier blades

and consequently more expensive wind turbine. Thus, there should be a compromise in selecting wind turbine mass moment of inertia and generated power to be cost effective.
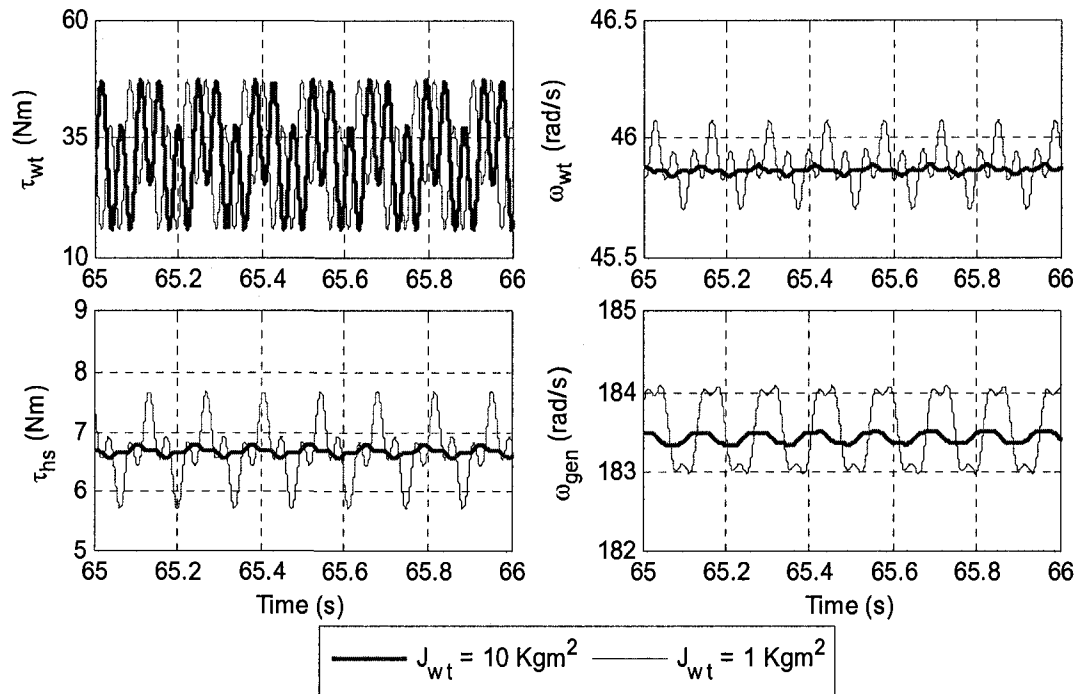
Fig. 2-13 Simulation results for case 1

Case 2) This case highlights the effect of the wind turbine mass moment of inertia on filtering of the wind speed variations as far as generator torque and speed are concerned. The results for this case are shown in Fig. 2-14. For power system studies, it is suggested in [20] to consider some harmonics on the wind speed with frequencies in the range of 0.1 to 10 Hz.

The wind speed is considered to be $Vw = 8.25 + 0.2\ sin2\pi t + 0.2\ sin6\pi t + 0.2\ sin20\pi t$ m/s. The coefficients A and B of the oscillatory torque in equation 2-10 are set equal to zero to be able to easily observe the effect of only wind speed variations on the system responses. The responses are shown for wind turbine with mass moment of inertia

36

(J_{wt}) equal to 1 and 10 kgm^2. According to equation 2-18, the shaft damping (B_{sh}) are

0.7168 and 0.8120 Nms/rad, respectively. The responses are shown in steady-state.
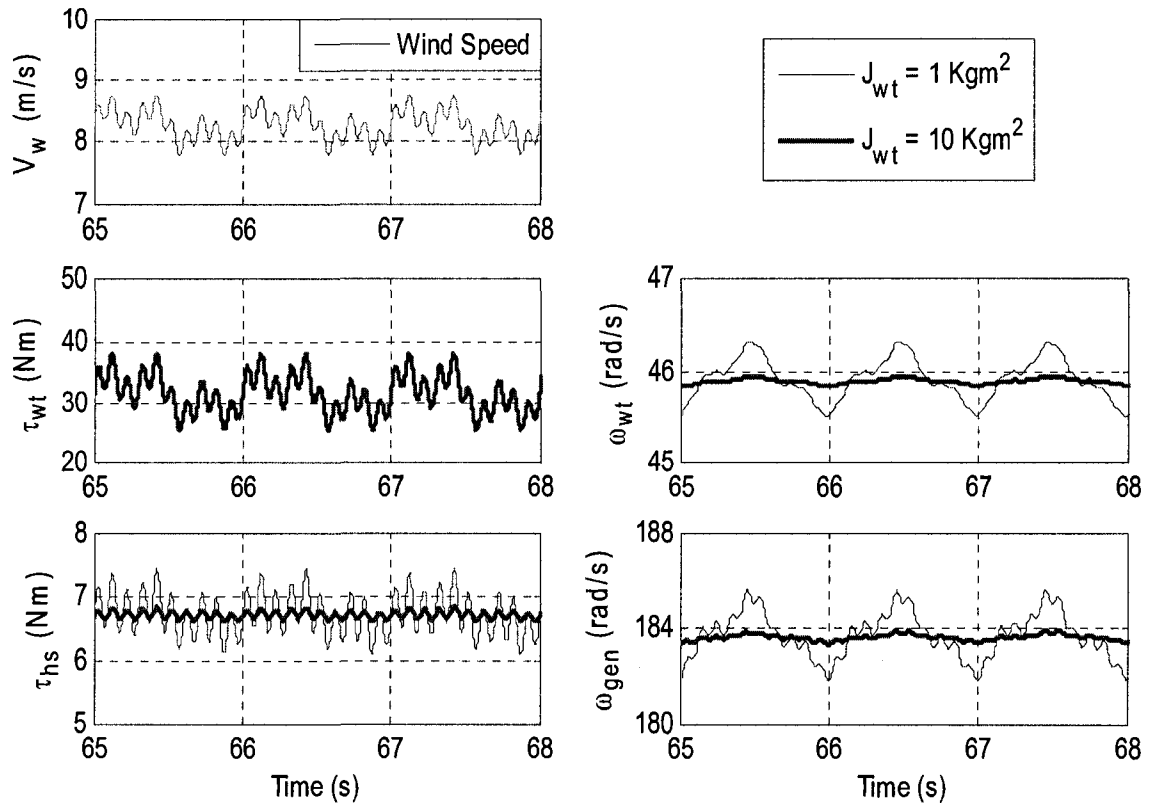
Fig. 2-14 Simulation results for case 2

The results reveal that the torque produced by the wind turbine is the same for both smaller and bigger masses moment of inertias. But, the high speed side shaft torque and the generator speed have less variations for the wind turbine with higher mass moment of inertia.

Case 3) This case is presented to show how the natural frequency of the system can be excited by a harmonic on the wind speed. The results for this case are shown in Fig. 2-15. The oscillatory torque coefficients A and B in equation 2-10 are set equal to

zero. Therefore, the variations on the system responses are due to only wind speed

harmonics. Two wind speed profiles are considered for the system with the same

parameters. They are $Vw = 8.25 + 0.4\ sin6\pi t$ m/s and $Vw = 8.25 + 0.4\ sin24\pi t$ m/s. The

responses are presented in steady-state.
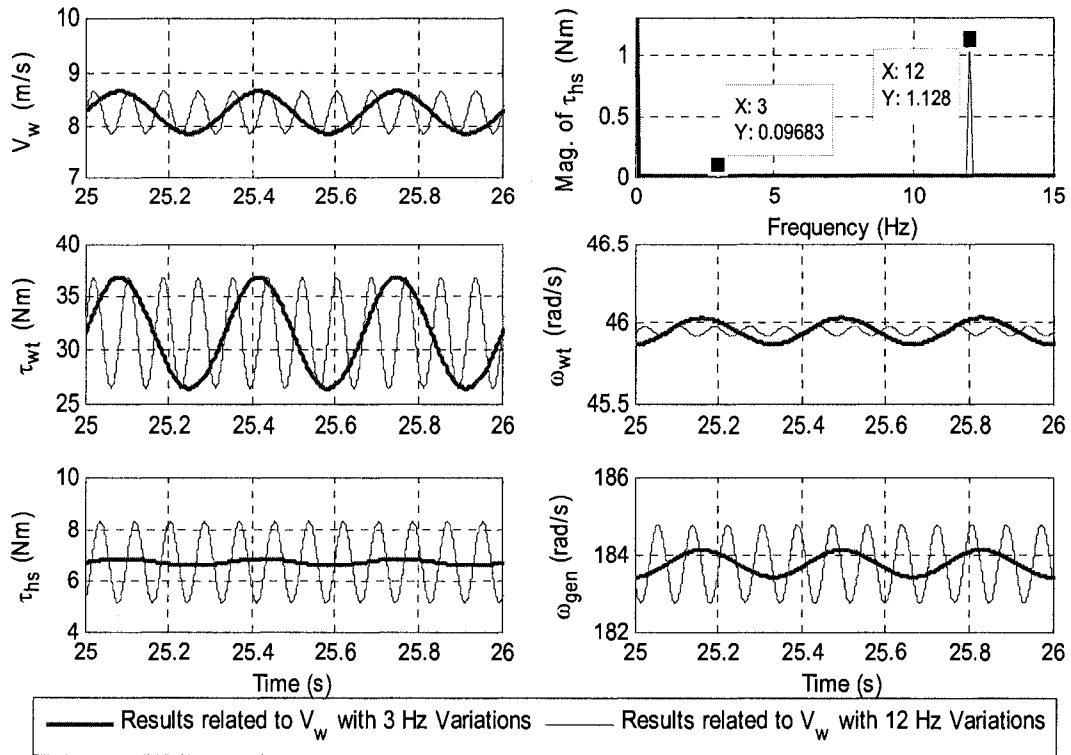
Fig. 2-15 Simulation results for case 3

As it can be seen from the results, the variations on the high speed side shaft

torque for the wind speed with 12 Hz variations is significantly larger than when wind

has a 3 Hz component. The reason is that, 12 Hz is very close to the system's natural

frequency which is, according to equation 2-14, 12.16 Hz. Thus, larger variations should

be expected on the output responses when the wind speed presents variations at

frequencies closer to the system's natural frequency. It should be noted that the FFT of

the high speed side shaft torque shows the 3 and 12 Hz components which correspond to

38

3 and 12 Hz variations on the wind speed. It can be also seen that the wind turbine speed variation for the wind speed with 3 Hz component is larger than the case where it has 12 Hz component. It is because of the fact that the torque with the lower frequency results in a larger variation on a mass with inertia.

Case 4) This case shows how oscillatory torque can excite the natural frequency of the system. The results for this case are shown in Fig. 2-16, in steady-state. The oscillatory torque is in effect. The wind speed is constant at 8.25 m/s. Therefore, the variations on the system responses are due to the oscillatory torque only. Systems with two different shaft torsional spring constants (K_{sh}), 5100 and 1710.8 Nm/rad are considered. It should be noted that according to equation 2-18, the shaft damping constants (B_{sh}) are 1.35 and 0.7837 Nms/rad, respectively.

Referring to Fig. 2-16, it can be clearly seen that the variations on the high speed side shaft torque is much larger in the case where K_{sh} is 5100 Nm/rad. The reason is that the natural frequencies of the system, based on equation 2-14, with K_{sh} = 5100 Nm/s and K_{sh} = 1710.8 Nm/s are 20.99 and 12.16 Hz, respectively. On the other hand, the 3rd harmonic of the wind turbine rotor speed is equal to 21.875 Hz. Since, this frequency (3rd harmonic) is much closer to the natural frequency of the system with K_{sh} = 5100 Nm/s, larger variations should be expected for the case where K_{sh} = 5100 Nm/s comparing to the case where K_{sh} = 1710.8 Nm/s.
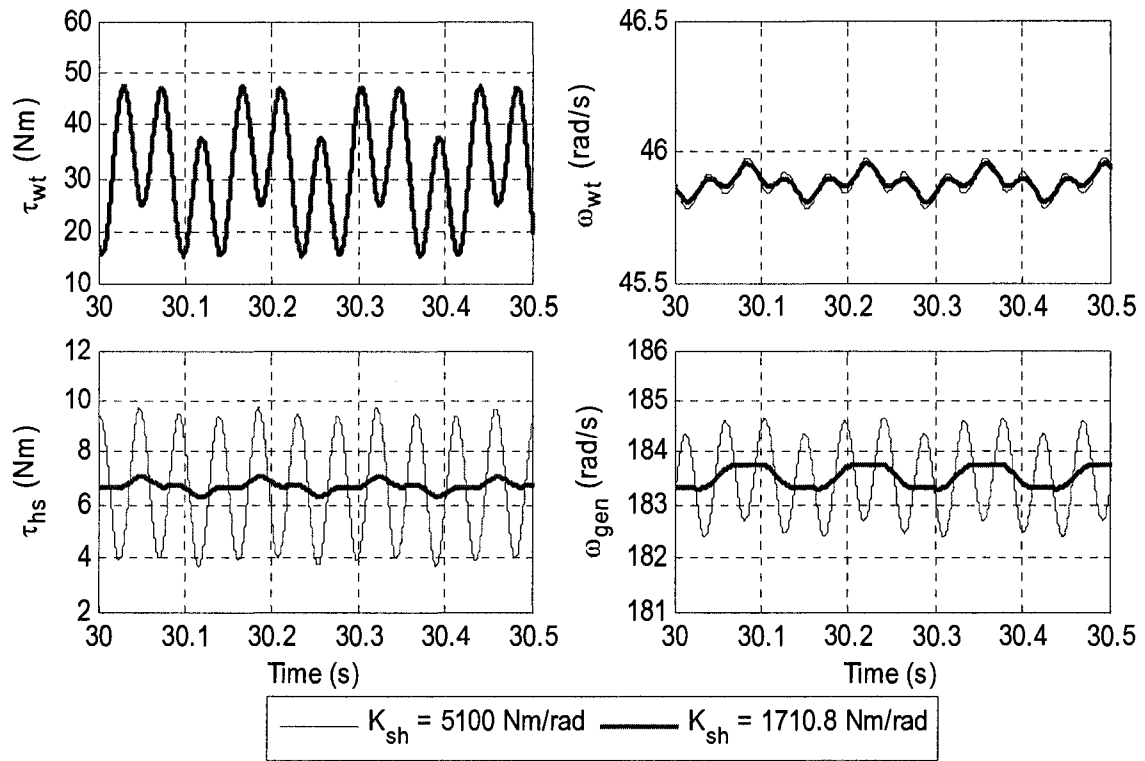
Fig. 2-16 Simulation results for case 4

Case 5) In this case the effect of wind speed step changes on the system responses are investigated. It includes transient as well as steady-state responses for the wind turbines with two different masses moment of inertias, 3 and 7 kgm^2. The results for this case are shown in Fig. 2-17. The wind speed is selected at 8.85 m/s. The mechanical load coefficient is $b = 246 \times 10^{-6}$ Nms^2/rad^2. In this case the generator power is 1500 W, which will be equal to rated power of the wind turbine emulator presented in Chapter 3. According to equation 2-18, for $J_{wt} = 3$ and 7 kgm^2, the shaft damping constants equal 0.7837 and 0.8065 Nms/rad, respectively. Fig. 2-17(a) shows the wind turbine responses, Fig. 2-17(b) shows the generator responses, and Fig. 2-17(c) is the zoom of the high speed side shaft torque.

40

The results show that the transient response for wind turbine with higher mass moment of inertia is slower. Another point is that the wind speed change causes overshoot or undershoot on the wind turbine torque and power responses but the other responses such as wind turbine rotor speed and the high speed side responses are under-damped.

The other fact is that every time the wind speed changes, the system's mechanical mode will be excited. This fact is shown in Fig. 2-17(c). The natural frequencies of the system for J_{wt} equal to 3 and 7 kgm^2, according to equation 2-23, are 12.16 and 11.81 Hz, respectively. According to Fig. 2-17(c), the calculated values of natural frequencies for the wind turbine with the masses moment of inertias of 3 and 7 kgm^2 are 12.19 and 11.76 Hz, respectively. The small differences are because of the accuracy of simulation results, since they have been executed with fixed step sampling time. It should be noted that the condition for exciting the natural frequency, introduced by equation 2-15 as discussed in section 2.3.1, is to somehow keep the generator speed constant. Since this condition cannot be provided unless the generator is connected to a strong grid (regulated system), the excitation of this mode does not occur.
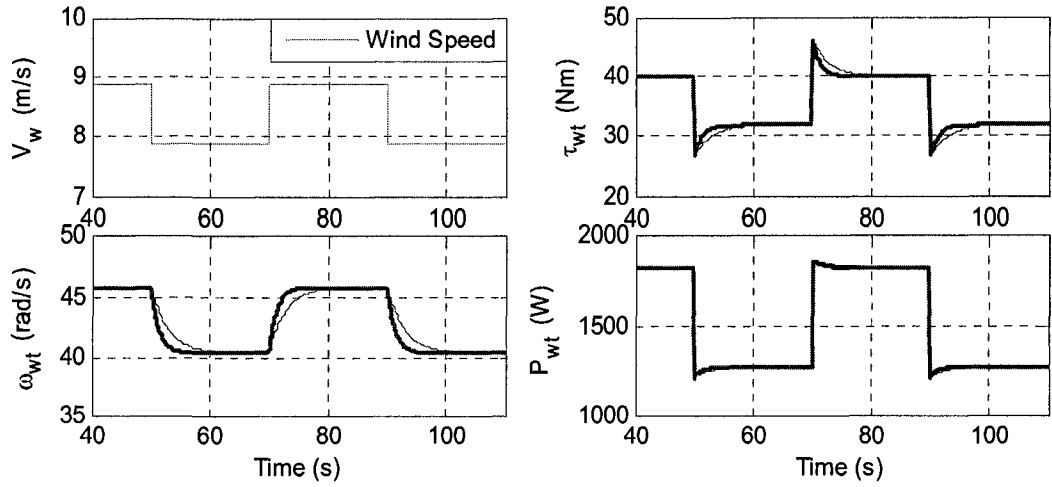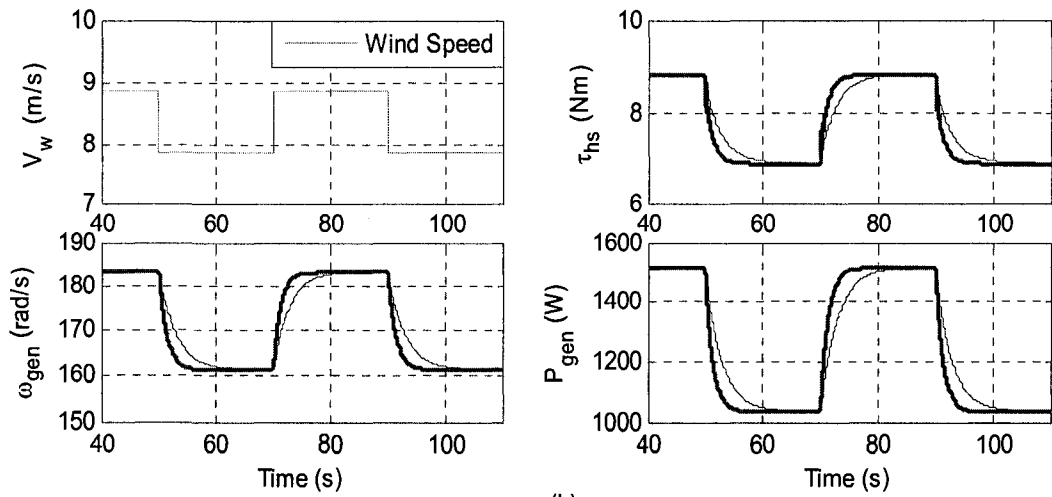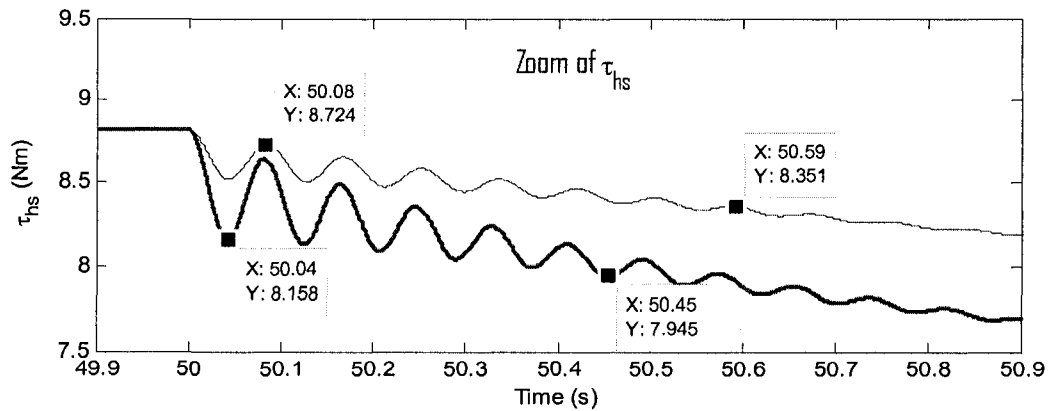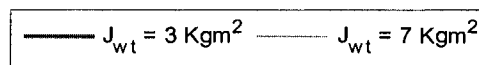
Fig. 2-17 Simulation results for case 5

Case 6) This case is intended to investigate the effect of load step changes on the system responses. It includes transient as well as steady-state responses. The results are shown in Fig. 2-18. The wind speed is selected at 8.5 m/s. The mechanical load coefficient is $b = 220 \times 10^{-6}$ Nms^2/rad^2. In this case the generator power is about 1300 W. These values are chosen since the wind turbine emulator in Chapter 3 will be tested with the same values for ease of comparison. Selecting these values allow the following load step changes with slightly exceeding the rated speed and torque of the prime mover in experimental set-up of Chapter 3. The load step changes are $\pm 40 \times 10^{-6}$ Nms^2/rad^2. Fig. 2-18(a) shows the wind turbine responses and Fig. 2-18(b) shows the generator responses. Fig. 2-18(c) is the zoom of the high speed side shaft torque and the generator speed.

The importance of the load change, as it can be seen from the results, is the excitation of the system's mechanical mode. Referring to equation 2-14, the natural frequency of the system is 12.16 Hz. According to the points highlighted in Fig. 2-18(c) the calculated natural frequency is 12.12 Hz. The slight difference is for the same reason as discussed in the end of previous case. The other point is that the responses on the wind turbine side are all over-damped. On the other hand, the load changes result in overshoot and undershoot on the generator torque and power responses.
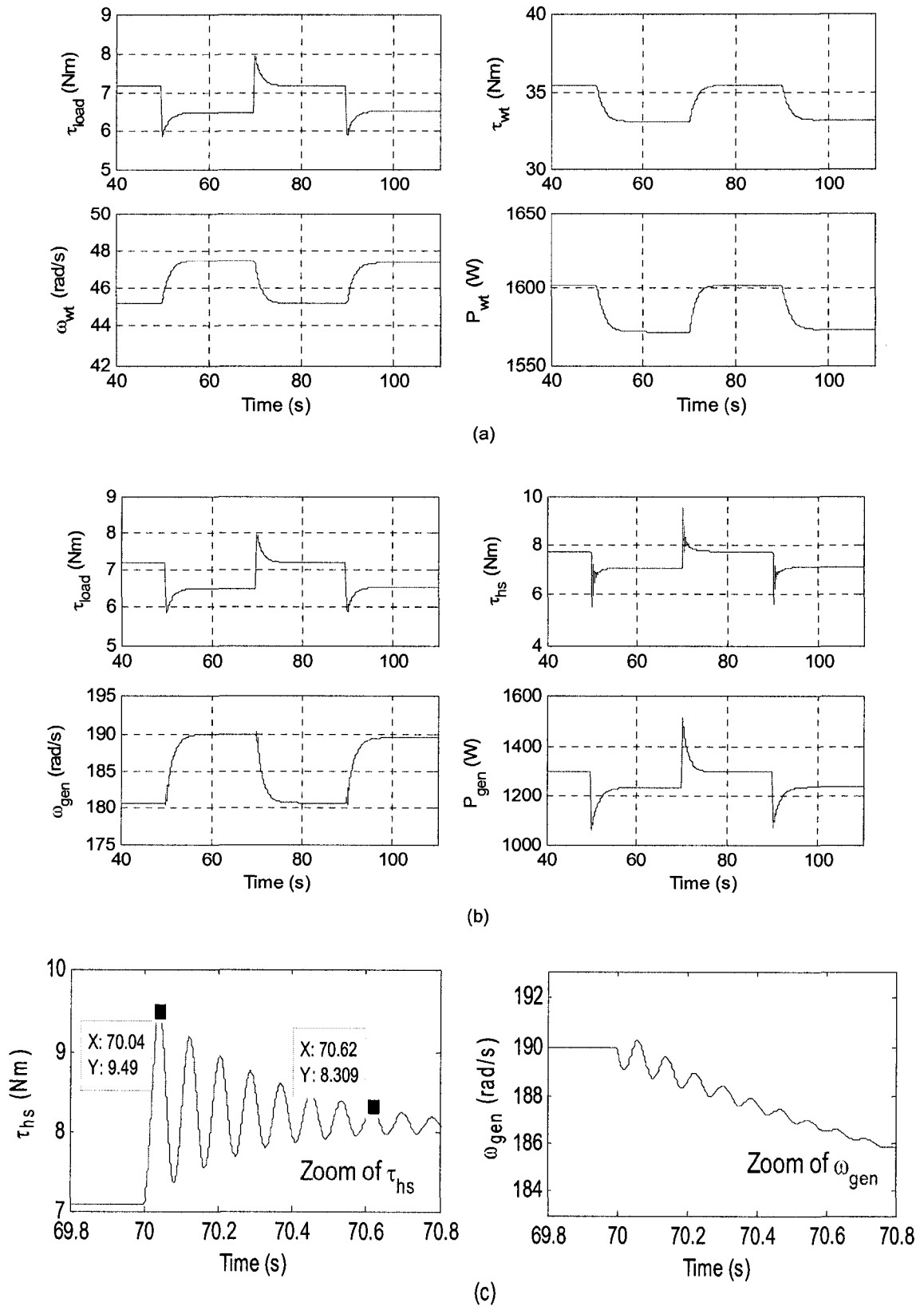
Fig. 2-18 Simulation results for case 6

44

2.6 CONCLUSIONS

This chapter has focused on the modeling of WECSs. In doing this, the power coefficient, and torque coefficient were introduced. Consequently, the power and torque equations were expressed and the torque-speed and power-speed characteristics of a typical wind turbine based on the given $C(\lambda)$ curve were presented. The drive train with a flexible shaft and gearbox were discussed and the equations for calculating natural frequencies of a 2-mass system with 2 degrees of freedom were given. The system under consideration was presented in Fig. 2-9 which mainly includes the mechanical model of the wind turbine, the electric generator, and the load. The wind turbine rotor was simply modeled as a mass moment of inertia and friction damping mainly due to the blades and the hub.

The wind turbine drive train was considered as a shaft, which was modeled with its torsional spring constant and damping constant, and an ideal (lossless and backlash free) gearbox. The electric generator was modeled with its mass moment of inertia and friction damping. An expression between load torque and speed of generator was assigned as a load model. After expressing the differential equations governing the system, the developed block diagram was presented in Fig. 2-10. Based on the block diagram and other equations the system was modeled in MATLAB/Simulink. The simulation results were presented and some important facts as summarized below were observed.

> ➢ Effect of the wind turbines with higher mass moment of inertia in filtering the wind speed variations and pulsations due to oscillatory torque on the generator torque.

45

➢ System resonance occurrence due to wind speed variations, load variations, and also due to oscillatory torque.

➢ Slower transient response for the system with higher wind turbine mass moment of inertia.

CHAPTER 3

DESIGN AND IMPLEMENTATION OF A WTE

3.1 INTRODUCTION

The mechanical parts of a wind turbine, including the rotor and the drive train, were modeled and discussed in Chapter 2, as the first step. The second step is to design and implement a system to follow the reference torque at the high speed side shaft, as if driven by the wind turbine. The system includes a prime mover, power electronics converter, and a controller in addition to the wind turbine model. The wind turbine model generates the reference torque and communicates with the system through a real-time software.

As it was discussed in Chapter 1, after reviewing the literature a PMDC machine is chosen as prime mover. In this case, by knowing the relationship between torque and current of the DC machine, it is possible to enforce the machine to produce the desired torque by controlling its current. A switch-mode DC-DC converter and a hysteresis current controller are chosen to enforce the prime mover to follow the reference torque on its shaft. It should be noted that the prime mover will run a PMDC machine as dynamometer, which behaves as a mechanical load. In this case without having a generator and variable electrical load, it is possible to make the system operate at different operating points (torque vs. speed characteristic of the wind turbine) by controlling the torque of the dynamometer.

Section 3.2 describes the PMDC machines and their characteristics. In section 3.3 the power electronics and type of controllers are discussed. Section 3.4 is devoted to

47

describing the logic of the WTE. The experimental set-up and the methods of implementation of the WTE are discussed in section 3.5. The experimental results are provided in section 3.6 and section 3.7 summarizes this Chapter and provides the conclusions.

3.2 PMDC MACHINES

DC machines have been used in motor drives since long time. They have very good drive performance which makes them relatively easy to control to follow the reference speed and/or torque. The main disadvantage of DC machines was very high maintenance requirement for brushes and commutators. Development in brushes and commutator technologies made it possible to design them with longer life time and lower maintenance requirement. With the advancement in rare-earth magnet, the PMDC machines are designed with very high torque-to-volume and reasonable prices. Recently, with the advancement in power electronics, the squirrel cage induction machines which have low cost and rugged construction are used in motor drives [24, 25].

There are different schemes to control the induction motor. Vector-controlled schemes are among them which were proposed by researchers. They require more complicated control strategies in comparison with DC machines due to their torque-speed characteristics and AC quantities. Besides, their performances in motor drive applications highly depend on the machine modeling and parameters. In this Thesis, because of the availability of DC machines and power electronics switches suitable for DC machines in the P. D. Ziogas Laboratory, and also the fact that, it is easier to control DC motors compared to induction motors, a PMDC machine is used as prime mover.

3.2.1 MODEL AND CHARACTERISTICS [24, 25]

Based on the fact that PMDC machines produce constant flux as field, the relationship between machine variables and parameters are as follows:

$$\tau_{em}(t) = K_t \, i_a(t) \tag{3-1}$$

Where τ_{em} is the electromechanical torque of the machine in Nm, K_t is the toque constant of the machine in Nm/A, and i_a is the machine's armature current in A.

$$e_b(t) = K_b \omega_m(t) \tag{3-2}$$

Where e_b is back emf of the machine in V, K_b is the speed constant of the machine in Vs/rad, and ω_m is the machine speed in rad/s. It should be noted that in the SI unit system the values of K_t and K_b are equal. By applying KVL to Fig. 3-1, which is the equivalent circuit of the DC machine in motoring operation, the following equation can be written:
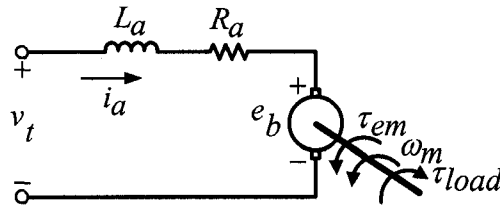
Fig. 3-1 PMDC machine equivalent circuit in motoring operation

$$\frac{di_a(t)}{dt} = \frac{1}{L_a}v(t) - \frac{R_a}{L_a}i_a(t) - \frac{1}{L_a}e_b(t) \tag{3-3}$$

Where v_t is the terminal voltage in V, L_a is the armature inductance in H, and R_a is armature resistance in Ω. Furthermore, the torque and speed of the machine can be related by the following equation:

$$\frac{d\omega_m(t)}{dt} = \frac{1}{J_m}\tau_{em}(t) - \frac{1}{J_m}\tau_{load}(t) - \frac{B_m}{J_m}\omega_m(t) \tag{3-4}$$

49

Where J_m is the mass moment of inertia of the machine in kgm^2 and B_m is the machine friction coefficient in Nms/rad. Considering equations 3-1 to 3-4 the following equation expresses the DC motor in the form of state variables:

$$\begin{bmatrix} \dfrac{di_a(t)}{dt} \\[4mm] \dfrac{d\omega_m(t)}{dt} \end{bmatrix} = \begin{bmatrix} -\dfrac{R_a}{L_a} & -\dfrac{K_b}{L_a} \\[4mm] \dfrac{K_t}{J_m} & -\dfrac{B_m}{J_m} \end{bmatrix} \begin{bmatrix} i_a(t) \\[2mm] \omega_m(t) \end{bmatrix} + \begin{bmatrix} \dfrac{1}{L_a} \\[4mm] 0 \end{bmatrix} v_t(t) + \begin{bmatrix} 0 \\[4mm] -\dfrac{1}{J_m} \end{bmatrix} \tau_{load} \qquad (3\text{-}5)$$

Based on the above equations the DC motor model (block diagram in s domain) is shown in Fig. 3-2.
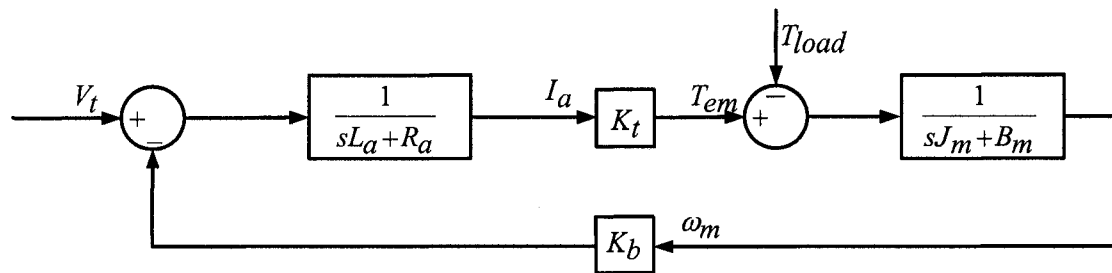
Fig. 3-2 PMDC motor model [25]

Fig. 3-3 shows the characteristics of PMDC machine. Fig. 3-3(a) shows the relation between terminal voltage and machine speed where the torque or equivalently armature current is kept constant at its rated value. In this case, the machine speed varies linearly with varying terminal voltage. Therefore, at rated terminal voltage the machine reaches the rated speed. The difference between v_t and e_b corresponds to $i_a R_a$ voltage drop. In Fig. 3-3(b) the relation between the torque and speed of the machines is presented for individual terminal voltages. The characteristic implies that for a given terminal voltage the machine can operate from zero to rated torque. One can see that for a given terminal voltage the speed variation is limited to a very small range. As a result of

these characteristics, it can be concluded that the machine can operate at any point in the safe region (operating region) as marked ABCD, by controlling the terminal voltage and machine torque. This characteristic provides the opportunity to use a DC machine as prime mover for implementing WTE.
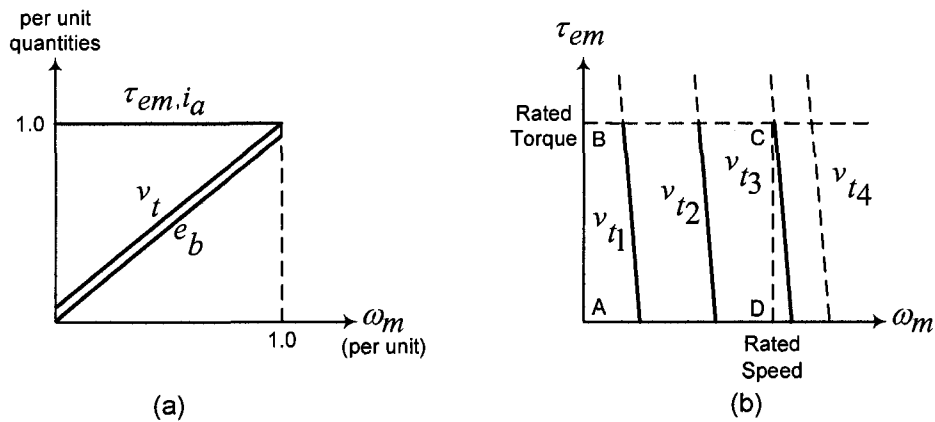
Fig. 3-3 PMDC machine characteristics; (a) Continuous torque-speed capability; (b) torque-speed characteristics for different terminal voltages where $v_{t4} > v_{t3} > v_{t2} > v_{t1}$ [24].

3.2.2 PMDC MACHINE PARAMETERS

The PMDC machine parameters, including nameplate data, information from data sheet, and estimated parameters, are provided in Table 3-1. The most important parameter of the PMDC machine in implementing WTE is the torque constant K_t. This parameter is estimated based on the method presented in [26] which is briefly described below. The PMDC under test has been driven by another motor, operating as generator at no-load. The generator voltages and speeds were measured and recorded. Therefore, according to equation 2-2 the speed constant (K_b) was calculated. As stated earlier in this chapter in the SI unit system, $K_t = K_b$.

The friction coefficient (B_m) and the mass moment of inertia (J_m) of the machine are estimated according to the methods proposed in [26] and [27], respectively. They are briefly described here. Calculation of friction coefficient is done based on the fact that at higher speed the main power loss and consequently the loss torque are due to the mechanical rotational speed. Therefore, tests and readings are done for the speed of 1400 RPM to about 10% above the rated speed of the machine. The machine is operated as motor at no load. By varying its terminal voltage various speeds were reached. In each step, voltage, current, and speed of machine were recorded. Then, the friction coefficient was calculated according to the following equation:

$$\Delta \tau_{em} = K_t \Delta i_a = B_m \Delta \omega_m \tag{3-6}$$

Where Δ corresponds to the difference of each quantity for two consequent steps.

Table 3-1 PMDC machine rating and parameters

Baldor PMDC Machine Rating and Parameters			
Nameplate and Data Sheet		Measured in the Laboratory	
Power (hp)	2	Torque Constant (Nm/A)	1.03947
Voltage (V)	180	Speed Constant (Vs/rad)	1.03947
Current (A)	8.5	Friction Coefficient (Nms/rad)	0.00153625
Speed (RPM)	1750	Mass Moment of Inertia (kgm^2)	0.01015
Armature Resistance (Ω)	0.8555	Armature Inductance (mH)	6.966

Finally, the average of the calculated friction coefficients is considered as the estimated value as indicated in Table 3-1. The mass moment of inertia of the machine was estimated by operating the machine as a motor at no load. At the time where the

speed was about 1900 RPM, its breaker was opened. In this case, by referring to equation 3-4 and setting τ_{em} and τ_{load} to zero the solution of the differential equation is:

$$\omega(t_1)=\omega(t_o)e^{\dfrac{-B_m(t_1-t_o)}{J_m}} \qquad (3\text{-}7)$$

Since the speed versus time was plotted during the test, speeds at the time t_1 and t_o are known and the only unknown in equation 3-7 is J_m which was calculated as 0.009747 kgm^2. This was the estimation of the mass moment of inertia of the PMDC machines by the method explained above. But, the WTE itself also provided the opportunity to estimate the mass moment of inertia of the PMDC machines which is briefly discussed in section 3.5.4. The estimated value of mass moment of inertia of the PMDC machine by using WTE was 0.01015 kgm^2; this value is used as the estimation of each PMDC machine mass moment of inertia.

3.3 POWER ELECTRONICS AND CONTROLLERS

To control the torque and speed of a DC machine, the average quantities such as average armature current and terminal voltage are of concern. This can be done by line-frequency controlled converters or switch-mode DC-DC converters. These concepts and types of controllers involved are briefly described below.

3.3.1 LINE-FREQUENCY CONTROLLED CONVERTERS [24]

These types of converters consist of thyristors which can be configured to work in single-phase or three-phase systems. In Fig. 3-4 only single-phase configurations are shown. In both configurations by creating proper firing angles for each thyristor the

output current can be enforced to follow the reference current. Two-quadrant configuration of this type of converter is not suitable for DC motor breaking since the current cannot be reversed. But, it is suitable for operating the reversible DC motors in both directions. The four-quadrant configuration can be achieved by using two back-to-back two-quadrant converters as shown in Fig. 3-4(c).
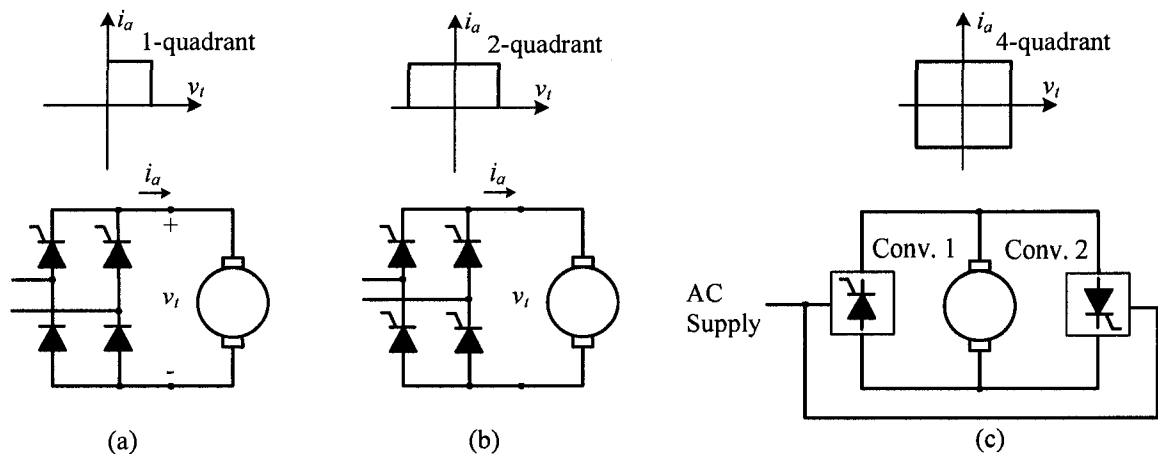
Fig. 3-4 Line-frequency controlled converters configuration; (a) 1-quadrant converter; (b) 2-quadrant converter; (c) 4-quadrant converter [24]

The most popular controllers for this type of converters are PI controllers. The general concept of operation is shown in the form of block diagram in Fig. 3-5. This type of converter with PI controller is not suitable for the wind turbine emulator. Its controller bandwidth, which has to be smaller than the equivalent switching frequency of the converter, is not sufficient to emulate the harmonics of the oscillatory torque of wind turbine output on the prime mover shaft which is addressed in [6]. For this reason, these types of converters are not used for implementing WTE in this Thesis.
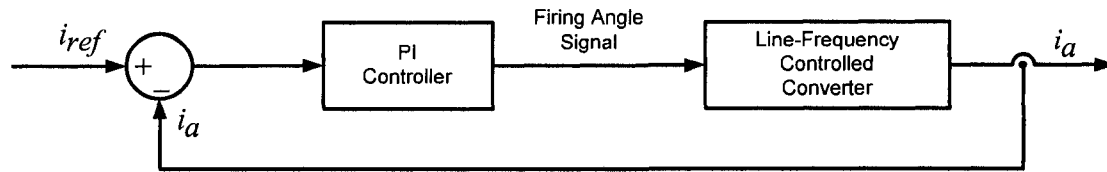
Fig. 3-5 Control concept of line-frequency controlled converter [24]

3.3.2 SWITCH-MODE DC-DC CONVERTERS [24]

These types of converters consist of power electronics switches such as bipolar junction transistors (BJTs), insulated-gate bipolar transistors (IGBTs), or power MOSFETs. As it is clear from the title of these converters they convert DC into DC quantities. Three configurations of these converters for controlling a DC machine are shown in Fig. 3-6. In each case, the concept is to control the duty cycle of a switch or switches to make the output voltage (v_t) or output current (i_a) follow the reference values.

Operating at higher switching frequencies is desirable for reducing the size of the filters. But, increasing switching frequency causes in higher switches losses. Thus, selecting the operating switching frequency is always a tradeoff between these two facts. For two-quadrant and four-quadrant converters a dead-time must be provided for gating signals of the switches in each leg to avoid short circuit. It means that a delay time more than turn-off time of the switches must exist between the trailing edge of one switch and rising edge of the other switch in one leg. Two types of control strategies can be applied to regulate the output current of converters; Fixed-frequency control and tolerance band (hysteresis) control which are briefly described below.
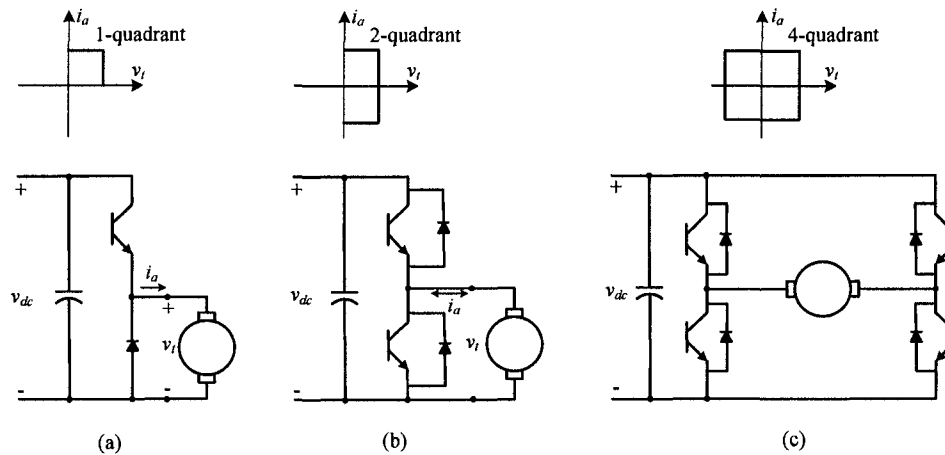
Fig. 3-6 Switch-mode DC-DC converter configurations; (a) 1-quadrant converter; (b) 2-quadrant converter; (c) 4-quadrant converter [24]

Fixed-frequency current control: In this type of control the reference current and actual current are compared and based on their difference a control voltage ($v_{control}$) will be generated. The control voltage is compared with a triangle waveform with a fixed switching frequency and the difference is fed to a comparator which provides the gating signal(s). A typical control block diagram with a PI controller for generating $v_{control}$ is shown in Fig. 3-7. Referring to Fig. 3-6(a), for instance, if the difference between reference current and actual current increases a larger $v_{control}$ will be created. Thus, the switch will be open for a longer time. This in turn results in a higher average output voltage of converter which makes the DC machine (motoring operation) to draw more current to follow the reference current.
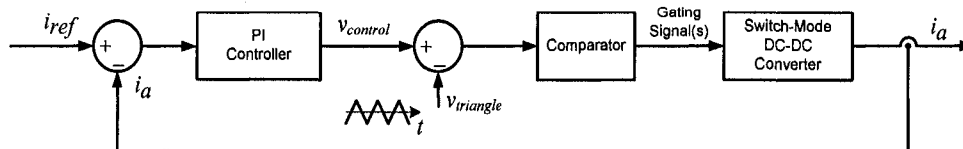
Fig. 3-7 Fixed-frequency current control block diagram [24]

56

Tolerance band (hysteresis) current control: This type of current control scheme is based on the definition of a tolerance band around the reference current and enforcing the actual current to be in that band. The concept and the gating signal pulses for a 1-quadrant converter are shown in Fig. 3-8(a).

It is clear that every time the actual current touches the upper or lower limit of the tolerance band the state of the switch must be change from on to off state and vice versa to be able to keep the actual current in the band limit. A general control scheme block diagram is shown in Fig. 3-8(b). There are three facts that cause in increasing the switching frequency in this scheme; higher value of DC input voltage, narrower tolerance band, and shape of the reference current. Since having faster response is required for the emulator to create larger variations due to the wind speed and load change and also the wind turbine torque pulsations the hysteresis control is selected for implementation of the WTE in this Thesis.

(a)   (b)
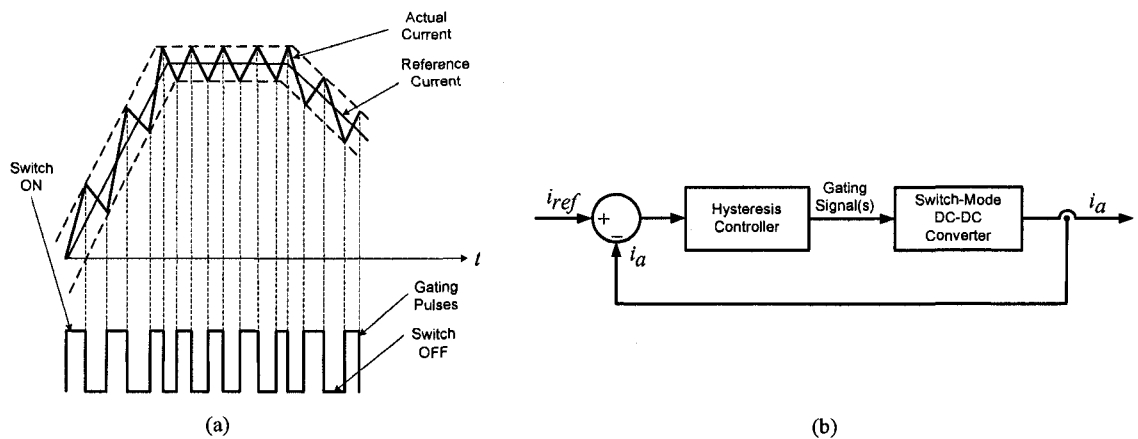
Fig. 3-8 Tolerance band current control; (a) waveforms and switching concept; (b) control block diagram [24]

3.4 CONTROL LOGIC OF THE WTE [6]

Fig. 3-9 shows the schematic control logic of the WTE. This WTE represents a 2-hp wind turbine since a 2-hp PMDC machine is used as the prime mover. It should be noted that, the WTE can be used for wind turbines with higher power by employing prime movers with higher ratings. The main concept is based on the fact that (referring to Fig. 2-4) for a certain wind speed and certain wind turbine rotor speed (or equivalently the prime mover speed by considering the gear ratio) there would be one and only one torque on the stable region of the torque-speed characteristic.

The operating point, for a certain wind speed, on the torque-speed characteristic depends on the load which wind turbine sees. Therefore, by imposing a load torque on the shaft of the prime mover, the operating point of wind turbine will be established. To impose a mechanical load torque on the shaft of the prime mover, a 2-hp PMDC machine is used as dynamometer.

Thus, by measuring the dynamometer speed and feeding it back to wind turbine model the reference torque for the prime mover will be created. The torque will be converted to current which is called the prime mover reference current. On the other hand, the actual current of the prime mover is measured. It will be compared with the prime mover reference current through the prime mover hysteresis current controller and the switching gating signals will be created.
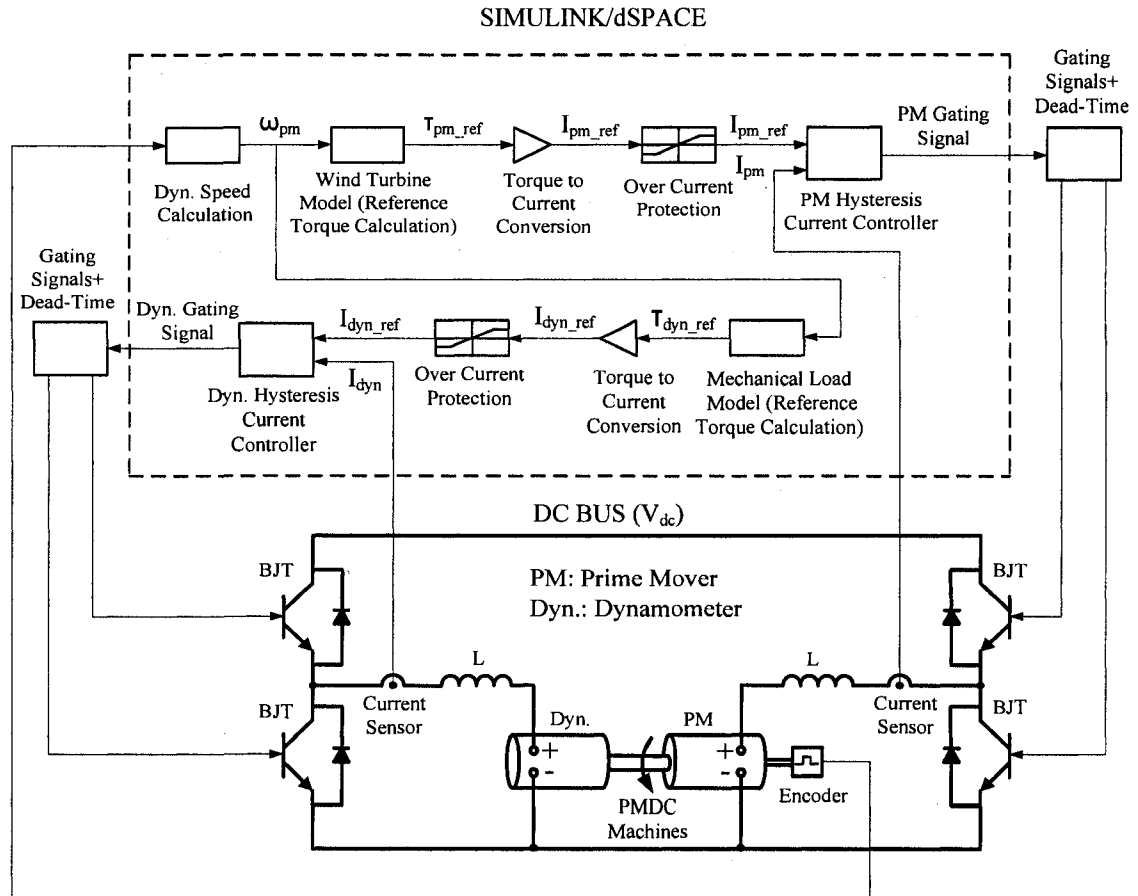
Fig. 3-9 WTE control logic schematic diagram

With regard to controlling the dynamometer, a relationship between the load torque and the dynamometer speed is defined in the MATLAB/Simulink model. Then, the created torque will be converted to the current. This current is called the reference current of the dynamometer. The actual current of the dynamometer is measured. It will be compared with the dynamometer reference current through the dynamometer hysteresis current controller and the switching gating signals will be created. The creation of gating signals and dead time are briefly explained in sub-section 3.5.3.

3.5 EXPERIMENTAL SET-UP

Fig. 3-10 shows the experimental set-up which is used for implementing the WTE. Two 2-hp PMDC machines are used as prime mover and dynamometer. Two 2-quadrant switch-mode DC-DC converters are used for controlling the currents of the machines. A 3-phase full bridge rectifier is used to provide the DC voltage for supplying the power circuit of the prime mover and the dynamometer. A dSPACE ds-1103, a digital controller for rapid prototyping that can be directly programmed with the simulink file used for the simulation, is used. It is accompanied with a user interface, ControlDesk, for operating, managing, and monitoring the experiments.

It should be noted that for the implemented WTE, a one-quadrant DC-DC converter for the prime mover and a one-quadrant converter for the dynamometer circuit will be suitable since the current direction in each circuit will remain the same. But, actually a two-quadrant DC-DC converter has been used for each circuit. This provides the opportunity for developing the proposed WTE for the future works as explained below.

As it is noted in the literature, sometimes the generator will be used for the start up of the wind turbine. Having two-quadrant switch-mode DC-DC converter provides the opportunity to perform this task. In this case, the dynamometer will be used for starting up the wind turbine by enforcing it to draw current in reverse direction. The prime mover, in this case, will be enforced to draw current in the reverse direction to oppose the dynamometer acting like wind turbine as a load for the generator.

The resistor, R, is used for discharging the capacitor for the time when the system is not in use. Its value is 3.3 kΩ. The capacitor, C, is used to reduce the ripple on the

rectifier output voltage. The inductors, L, are used to reduce the current rate of change of the prime mover and the dynamometer in each simulation time step. The methods of calculating values of the capacitor and inductors are described in the following sub-section.
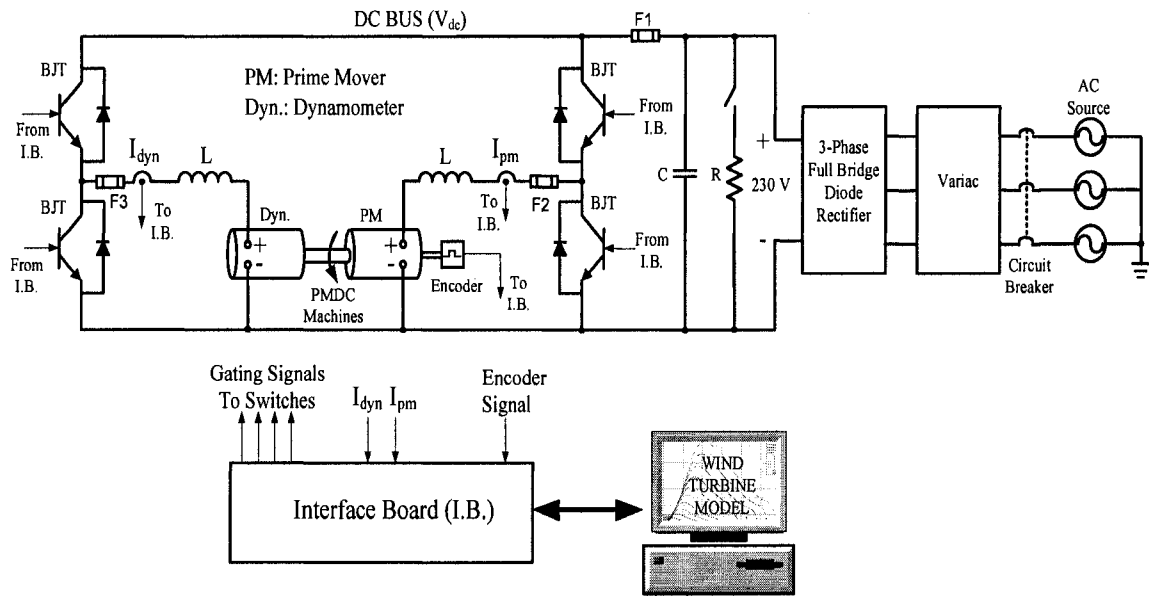
Fig. 3-10 WTE experimental set-up

3.5.1 PARAMETERS SELECTION

Capacitor C: The value of the capacitor C is not a critical point in the design of the WTE. Since the duty cycle of the switches will be automatically adjusted to provide the required voltage for the DC machine as long as the DC bus voltage (V_{dc}) is greater than the voltage required for the full load operation. But it is desirable to keep the voltage ripple low around the average value of the DC bus voltage; because one of the factors of emulating higher torques variations is to have a higher instantaneous voltage. Thus if the

voltage ripple will be high, it might be possible that at the time of step change in load the instantaneous voltage will be much lower than its average value.

The detail of the calculation is not provided. But the calculations are done based on , first, the theory and waveforms of the 3-phase full bridge diode rectifiers defined and discussed in [24] and second, on the well known equations of the energy stored in a capacitor which is $E = 1/2CV^2$ and power and energy relationship $E = Pt$. Where E is the stored energy in the capacitor in J, C is the capacitance of the capacitor in F, V is the capacitor voltage in V, P is the load power in W, and t is the time which the capacitor voltage drops from its maximum to minimum value in s. Therefore, considering that the voltage variation will be between 230.5 and 229.5 V, the minimum capacitor's capacity required to maintain this condition is 19,830 μF. The capacity of the capacitor which was used in the experimental set-up was 21,600 μF.

Inductors L: The inductors are connected in series with the prime mover and dynamometer to limit the rate of change of the current passing through the circuit. The calculations will be provided for the prime mover circuit only since, the same logic can be applied to the dynamometer circuit. Fig. 3-11 shows the prime mover circuit in two operating conditions. Fig. 3-11(a) represents the condition when the upper switch is on, this condition causes the current to rise. Fig. 3-11(b) represents the condition when the lower switch is on, this condition causes the current to fall.

The value of L_t is the total reactance of the circuit (DC machine armature reactance plus the reactance of inductor L). The value of R_t is the total resistance of the circuit (DC machine armature resistance (0.855 Ω) plus the resistance of the inductor L (0.14 Ω). The voltage e_t is the back emf voltage plus 2 volts voltage drop due to the

brushes. Considering that the prime mover is running at full speed, 1800 RPM, which is the concerned speed when the WTE will be used in Chapter 4 to run an induction generator. Thus for the full speed (188.5 rad/s) considering that speed constant, specified in Table 3-1, is 1.03947, the voltage e_t will be 198 V. Therefore the terminal voltage, V_{dc}, for full load and full speed operation will be 198 + 8.5 = 206.5 V. The voltage V_{dc} is selected equal to 230 V which is about 10% higher than the required voltage for full speed and full load operation.
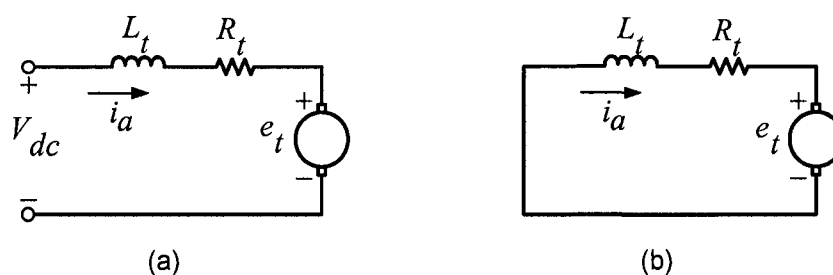
Fig. 3-11 Equivalent circuit of the prime mover in two operating conditions; (a) Upper switch is on; (b) Lower switch is on

Selecting the value of inductor L is a tradeoff between the maximum rate of change of armature current of the prime mover and the minimum tolerance band limit of hysteresis current controller which can be achieved. This matter will be clearer by numerical calculations presented below. The calculation will be presented for a 35 mH inductor which was available in the laboratory. The prime mover armature reactance is about 7 mH. Thus, L_t is about 42 mH and R_t is about 1 Ω. Referring to Fig. 3-11(a), by applying KVL to the circuit, the rate of rise of the current in full load operation when current is 8.5 A and prime mover is running at 1800 RPM, will be as below in A/s:

$$V_{dc} - e_t - i_a R_t = L_t \frac{di_a}{dt} \Rightarrow \frac{di_a}{dt} = 560$$

This can be converted to rate of rise of torque by multiplying it by 1.03947 (torque constant) which will be 582 Nm/s.

Referring to simulation results in Chapter 2, any step variations in the system input and output such as wind speed and load variations cause in excitation of the system's natural frequency which appears in a sinusoidal form on the reference torque (on the shaft of the prime mover) with the frequency of 12.16 Hz, for the parameters given in Table 2-1. That is $\tau_{ref\_variation} = C_l \; sin2\pi \times 12.16t$ Nm. Therefore, the maximum variation of the torque will be $2\pi \times 12.16 \times C_l$. It can be concluded that C_l = 582 / $(2 \times \pi \times 12.16)$ = 7.6 Nm.

This means that the prime mover can emulate the variations which cause in the torque variation with the amplitude of up to 7.6 Nm on the shaft of prime mover. In the calculations it is assumed that the oscillatory torque is not in effect. In section 4.3.1 of Chapter 4 the effect of oscillatory is also accounted for in calculating the emulating capability of the WTE. It should be noted that this is considered to be the variations which cause in additional load on the wind turbine when it is already running at full load. By applying KVL to the circuit of Fig. 3-11(b) the rate of fall of the torque will be 4917 Nm/s which is much higher than the rate of rise of the torque.

Considering the circuit in Fig. 3-11(b) and the fact that the time step of the simulation is 45 µs (the minimum value which the MATLAB/Simulink model was converted for real time application) and dead time of 4 µs, at full speed and full load, the current reduction in each step is $4917 \times 49 \times 10^{-6}$ = 0.24 A. In this case if the tolerance band of the hysteresis current controller will be set less than this value, the average value of

actual current will be less than the average value of the reference current. But the tolerance band was actually set to 0.35 which is higher than calculated value. This difference might be resulted from the discrepancies between measured or estimated parameters with the real values such as DC machine armature resistance and inductance, brushes voltage drop, and DC machine speed constant. If smaller inductor will be used, it causes in higher rate of fall in current which means the tolerance band should be made wider. One of the disadvantages of using wider tolerance band is that it results in higher variations on the prime mover current which is not desirable when the machine is running at full load.

3.5.2 METHODS OF USING MEASURED SPEED SIGNAL

Method-A (directly using measured speed signal): It is desirable to directly (without filtering) use the speed signal for implementation of the WTE as shown in Fig. 3-9. This has been tried with 3 types of rotational speed measuring devices. Tachometer, Optoschmitt sensor, and incremental encoder were used. The signal quality (high variations or ripples around average value) of the first two devices did not let to emulate wind turbines with the masses moment of inertias higher than 0.1 kgm^2. For the values above 0.1 kgm^2, the created reference torque was boundlessly growing.

Therefore an incremental encoder with 3000 pulses/revolution was used to overcome the problem. The incremental encoder typical speed signal (output) and its frequency spectrum are shown in Fig. 3-12. The frequency spectrum of the speed signal shows the nonzero magnitude for all frequencies. But ideally the only nonzero component should be at 0 Hz, DC value. The largest magnitude (for nonzero frequencies)

is at 30 Hz. This frequency changes by the speed of the dynamometer and is due to misalignment of the shafts of the dynamometer and the incremental encoder.

As the experimental results in Chapter 4 show, the 30 Hz component of the speed signal produces a 30 Hz component on the reference torque. But as far as this frequency is not close to the system's natural frequency (equation 2-14), it does not cause system instability. The most crucial frequencies are the ones that are close to the system's natural frequency. The results presented in Chapter 4 indicate the effect of the existence of nonzero components close to system's natural frequency on the system responses which brings limitations on selecting some parameters of the wind turbine. For this reason, the method-B which is discussed in the next subsection is proposed to reduce the effect of system's natural frequency excitation.
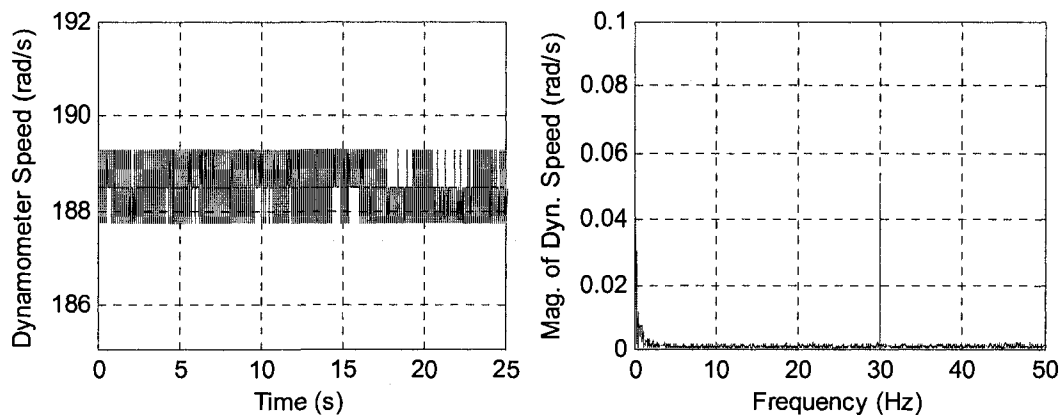
Fig. 3-12 Dynamometer speed signal and its frequency spectrum

Method-B (using actually modified speed signal): The main objective of this method is to highly reduce the magnitude of frequencies around the system's natural frequency on the measured speed signal even though they are normally very low by using 3000 (pulses/revolution) incremental encoder. This can be done by using a low pass filter

with its cut off frequency lower than the system's natural frequency. In this case, first, the magnitudes of the components that can excite the system mechanical modes will be attenuated which is not desirable (affecting the system dynamics). Second, the speed variations which are due to variations of the reference torque should be kept intact as much as possible otherwise instability occurs due to the phase lag created by the low pass filter. So in brief, using a low pass filter alone for filtering of the speed signal will cause in system's instability and also affecting the system dynamic. Therefore by combining these two requirements an actually modified speed signal can be created by adding *estimated* speed variations to the average value of the actual speed signal as shown in Fig. 3-13.

In this figure, T_{act} is the actual torque generated on the shaft of the prime mover which is assumed to be equal to T_{ref} created by the wind turbine model. J_T and B_T are total mass moment of inertia and total friction constant of the prime mover and the dynamometer. T_{dyn} is the load torque plus the dynamometer losses torque except its friction torque since it is considered as part of the prime mover and dynamometer model. Ω_{dyn} is the dynamometer measured speed signal. The quantities marked by *, are the estimated values of the related quantities. The two low pass filters have the same transfer functions.

If the estimation of the system's parameters were 100% accurate, using $\Omega^*_{dyn}(s)$ directly instead of $\Omega_{dyn}(s)$ would be the easiest and the most effective way to overcome the problem described before in method-A. But, since the accurate estimation of B_T and T_{dyn} was not possible in the laboratory (their values have high impact on the average of

the estimated speed), it was decided to use the average of the actual speed signal as the

base and just use the estimated speed signal for estimation of speed variations.

Thus, referring to Fig. 3-13, signal $X(s)$ is the average value of the actual speed

signal. Signal $W(s)$ is the estimated value of speed variation around its average value. It is

added to the average value of the actual speed signal, $X(s)$, to obtain the signal $Z(s)$ which

is the actually modified speed signal. So, the average value of signal $Z(s)$ is equal to the

average of $\Omega_{dyn}(s)$ with much less noise and disturbances (especially the components

around the system's natural frequency).
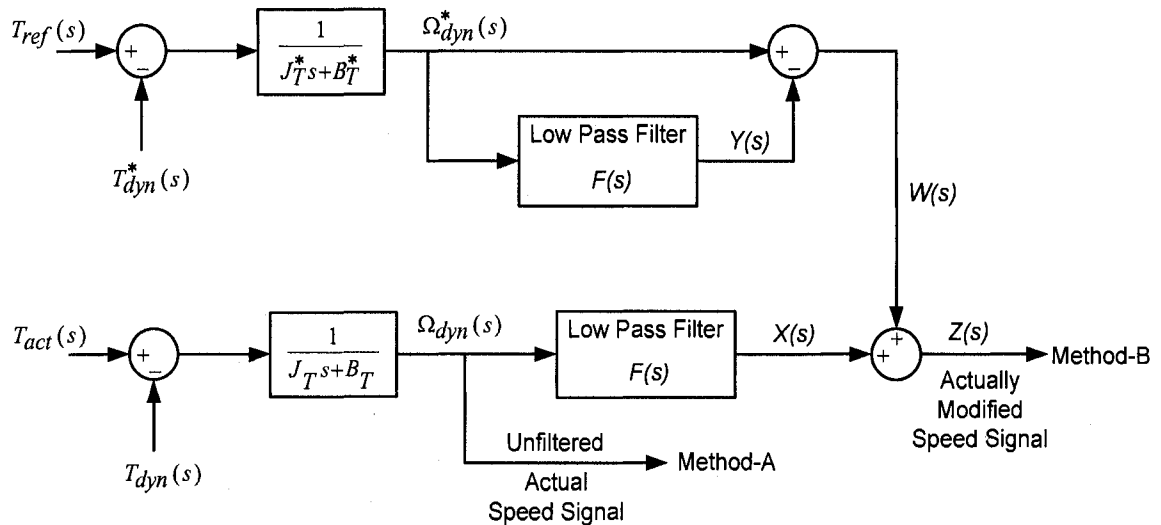
Fig. 3-13 Block diagram for creating actually modified speed signal

It should be noted that the speed of the dynamometer cannot have a step change

because of the masses moment of inertias of the prime mover and the dynamometer. Any

change on the average value of the dynamometer speed, therefore, appears in the form of

a ramp. Using a low pass filter on the actual speed signal causes some delay and therefore

some error during the speed transition. This error can be calculated as:

$$E(s) = \Omega_{dyn}(s) - \Omega_{dyn}(s) \times F(s) \tag{3-8}$$

This error will be compensated by the signal W(s) as shown below:

$$W(s) = \Omega_{dyn}^{*}(s) - \Omega_{dyn}^{*}(s) \times F(s) \tag{3-9}$$

This is the estimated speed signal minus its filtered (average) value. Since the estimated speed signal itself has some errors with respect to the actual speed signal, it brings some limitations on reducing the cut off frequency of the low pass filter at will. In other words, by inspecting equation 3-10 (based on Fig. 3-13), it is obvious that if $\Omega_{dyn}^{*}(s) = \Omega_{dyn}(s)$, the signal Z(s) will be equal to Ω_{dyn}(s) independently of the transfer function F(s).

$$Z(s) = \Omega_{dyn}^{*}(s) - \Omega_{dyn}^{*}(s) \times F(s) + \Omega_{dyn}(s) \times F(s) \tag{3-10}$$

Experimental results show that as the cut off frequency of the low pass filters were set to lower values the error between the estimated and actual speed signals increased. It can be stated that the closer the estimated speed signal is to actual speed signal, the lower is the cut off frequency of the low pass filters that can be used. The other way of observing the problem of the error is that the time constant of the prime mover and the dynamometer model is J_T/B_T = 0.0203/0.0030725 = 6.6 s. Therefore, the closer the time constant of the low pass filters is to the prime movers and the dynamometer time constant the higher error is expected during the ramp transition of the speed signal.

For the first order low pass filters, the time constant is inversely proportional to the cut off frequency. Thus, to have less error (between estimated and actual speed signal) the cut off frequency of the filter must be increased but by increasing the cut off frequency the amount of the attenuation on the signals especially around system's natural

frequency will be reduced. Thus, the other option which is a second order filter is used for two main reasons. First, attenuation of the frequencies higher than the cut off frequency of the filter for the second order is higher. The attenuation is -40 dB/dec for a second order filter and is -20 dB/dec for a first order filter. Second, for a specified cut off frequency by changing the damping factor, the speed of the filter which is its rise time, can be adjusted.

The second order low pass filters are discussed in detail in [28] and will be briefly explained below. The general form of the transfer function of the second order low pass filter is:

$$F(s) = \frac{\omega_n^2}{s^2 + 2\xi\omega_n s + \omega_n^2} \tag{3-11}$$

Where $\omega_n = 2\pi f_n$ in rad/s, f_n is the natural frequency in Hz, and ξ is the damping factor. The rise time (time to go from 10% to 90% of the final value in s) of the filter is given as:

$$T_r = \frac{2.16\xi + 0.6}{\omega_n} \qquad 0.3 \le \xi \le 0.8 \tag{3-12}$$

Considering the above equations, it is possible to select the natural frequency for enough attenuation of the frequencies above the cut off frequency and to reduce the value of ξ for faster filter response for reducing the error during the transition. After extensive tests the system responses were examined and the responses were acceptable for wide ranges of the second order low pass filters in terms of their cut off frequencies and damping factors. Thus, the experimental results in this Chapter and Chapter 4 are provided for low pass filters with the following transfer function:

$$F(s) = \frac{(9\pi)^2}{s^2 + 5.4\pi s + (9\pi)^2}$$ (3-13)

In equation 3-13, the natural frequency (f_n) is 4.5 Hz and ξ is 0.3. Therefore, the rise time is 0.044 s. The results will show that this filter provides enough attenuation around the system's natural frequency for each case and also provides fast response so that the error between the estimated and actual speed signals is not noticeable.

3.5.3 THE DSP SYSTEM [29]

Fig. 3-14 shows the input/output signals to and from ds-1103 control board. The DSP development system which is used for implementation of the WTE is called dSPACE. It has many features but the main features which are used for this experimental set-up are briefly discussed here. By installing dSPACE it provides additional block-set libraries in MATLAB/Simulink. One of them is the master PPC library which includes ADC, DAC, and incremental encoder blocks.

ADC blocks are used in the MATLAB/Simulink model of the system to convert analogue input signals to digital signals. The DAC blocks are used in the MATLAB/Simulink model of the system to convert the signals created in the model to analogue signals. The voltage levels that the ds-1103 can take as input signals and can send as output signals are in the ±10 V range. The inputs/outputs on the ds-1103 board are BNC connectors which provide easy and quick connections to other interface boards via coaxial cables.

For this experimental set-up the outputs from dSPACE are only the gating signal for each leg (prime mover switches and dynamometers switches). Since the maximum

current that dSPACE can supply through these outputs is 5 mA, an electronic interface

board was used to provide the required current for the drive circuit of the switches which

is about 25 mA. In addition to this, from each gating signal created in the

MATLAB/Simulink model, gating signals for upper and lower switch of each leg

including about 4 μs dead time between the signals of the switches in each leg was

created by using electronic circuits. The electronic circuit is provided in Appendix B.
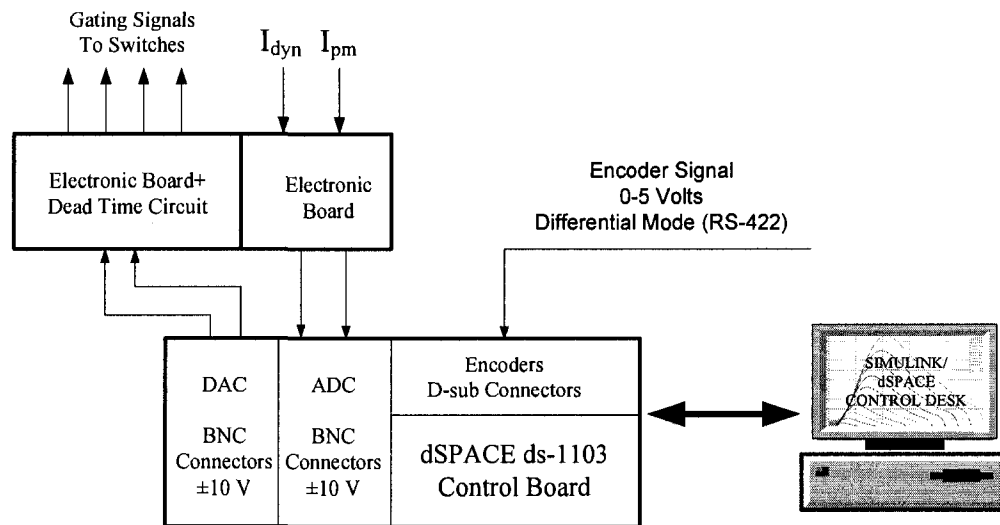
Fig. 3-14 Input/output signals to and from dSPACE ds-1103 control board

The inputs to ds-1103 board are prime mover current, dynamometer current and

the most critical signal, the speed signal. As it was mentioned in the previous subsection,

the implementation of WTE using directly the speed signal is very sensitive to the noise

and disturbances. For this reason, the special inputs which are available on the ds-1103

board and allocated to incremental encoder signals are very crucial for this

implementation.

They are seven D-sub connector type inputs. Six of them accept encoder signals in the form of digital signal and one of them accepts the signal of the encoder in the form of analogue. Each input can be set to accept the signals in the form of single ended or differential mode (RS-422). This can be done by placing the Encoder Master Setup block, in the Master PPC library as mentioned before, in the Simulink model of the system. An incremental encoder with 3000 pulses/revolution, with differential mode (RS-422) signals and digital output, 0 − 5 V, was used. Special cable with twisted pairs with overall shield and separate shield for each pair was used to minimize the noise on the signal.

After converting the Simulink model for real time application (by clicking the build button), all the blocks in the model will be accessible by dSPACE/ Control Desk software. This software provides many features such as measuring instrumentation, sliders, control buttons, and data acquisition tools. All these, make it possible to change the value of each block in the model while system is running (online), to observe the waveforms at any point in the model, and to capture the data as m file, which can be used in MATLAB for analysis or plotting.

3.5.4 MATLAB/SIMULINK MODEL

The MATLAB/Simulink model which was used for implementation of the experimental set-up is shown in Fig. 3-15. It mainly consists of wind turbine model, prime mover hysteresis current controller, prime mover measured current, dynamometer hysteresis current controller, dynamometer measured current, dynamometer speed signal, dynamometer measured current, and dynamometer torque estimation sub-system.

The hysteresis current controllers create the gating signals for the prime mover power circuit upper switch and dynamometer power circuit lower switch shown in Fig. 3-9 and Fig. 3-10. The model is prepared in such a way to be able to operate with either directly using the dynamometer speed signal (method-A) or using actually modified dynamometer speed signal (method-B) as marked in the top-left of the model. These methods were introduced and discussed in subsection 3.5.2.

With regard to calculating the total mass moment of inertia of the prime mover and dynamometer (J_{pm+dyn}), referring to the method discussed in section 3.2.2, it was estimated as 0.019495 kgm^2. Implementation of the WTE also provides an opportunity to estimate the mass moment of inertia. After several tests, by varying the values of K_{sh} and J_{wt}, the resonance frequencies of the reference torque have been measured using FFT analysis of the reference torque signal.
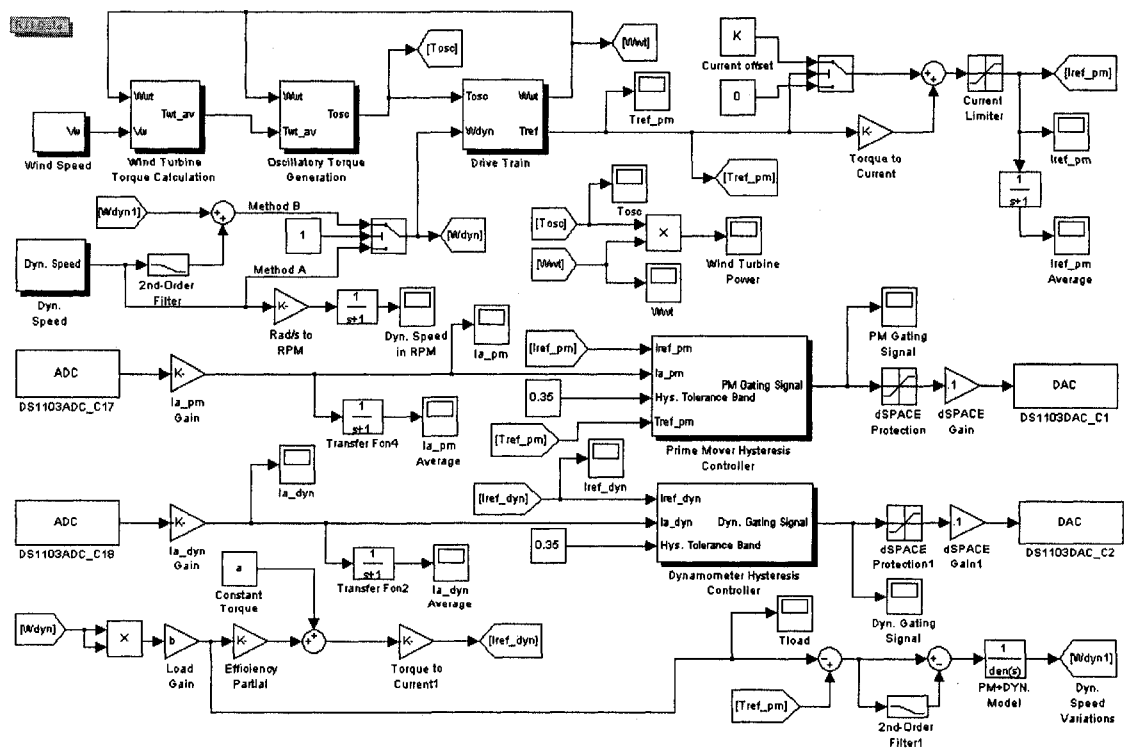

Fig. 3-15 MATLAB/Simulink model for implementation of the experimental set-up

74

Then, according to equation 2-14 corresponding J_{pm+dyn} were calculated in each case. The average value of the measured J_{pm+dyn} was calculated as 0.0203 kgm^2. The error between the average value and the values obtained in each case is less than 1.5 %. The error between the estimated value of J_{pm+dyn} by the method introduced in Section 3.2.2, 0.019495 kgm^2, and using WTE, 0.0203 kgm^2, is about 4%. In Fig. 3-15, the "PM+Dyn. Model" block is set equal to 1/(0.0203s+0.0030725), where 0.0203 kgm^2 and 0.0030725 Nms/rad are the estimated values for the total mass moment of inertia and the total friction coefficient of the prime mover and the dynamometer, respectively.

In this model the created load torque is in the form of $T_{load} = b\omega^2$. The value of b in the experimental results is multiplied by the factor 0.94. The reason is the losses of dynamometer, therefore, by reducing the load torque by that factor (0.94) the operating points of the results in this Chapter (experimental results) are close to the operating points of the results (simulation results) in Chapter 2. By doing this, comparison between the experimental results and simulation results will be more straightforward.

In Fig. 3-15, there are two subsystems which are the prime mover and the dynamometer hysteresis current controller. They are used to control the current of the prime mover and of the dynamometer to follow their reference currents created in the MATLAB/Simulink model. The models for both cases are nearly the same. Thus, the prime mover hysteresis current controller is discussed here. This model was available in the files of Mr. Avishek Mukherjee (former student in the electrical department) in the P. D. Ziogas Power Electronics Laboratory, and with a slight change is used in this Thesis. The model is shown in Fig. 3-16.

The logic is, while the actual current of the prime mover remains in the tolerance band (which is defined around the reference current of the prime mover) the state of upper switch (the top switch in the power circuit of the prime mover) remains the same. If the prime mover current will be higher than upper limit of the tolerance band the upper switch will be turned off. If the prime mover current is less than the lower limit of the tolerance band the upper switch will be turned on. This concept is fulfilled by using a J-K flip-flop.

Fig. 3-16 Prime mover hysteresis current controller model
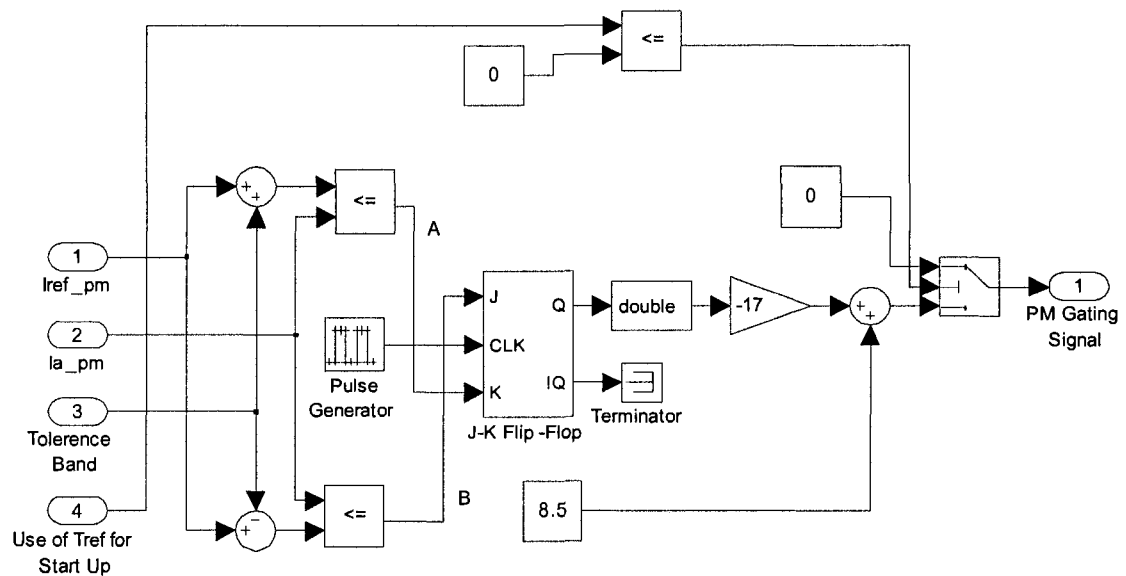
It should be noted that the model for the dynamometer is the same as the model for the prime mover except that the lines marked A and B will be connected to J and K inputs of the flip flop, respectively. Also, the statements mentioned earlier for the upper switch of the prime mover converter leg must be considered for the lower switch of the dynamometer converter leg.

3.6 EXPERIMENTAL RESULTS

Experimental results are provided in six different cases which include the steady-state and transient responses. The conditions and parameters in all six cases are the same as conditions and parameters in the cases shown in Chapter 2 (simulation results Section) for ease of comparison between the experimental and simulation results. The parameters for the experimental results are the same as the parameters in Table 2-1, unless otherwise stated.

As it was discussed in Section 3.5.2, the WTE can be implemented by two methods of using the dynamometer speed signal. Method-A (the speed signal is directly used) and method-B (the actually modified speed signal is used). Since the results by two methods are presented for all cases in Chapter 4 for comparison, to avoid lengthening the Thesis, the results in this Chapter are provided for the case where method-B is used. The reference torque (τ_{ref}) relates to the high speed torque (τ_{hs}) and the dynamometer speed (ω_{dyn}) relates to the generator speed (ω_{gen}) in Chapter 2.

Case 1) This case highlights the effect of the wind turbine mass moment of inertia on filtering of the oscillatory torque as far as generator torque and speed are concerned. The results for this case are shown in Fig. 3-17 and are taken in steady-state. The wind speed is constant at $V_w = 8.25$ m/s. The responses are shown for wind turbine with mass moment of inertia (J_{wt}) equal to 1 and 10 kgm^2. According to equation 2-18, the shaft damping (B_{sh}) are 0.7168 and 0.8120 Nms/rad, respectively.

The results show that the wind turbine and the dynamometer torque and speed responses correspond to the results provided in the case 1 of simulation results in Chapter 2. In Fig. 3-17(b) the zoom of the dynamometer speed signals are presented to indicate how close the actually modified speed signal and the actual speed signal are. In other words, the reference torque creates the expected variations on the dynamometer speed.

Based on the results, it can be concluded that for the wind turbine with higher mass moment of inertia the variations on the wind turbine rotor speed, reference torque (dynamometer shaft), and the dynamometer speed are lower than the case where wind turbine has lower mass moment of inertia. Higher mass moment of inertia can be achieved at the expense of larger and heavier blades and consequently more expensive wind turbine. Therefore, there should be a compromise in selecting wind turbine mass moment of inertia and generated power.
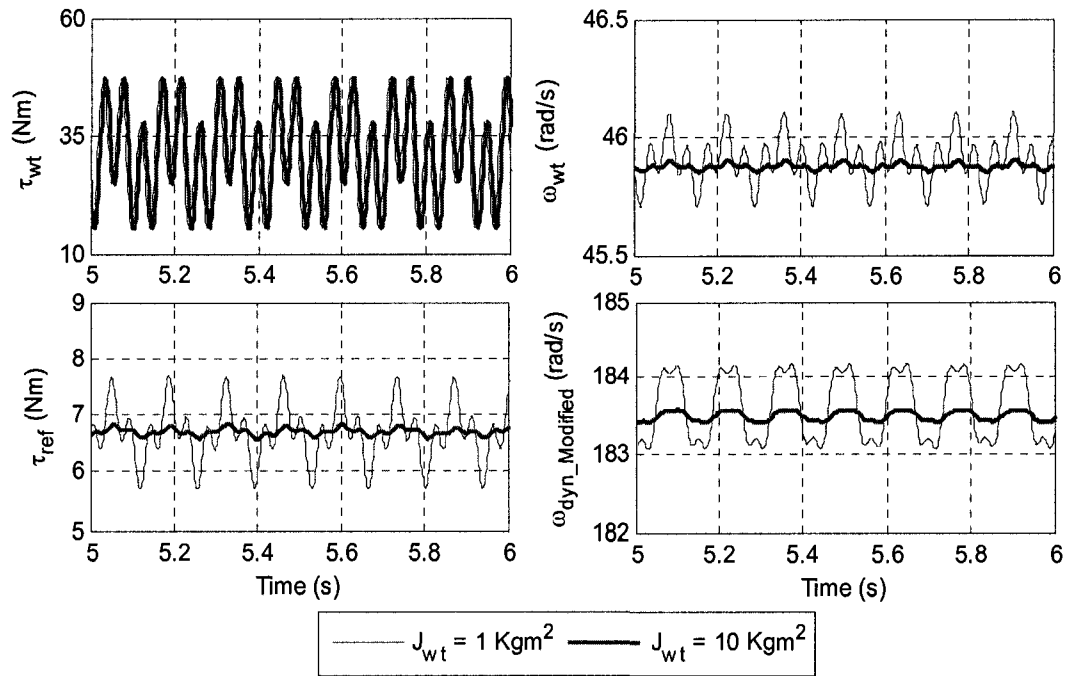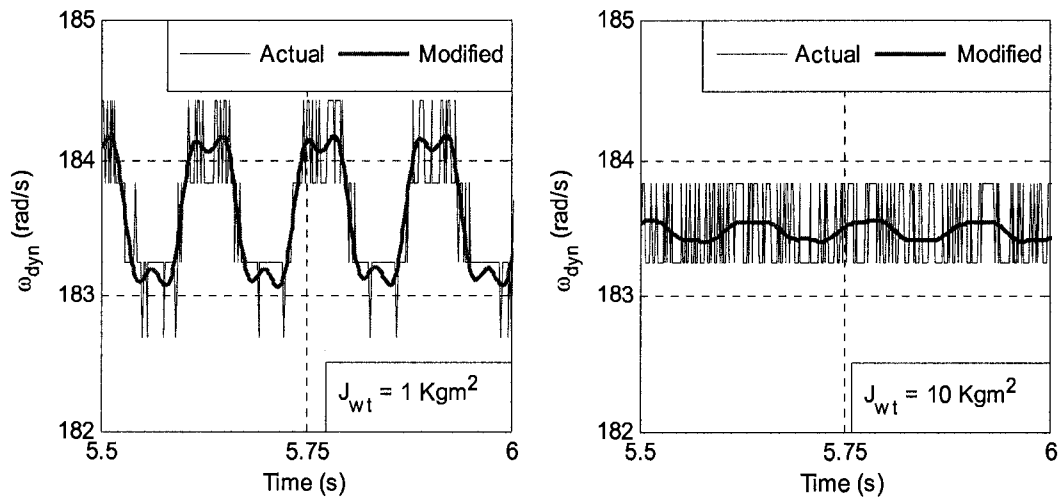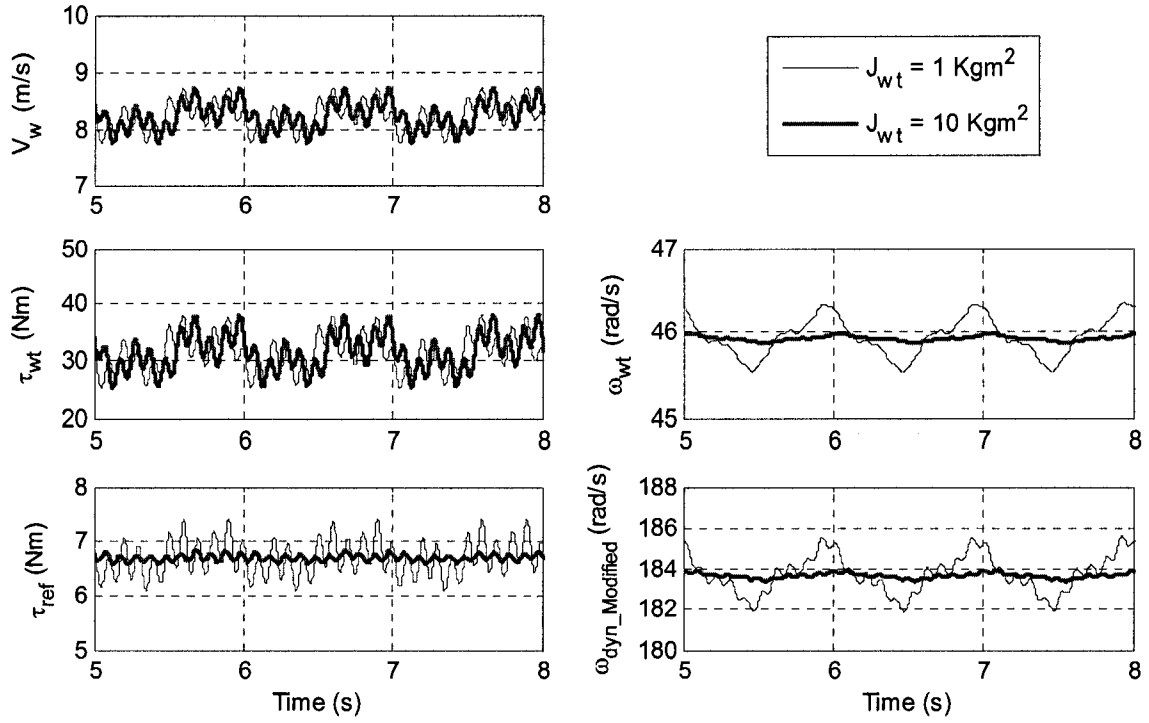
Fig. 3-17 Experimental results for case 1; (a) WTE responses; (b) Zoom of the
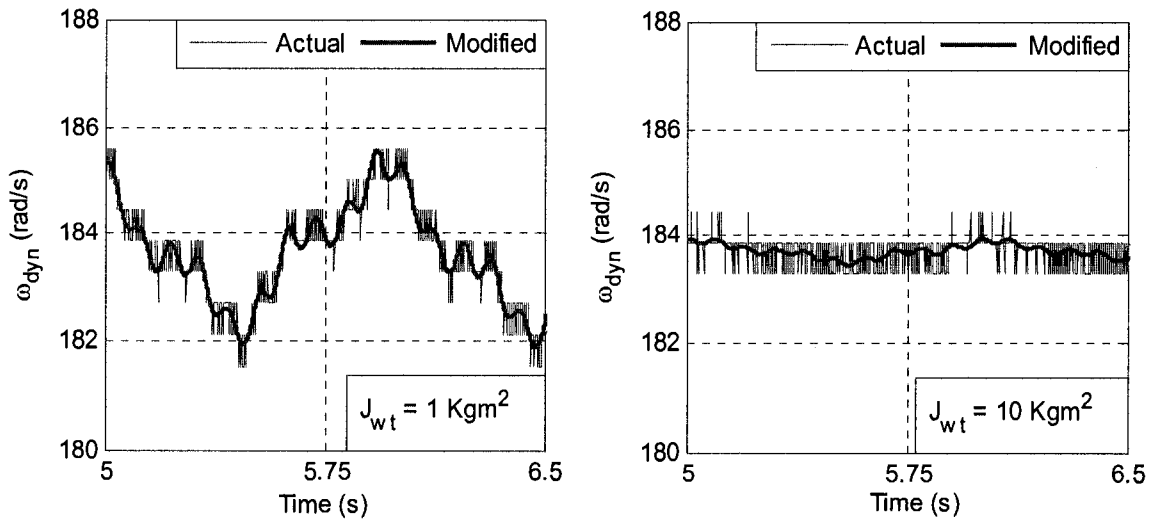
dynamometer speed signals

Case 2) This case highlights the effect of the wind turbine mass moment of inertia on filtering of the wind speed variations as far as the generator torque and speed are concerned. For power system studies, it is suggested in [19] to consider some harmonics on the wind speed and the frequencies of the harmonics are in the range of 0.1 -10 Hz. The results for this case are shown in Fig. 3-18.

The wind speed is considered to be $Vw = 8.25 + 0.2\ sin2\pi t + 0.2\ sin6\pi t + 0.2$ $sin20\pi t$ m/s. The coefficients A and B of the oscillatory torque in equation 2-10 are set equal to zero to be able to easily observe the effect of only wind speed variations on the system responses. The responses are shown for wind turbine with mass moment of inertia (J_{wt}) equal to 1 and 10 kgm^2. According to equation 2-18, the shaft damping (B_{sh}) are 0.7168 and 0.8120 Nms/rad, respectively. The phase difference between the wind speed profiles is due to the fact that the results for two cases are captured at different times. The responses are shown in steady-state.

The results show that the wind turbine and the dynamometer torque and speed responses correspond to the results provided in the case 2 of simulation results in Chapter 2. In Fig. 3-18(b) the zoom of the dynamometer speed signals are presented to indicate that how close the actually modified speed signal and the actual speed signal are. In other words, the reference torque creates the expected variations on the dynamometer speed. The results reveal that the wind turbine produced torque is the same for both lower and higher masses moment of inertias. But, the reference torque and the dynamometer speed have lower variations for the wind turbine with higher mass moment of inertia.

Fig. 3-18 Experimental results for case 2; (a) WTE responses; (b) Zoom of the

dynamometer speed signals

Case 3) This case is presented to show how the natural frequency of the system can be excited by a harmonic on the wind speed. The results for this case are shown in Fig. 3-19. The oscillatory torque coefficients A and B in equation 2-10 are set equal to zero. Therefore, the variations on the system responses are due to wind speed harmonics only. Two wind speed profiles are considered for the system with the same parameters. They are $Vw = 8.25 + 0.4 \ sin6\pi t$ m/s and $Vw = 8.25 + 0.4 \ sin24\pi t$ m/s. The responses are presented in steady-state.

The results show that the wind turbine and the dynamometer torque and speed responses correspond to the results provided in the case 3 of simulation results in Chapter 2. In Fig. 3-19(b) the zoom of the dynamometer speed signals are presented to indicate that how close the actually modified speed signal and the actual speed signal are. In other words, the reference torque creates the expected variations on the dynamometer speed.

As it can be seen from the results the variations on the reference torque for the wind speed with 12 Hz variations is significantly larger than when wind has 3 Hz variations. The reason is that variation of 12 Hz is very close to system's natural frequency which is, according to equation 2-14, 12.16 Hz. Thus, larger variations should be expected on the output responses when the wind speed presents variations at frequencies closer to the system's natural frequency. It should be noted that the FFT of the reference torque shows the 2.949 and 11.97 Hz components which are due to 3 and 12 Hz components on the wind speed.
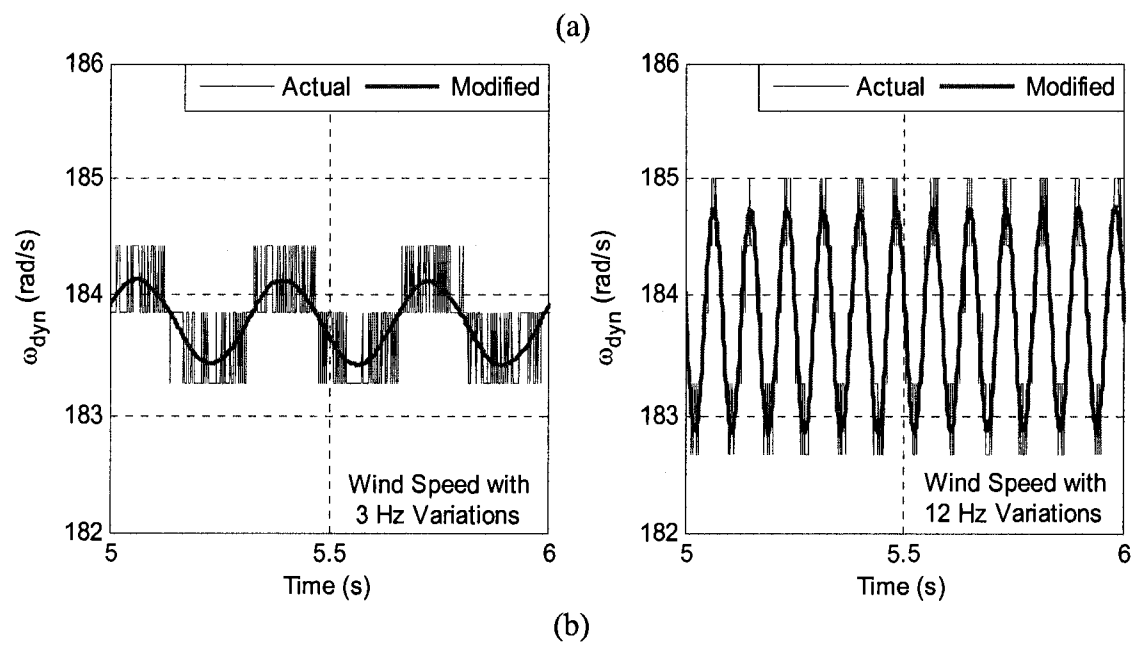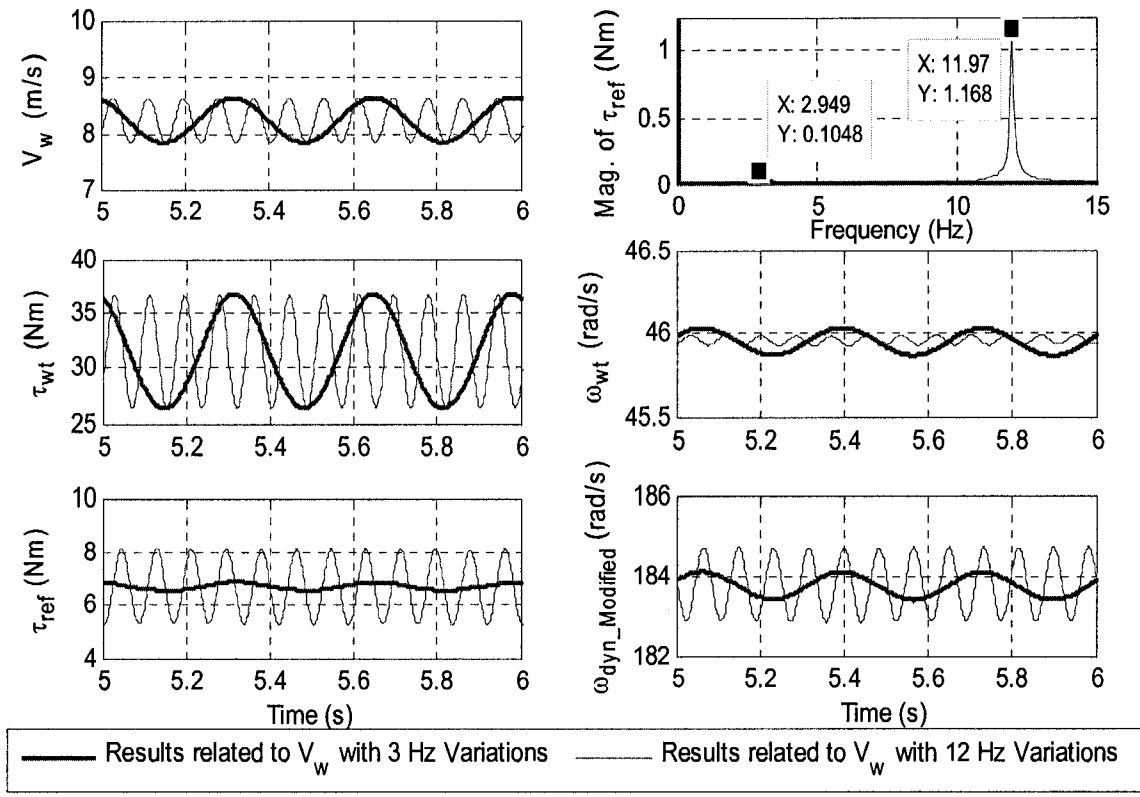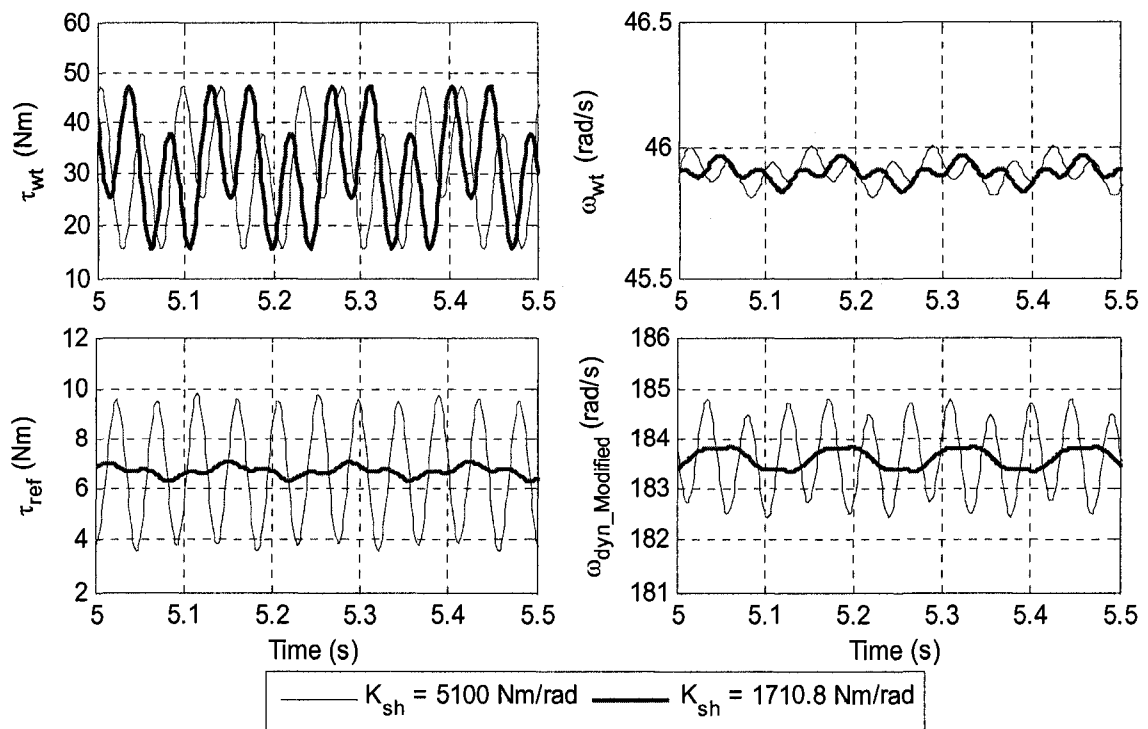
Fig. 3-19 Experimental results for case 3; (a) WTE responses; (b) Zoom of the
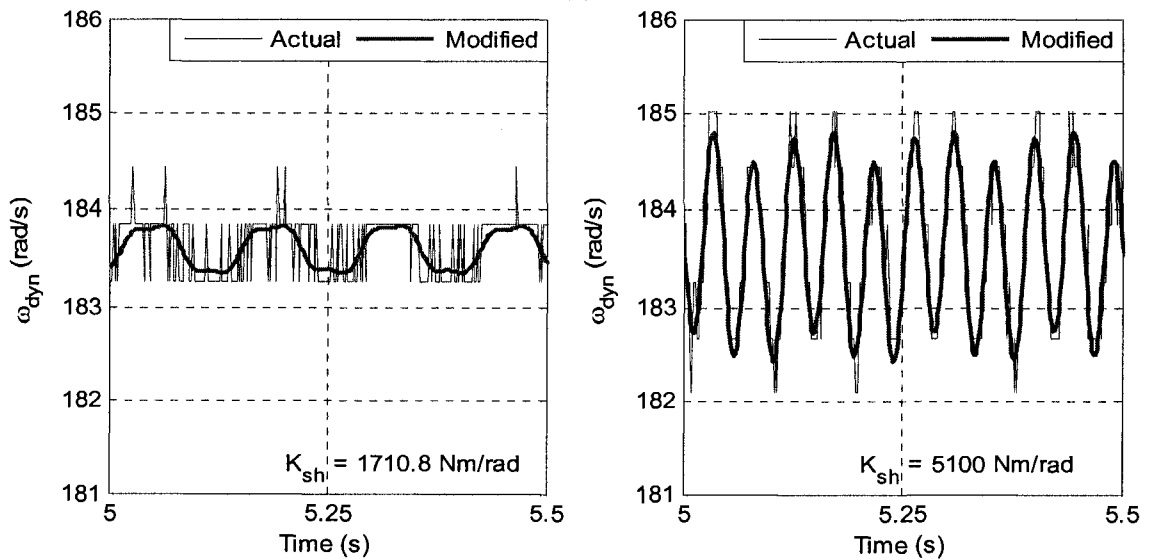
dynamometer speed signals

Case 4) This case shows that how oscillatory torque can excite the natural frequency of the system. The oscillatory torque is in effect. The results for this case are shown in Fig. 3-20 in steady-state. The wind speed is constant at 8.25 m/s. Therefore, the variations on the system responses are due to oscillatory torque only. Two systems with two different shaft torsional spring constants (K_{sh}), 5100 Nm/rad and 1710.8 Nm/rad are considered. It should be noted that according to equation 2-18, the shaft damping constants (B_{sh}) are 1.35 Nm/rad and 0.7837 Nm/rad, respectively.

The results show that the wind turbine and the dynamometer torque and speed responses correspond to the results provided in the case 4 of simulation results in Chapter 2. In Fig. 3-20(b) the zoom of the dynamometer speed signals are presented to indicate that how close the actually modified speed signal and the actual speed signal are. In other words, the reference torque creates the expected variations on the dynamometer speed.

Referring to Fig. 3-20, it can be clearly seen that the variations on the high speed side shaft torque is much larger in the case where K_{sh} is 5100 Nm/rad. The reason is because of the fact that the natural frequencies of the systems, based on equation 2-14, with K_{sh} = 5100 Nm/s and K_{sh} = 1710.8 Nm/s are 20.99 and 12.16 Hz, respectively. On the other hand, the 3rd harmonic of the wind turbine rotor speed is equal to 21.875 Hz. Since, this frequency (3rd harmonic) is much closer to the natural frequency of the system with K_{sh} = 5100 Nm/s, larger variations should be expected for the case where K_{sh} = 5100 Nm/s comparing to the case where K_{sh} = 1710.8 Nm/s.

Fig. 3-20 Experimental results for case 4; (a) WTE responses; (b) Zoom of the

dynamometer speed signals

Case 5) In this case the effect of wind speed step changes on the system responses are investigated. It includes transient as well as steady-state responses. The results for this case are shown in Fig. 3-21. The wind speed is selected at 8.85 m/s. The mechanical load coefficient is $b = 246 \times 10^{-6}$ Nms^2/rad^2. The system responses are provided for the wind turbines with two different masses moment of inertias, 3 and 7 kgm^2. According to equation 2-18, the shaft damping constants equal to 0.7837 and 0.8065 Nms/rad are considered, respectively. Fig. 3-21(a) shows the wind turbine responses, Fig. 3-21(b) shows the dynamometer responses, and Fig. 3-21(c) is the zoom of the reference torque. The results show that the wind turbine and the dynamometer torque and speed responses correspond to the results provided in the case 5 of the simulation results in Chapter 2.

The results show that the transient response for wind turbine with higher mass moment of inertia is slower. Another point is that the wind speed change causes overshoot or undershoot on the wind turbine torque and power responses but the other responses such as wind turbine rotor speed and the generator side responses are under-damped.

The other fact is that every time the wind speed changes, the system's mechanical mode will be excited. This fact is shown in Fig. 3-21(c). The natural frequencies of the system for J_{wt} equal to 3 and 7 kgm^2, according to equation 2-14 are 12.16 and 11.81 Hz, respectively. According to Fig. 3-21(c), the calculated values of natural frequencies for the wind turbines with the masses moment of inertias of 3 and 7 kgm^2 are 12.19 and 11.79 Hz, respectively, which correspond to the theoretical values.
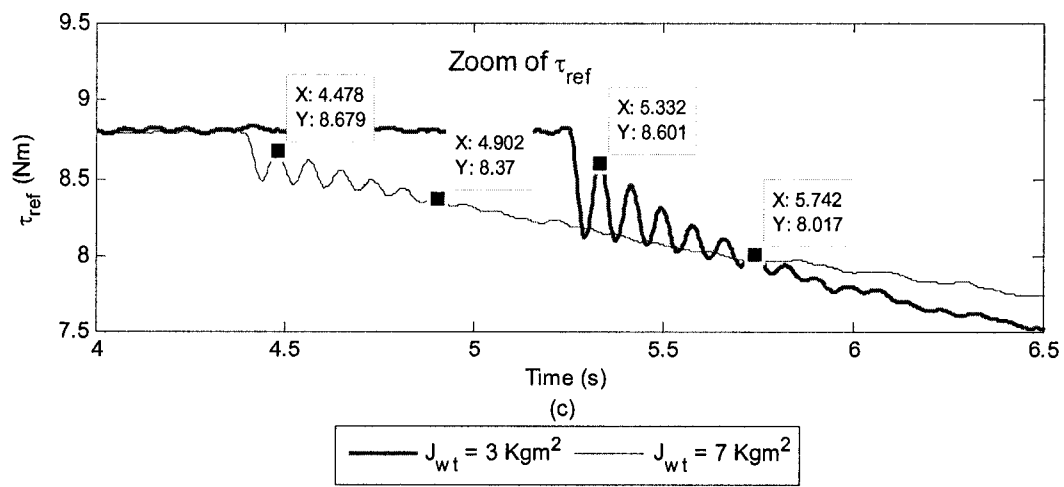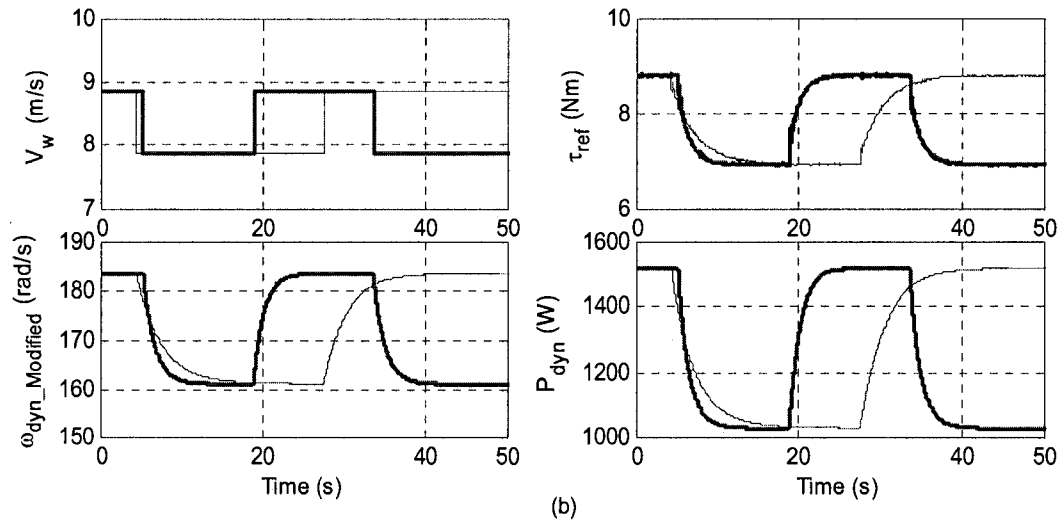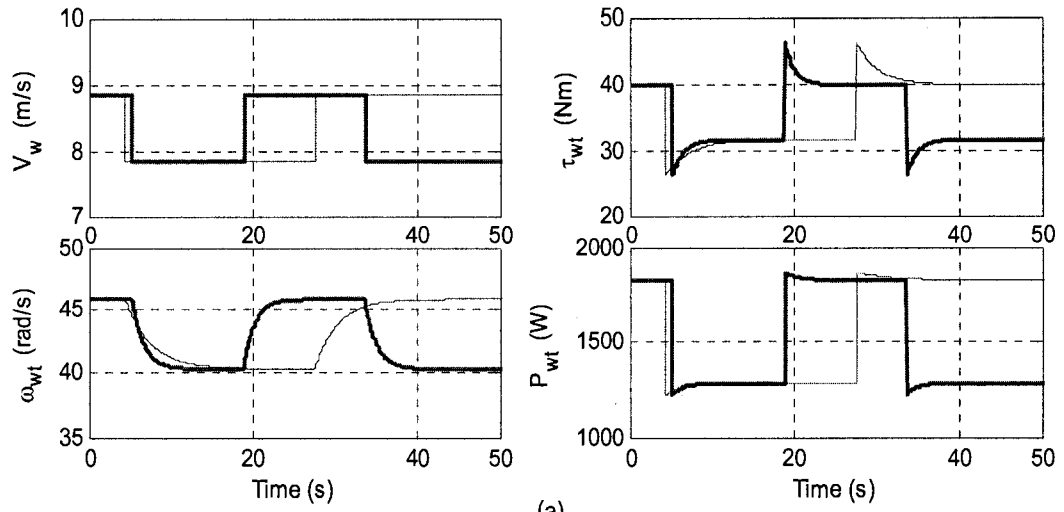
Fig. 3-21 Experimental results for case 5

Case 6) This case is intended to investigate the effect of load step changes on the system responses. It includes transient as well as steady-state responses. The results for this case are shown in Fig. 3-22. The wind speed is selected at 8.5 m/s. The mechanical load coefficient is $b = 220 \times 10^{-6}$ Nms^2/rad^2. The step changes in load are $\pm 40 \times 10^{-6}$ Nms^2/rad^2. Fig. 3-22(a) shows the wind turbine responses, Fig. 3-22(b) shows the dynamometer responses, and Fig. 3-22(c) is the zoom of the reference torque and dynamometer speed signals.

The results show that the wind turbine and the dynamometer torque and speed responses correspond to the results provided in the case 6 of simulation results in Chapter 2. In Fig. 3-22(b) the zoom of the dynamometer speed signals are presented to indicate that how close the actually modified speed signal and the actual speed signal are. In other words, the reference torque creates the expected variations on the dynamometer speed.

The importance of the load change, as it can be seen from the results, is the excitation of the system's mechanical mode. Referring to equation 2-14 the natural frequency of the system is 12.16 Hz. According to the points highlighted in Fig. 3-22(c) the calculated natural frequency is 12.07 Hz which is very close to calculated theoretical value. The other point is that the responses on the wind turbine side are all under-damped. But, the load change causes overshoot or undershoot on the dynamometer torque and power responses.
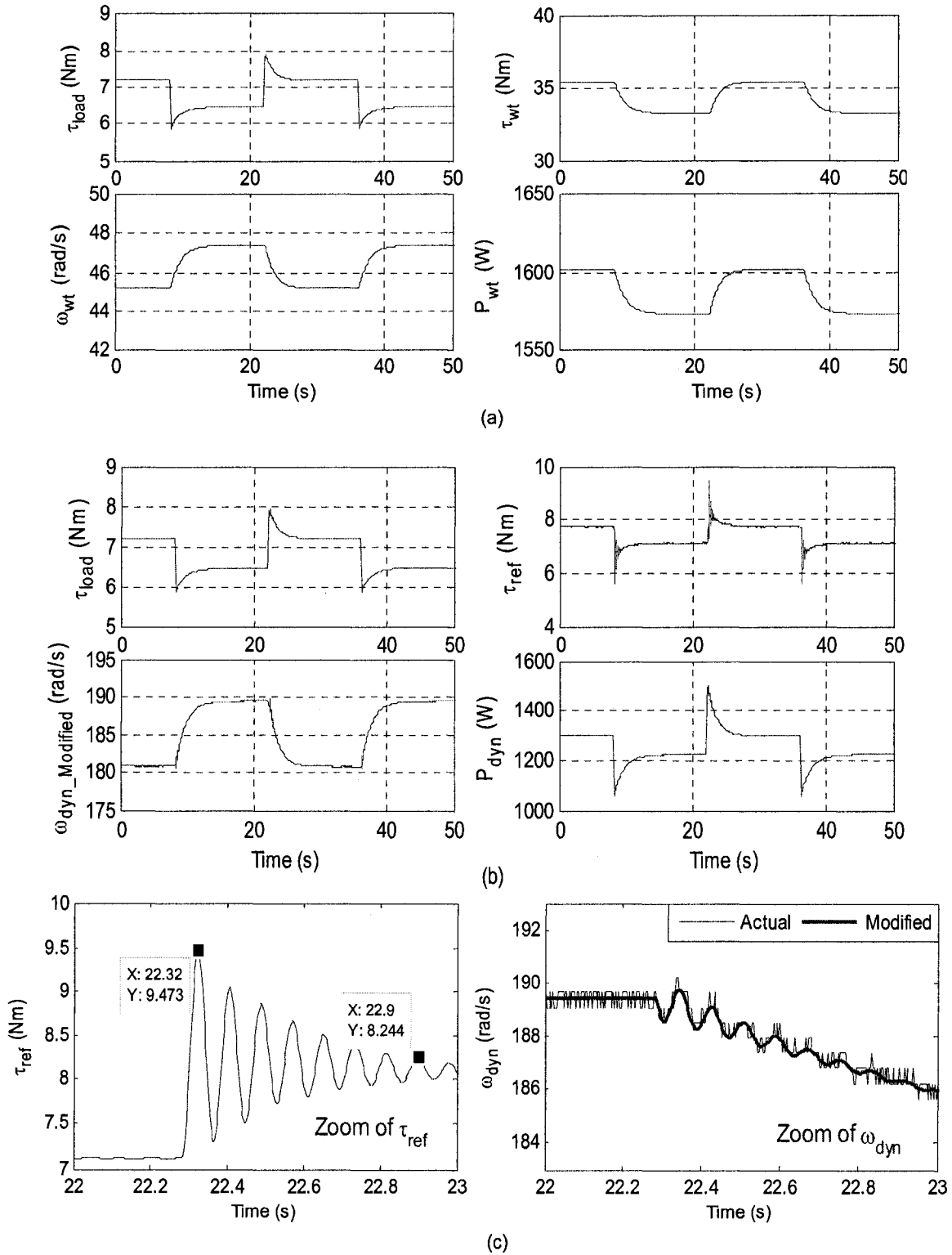
Fig. 3-22 Experimental results for case 6

3.7 CONCLUSIONS

The focus of this chapter was on the implementation of a 2-hp WTE. The logic of the WTE was introduced in Fig. 3-9. A 2-hp PMDC machine was used as prime mover. It produces the torque equal to the reference torque on its shaft by using a switch-mode DC-DC power converter and a hysteresis current controller. Another 2-hp PMDC machine was used to operate as a dynamometer which acts as a mechanical load. It is supplied by a switch-mode DC-DC power converter and a hysteresis current controller. This provided the opportunity to make the WTE to run at different operating points to perform different tests without requiring an electric generator and electrical load.

The experimental set-up was presented. The system parameters were calculated and their effects on system limitations were discussed. Two methods (method-A and method-B) of using the measured dynamometer speed signals were discussed, but the results were shown for implementation with method-B only.

The main features of the designed and implemented WTE are:

➢ Capable of emulating the wind turbines with different mass moment of inertias, drive train with flexible shaft with different torsional spring constants, and damping constants, and ideal gear box with different gear ratios.

➢ Capable of emulating the oscillatory torque.

➢ Provides the capability of experimentally verifying the facts highlighted in the conclusion of Chapter 2 as simulation results.

CHAPTER 4

AN APPLICATION OF THE WTE

4.1 INTRODUCTION

A WTE with a dynamometer as variable mechanical load was implemented in

Chapter 3. Since the goal of designing a WTE is to provide a controllable environment to

test different topologies of WECS, the dynamometer is replaced by a self-excited

induction generator. In this case it is possible to investigate the impact of the wind speed

variations, load variations, and wind turbine parameters on the generated electric power.
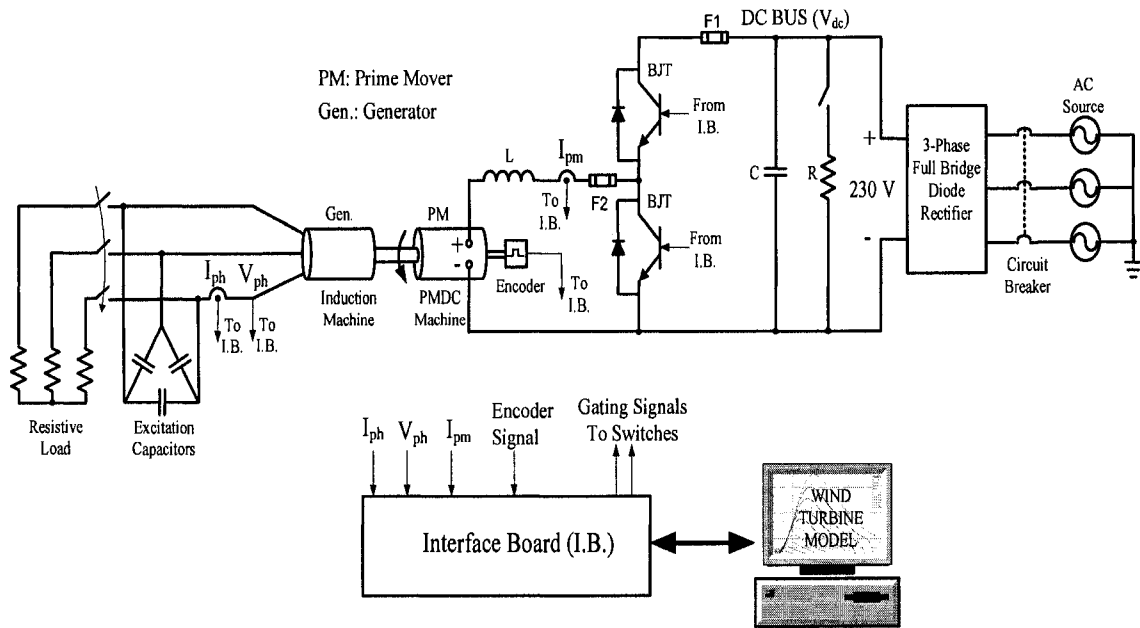
Fig. 4-1 Unregulated electric power generation using WTE.

It also provides the opportunity to investigate the effect of oscillatory torque and

excitation of the drive train natural frequencies on the generated electric power. Fig. 4-1

shows the implemented experimental set-up. It should be noted that the magnitude and

frequency of the output voltage of the generator can vary with load and wind speed variations; therefore this figure represents an unregulated WECS.

In many applications the generator voltage must be regulated. This means that the magnitude and frequency of the generated voltage must be kept within an acceptable defined range. For these reasons, different configurations of the generator and power electronics converters with different control strategies are currently used in the WECS industry.
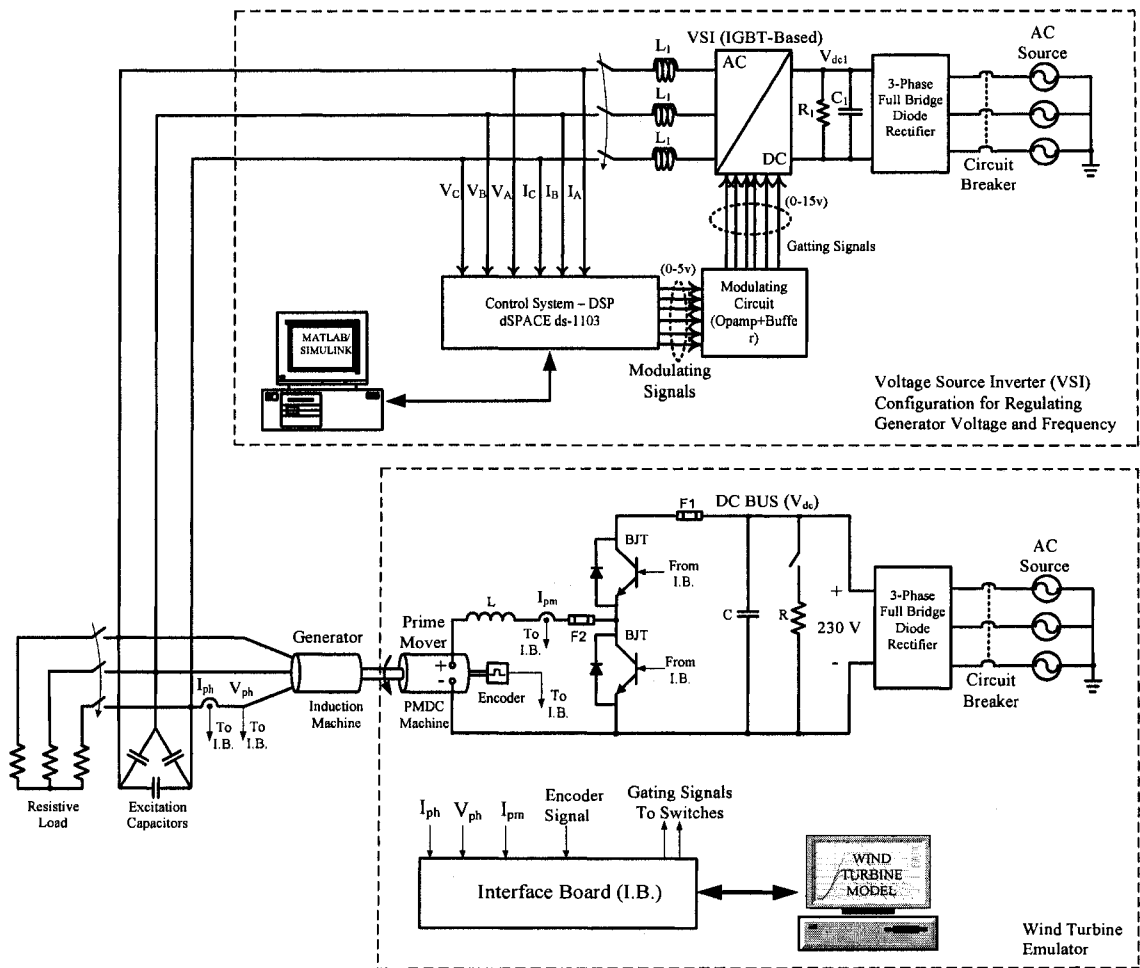
Fig. 4-2 Regulated electric power generation (Stand-Alone) using WTE

The implemented WTE is also used as prime mover to run a 2-hp self-excited induction generator in which its output power is controlled by a Voltage Source Inverter (VSI). It represents a stand-alone regulated WECS. This topology is shown in Fig. 4-2. The top part (VSI) was designed and implemented in [30]. The VSI is controlled in such a way that it produces different amounts of power in order to maintain the generator speed at its nominal value while wind speed and electrical load vary.

Section 4.2 provides some basic information about the induction generator and its model. Section 4.3 describes the experimental set-up of the implemented WTE which runs the induction generator in two cases; an unregulated WECS and a stand-alone regulated WECS. The experimental results are presented in Section 4.4 and Section 4.5 summarizes this Chapter and presents the conclusions.

4.2 INDUCTION GENERATOR MODEL, PARAMETERS, AND CHARACTERISTICS [30, 31]

To operate an induction machine as generator with rated voltage and frequency, it must be run slightly over the synchronous speed. It needs reactive power which provides the generator magnetization current [31]. In the case where it is connected to the grid, it draws reactive power from the grid. In stand-alone applications, the reactive power must be provided by a capacitor bank and/or by an inverter. A simplified, steady state, and per-phase model of the induction generator as presented in [31] is shown in Fig. 4-3. In the model, subscripts s and r correspond to stator and rotor parameters, respectively. Subscript m corresponds to magnetization current and magnetization reactance. V_t and V_g

correspond to terminal and air gap voltages, respectively. The relationships between the model parameters and quantities are discussed in detail in [31]. Some of those which are used in implementing the WTE are presented below:

$$n_s = 120\,f_s/p \qquad ; \qquad s = (n_s - n_r)/n_s \qquad ; \qquad P_{r\text{-}loss} = 3I_r^2 R_r$$

$$P_r = 3I_r^2 R_r(1-s)/s \qquad ; \qquad P_{s\text{-}loss} = 3I_s^2 R_s \qquad\qquad\qquad (4\text{-}1)$$

where n_s is the synchronous speed in RPM, n_r is the rotor speed in RPM, f_s is the nominal frequency in Hz, s is the slip, P_r is the generator's rotor mechanical power in W, $P_{s\text{-}loss}$ is the generator's stator copper loss in W, $P_{r\text{-}loss}$ is the generator's rotor copper loss in W, R_s is the generator's stator winding resistance in Ω, and R_r is the generator's rotor winding resistance in Ω.
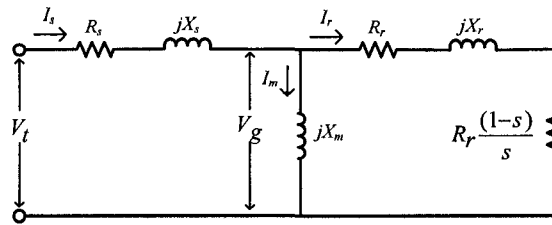
Fig. 4-3 Simplified model of an induction machine [31]

Table 4-1 Parameters of the induction machine [30]

Baldor Induction Machine Rating and Parameters			
Nameplate		Measured in the Laboratory	
Power (hp)	2	R_s (Ω)	1.33
Ph. Voltage (V)	208	R_r (Ω)	0.891
Ph. Current (A)	6.1	X_s (Ω)	1.44
Speed (RPM)	1725	X_r (Ω)	1.44
Frequency (Hz)	60	X_m (Ω)	37.9

The induction generator parameters were calculated and provided in [30]. They are presented in Table 4-1.

Fig. 4-4 shows two important characteristics of the self excited induction generator. They are frequency and air-gap line voltage versus generator speed curves. These curves are obtained with delta connected excitation capacitors, 25.66 μF each, shown in Fig. 4-1 and Fig. 4-2, which are calculated for the case where the generator supplies a half-rated load [30]. The procedures for obtaining these curves are described in detail in [30] and the results are just shown in Fig. 4-4. It is obvious from the curves that the variations on frequency and voltage of the generated electricity due to speed variation of the generator are high. On the other hand, regulating the generator voltage and frequency, especially in WECSs, are necessary for supplying many types of electrical loads. It should be noted that the relation between frequency and generator speed will be used for the load power measurement as discussed in Section 4.3.
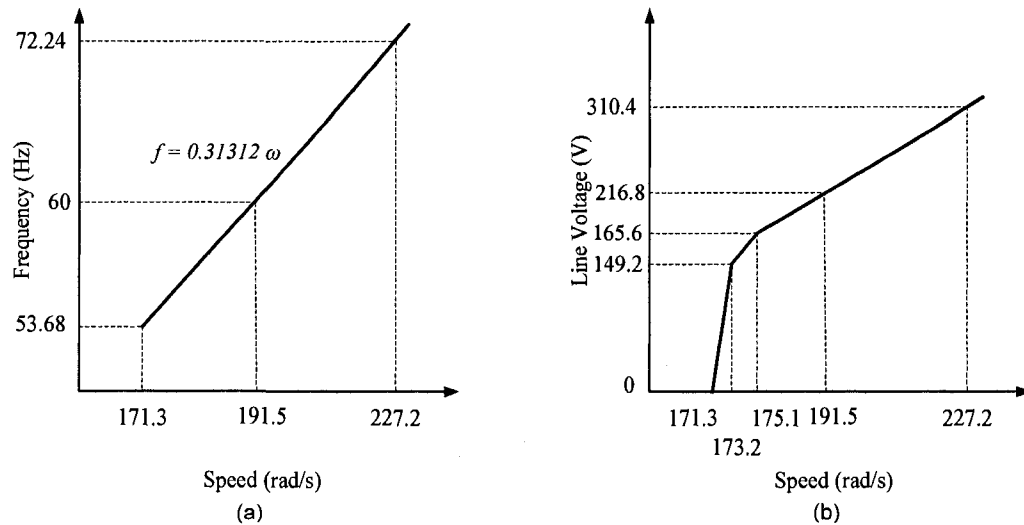

Fig. 4-4 Induction machine characteristics; (a) Frequency versus speed characteristic; (b) Air-gap line voltage versus speed characteristic [30]

4.3 EXPERIMENTAL SET-UP

All the discussions in the following subsections apply to both experimental set-ups, unregulated and regulated WECSs, shown in Fig. 4-1 and Fig. 4-2, respectively. The system parameters, design methods, and implementation of the VSI configuration are discussed in [30]. For this reason, in this section only the parts related to WTE are described.

4.3.1 WTE PARAMETERS SELECTION

The values of R and C are equal to 3.3 kΩ and 21,600 μF, respectively. These are the same as those mentioned in Chapter 3. However, the value of L (the inductor in series with the prime mover) differs from the value which has been selected in Chapter 3. The reason is related to the sampling time of MATLAB/Simulink Model. Because of the power measurement block which is added to the model, which contains time delay blocks, the processing time of the DSP system increases. The minimum sampling time that let the model to be converted for real time application was 70 μs.

By using the same method described in Chapter 3 and based on this new sampling time, the value of L is selected to be equal to 48 mH. The total inductance is $L_t = L + L_a$ where L is the inductor in series with the DC machine and L_a is the armature inductance of the DC machine. Therefore, the total inductance is $L_t = 55$ mH. The method discussed in Chapter 3 for calculating the rate of rise and fall the torque which the DC machine will be able to emulate can be applied to this Section. The DC bus voltage is selected as 230 V as mentioned in Chapter 3. Thus, for full load operation and rated generator speed the

prime mover will be able to follow the rate of rise of up to about 444 Nm/s and rate of fall of up to about 3900 Nm/s.

Any time the wind speed or load suddenly changes, it causes a change on the reference torque. Recall that this is the torque applied to the generator. The changes appear in the form of damped sinusoidal (due to the excitation of the mechanical mode) response until it reaches the steady-state condition. Therefore, a sudden or step change in wind speed or load does not cause an instantaneous change on the reference torque. This was verified by simulation results (Chapter 2) and experimental results (Chapter 3). Having this in mind, the reference torque variations will be due to this fact plus the variations due to 1st and 3rd harmonics of oscillatory torque. The worst case for having the highest rate of rise on the reference torque is that the maximum rate of rise for the 1st and 3rd harmonics and the reference torque excitation occur simultaneously. The following reference torque variation is considered:

$$\tau_{ref\_variation} = C_1 \sin(2 \times 7.6 \pi t) + C_2 \sin(2 \times 22.8 \pi t) + C_3 \sin(2 \times 14.1 \pi t) \qquad (4\text{-}2)$$

Where 7.6, 22.8, and 14.1 are the frequencies of the 1st harmonic, 3rd harmonic, and the system's natural frequency for $J_{wt} = 1$ kgm^2, respectively. Assuming that $C_1 = 0.37$ Nm and $C_2 = 0.35$ Nm which are the values shown in case 1 of the experimental results for $J_{wt} = 1$ kgm^2.

By differentiating equation 4-2, the maximum value will be reached when the cosines are set equal to one. By doing this and equating equation 4-2 to 444 Nm/s calculated before, C_3 can be obtained equal to 4.25 Nm. This means that the WTE with the selected parameters can emulate the variations on the wind speed and load which cause excitation of the reference torque with the amplitude of up to 4.25 Nm. In the

calculations, it was considered that the generator operates at full load. If the generator supplies lower load, the rate of rise of torque will be increased (due to less voltage drop across DC motor armature resistance). It is worth saying that the prime mover full load average torque is about 8.8 Nm.

The other fact which limits the reduction of the tolerance band limit is the amount of current reduction in one simulation time step (70 μs) and dead time of 4 μs as discussed in Chapter 3. This happens when the lower switch in Fig. 4-1 is on. Considering that the prime mover is running at 1800 RPM and at full load condition (8.5 A), referring to Fig. 3-11(b) and the equation: $\Delta V = L_t \Delta i_a / \Delta t_{sampling}$, the current reduction can be calculated: $\Delta i_a = 206.5 \times 74 \times 10^{-6}/(55 \times 10^{-3}) = 0.28$ A. For the same reason discussed in Chapter 3 the tolerance band limit has to be greater than 0.28 A which is thus selected equal to 0.35 A.

4.3.2 MATLAB/SIMULINK MODEL

The MATLAB/Simulink model used in the implementation of the experimental set-up is shown in Fig. 4-5. It mainly consists of the wind turbine model, the prime mover hysteresis current controller, the prime mover measured current, the generator speed signal, the generator measured phase voltage and current, and the power measurement block. The hysteresis current controller creates the gating signals for the prime mover power circuit upper switch. By using external electronic circuits, gating signals with appropriate power levels are created for both switches as discussed in Chapter 3. The model is prepared to be able to operate with directly using of generator speed signal

(method-A) or using modified generator speed signal (method-B). These methods are introduced and discussed in Chapter 3.

It should be noted that the generator phase voltage and current are used for power measurement only in the case when method-A is applied. But, when method-B is applied they are used for estimating the generator torque by using the equation $\tau = P/\omega$ as well as power measurement. The estimated torque will be used for estimating the variations of the generator speed as shown in the bottom-right part of Fig. 4-5. The estimated generator speed variations is added to the filtered actual generator speed signal (average of speed signal) and fed back to the wind turbine model as shown in the top-left (marked method-B) of Fig. 4-5. The power measurement block is explained in Section 4.3.2.
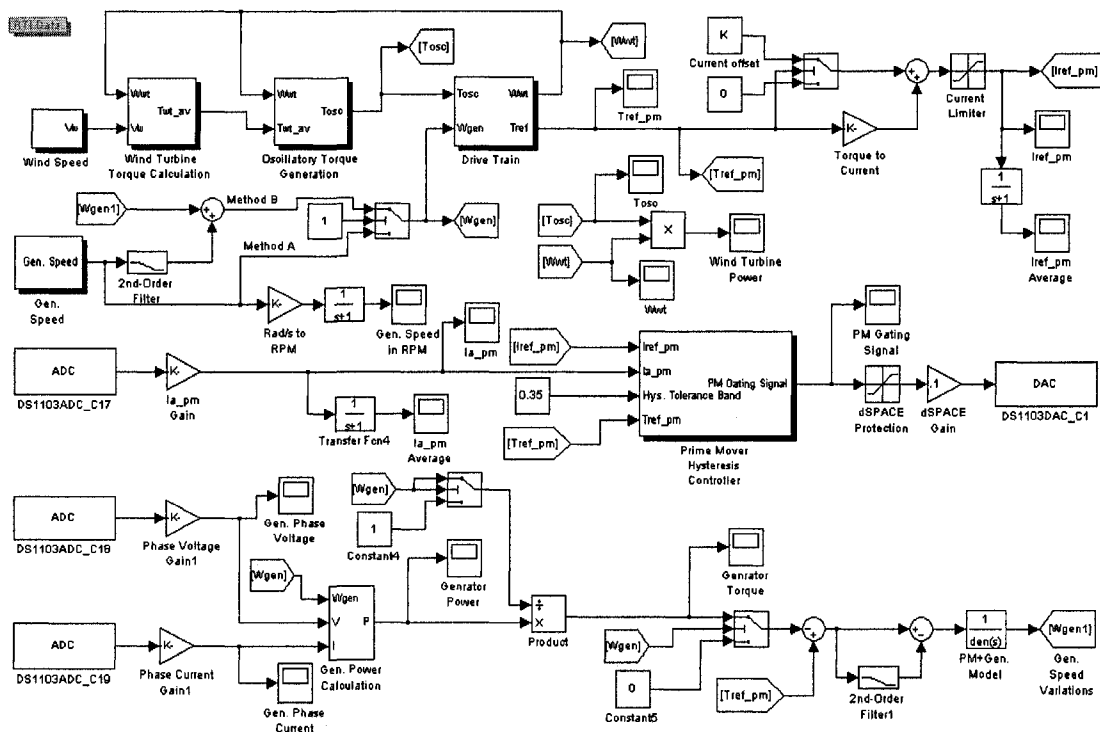

Fig. 4-5 MATLAB/Simulink model for implementation of the experimental set-up

With regard to calculating the total mass moment of inertia of the DC motor and

induction generator (J_{pm+gen}) and total friction coefficient of the DC motor and induction

generator, referring to the method discussed in Chapter 3, they were estimated 0.0185

kgm^2 and 0.00245 Nms/rad, respectively. The implementation of the WTE also provides

an opportunity to estimate the total mass moment of inertia of the prime mover (DC

motor) and the generator. After several tests, by varying the values of K_{sh} and J_{wt},

resonance frequencies of the reference torque have been measured using FFT analysis of

the reference torque. Then, according to equation 2-14, corresponding J_{pm+gen} were

calculated in each case. The average value of the measured J_{pm+gen} was calculated as

0.0174 kgm^2. The error of the average value is less than 1% for all cases. The estimated

values which are 0.0185 and 0.0174 kgm^2 have an error of about 6% with respect to each

other. Therefore, in Fig. 4-5 the "PM+Gen. Model" block is set equal to

1/(0.0174s+0.00245), where 0.0174 kgm^2 and 0.00245 Nms/rad are the estimated values

for the total mass moment of inertia and the total friction coefficient of the DC machine

and the induction machine, respectively.

4.3.3 POWER MEASUREMENT BLOCK

The power measurement block which is available in the MATLAB/Simulink

power systems library (version 5.3 of MATLAB) measures the power associated with the

input current and voltage to the block for the specific frequency. That frequency, for

instance 60 Hz, must be set in the block. Because the generator speed might vary

(unregulated operation) the frequency of the generator voltage changes in different

conditions. For this reason the power measurement block is slightly modified by using

the "look under mask" option provided in MATLAB/Simulink. In that block, the transport delay is replaced by "variable transport delay" block which is shown in Fig. 4-6. To calculate the period of the generated voltage which is the bottom input of the "variable transport delay" block the relationship between frequency and speed of the generator as shown in Fig. 4-4 (a), which is $f = 0.31312 \, \omega_{gen}$ was used.

The stator copper loss of the generator is added to the electrical load power. In this case the measured power is the sum of the electrical load power and the stator copper loss. This provides closer estimation of the total torque of the generator which is the load torque plus generator losses except the friction loss. Recall that friction loss is considered as part of the generator and prime mover model.
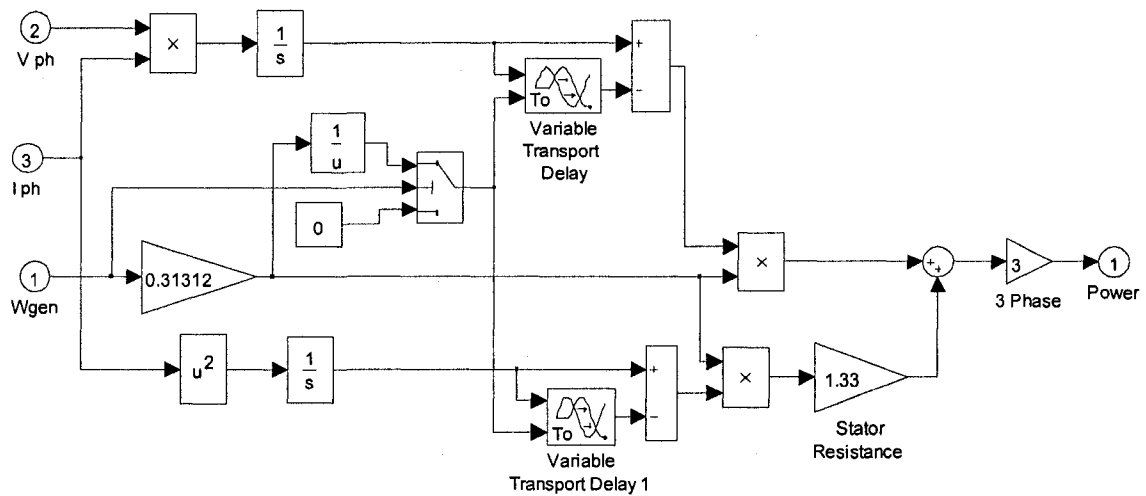

Fig. 4-6 Modified MATLAB/Simulink (version 5.3) power measurement block

4.4 EXPERIMENTAL RESULTS

The experimental results are presented in two major categories: Unregulated WECS and regulated WECS. Different cases are considered for each category and for

each case two methods of using generator speed signals introduced as method-A and method-B are provided. Since in the WECSs, from the electrical point of view, the main concern is about the generator torque and speed, and also to avoid lengthening the Thesis, the results related to internal quantities of the wind turbine are not presented in this Chapter.

It is worth emphasizing that method-A relates to directly using generator speed signal and method-B relates to using modified generator speed signal as described in Chapter 3. The reference torque in all results represents the torque produced on the prime mover shaft. The WTE parameters are the same as values provided in Table 4-2, unless otherwise stated.

Table 4-2 Parameters used for experimental results

Wind Turbine, Prime Mover, Generator, and Electrical Load Parameters			
Wind Turbine		Prime Mover + Generator and Electrical Resistive Load	
J_{wt} (kgm^2)	3	J_{pm+gen} (kgm^2)	0.0174
B_{wt} (Nms/rad)	0.1	B_{pm+gen} (Nms/rad)	0.00245
K_{sh} (Nm/rad)	1710.8	R_{ph} (Ω)	63
B_{sh} (Nms/rad)	0.7307		
n	4		

4.4.1 UNREGULATED WECS

The results in this Section are related to the unregulated WECS shown in Fig. 4-1. In this case, it is possible to investigate the effects of system parameters, wind speed variations, and load variations on the generated electricity, without any additional circuitry such as power electronic devices which enforces the generator to produce

electricity with constant voltage and frequency. Six different cases (steady-state and transient responses) are discussed in this section.

Case 1) In this case the effect of the wind turbine mass moment of inertia on suppressing the variations due to the oscillatory torque is investigated. The results for this case are shown in Fig. 4-7 and Fig. 4-8 for method-A and method-B, respectively. The system is tested for two values of J_{wt} equal to 1 and 10 kgm^2. According to equation 2-18, the values of B_{sh} related to each J_{wt} are calculated and set to 0.6756 and 0.7534 Nms/rad, respectively. The results are shown in the steady-state condition. The wind speed is kept constant at 7.87 m/s at which the generator generates 120 V, rated phase voltage, at half-rated load. Therefore, the variations on the reference torque should be due to the oscillatory torque (1st and 3rd harmonics) only.

With regard to the results related to method-B, the generator speed (ω_{gen_Actual}), represents the speed signal which is measured directly without any filtering. The generator speed ($\omega_{gen\_Modified}$), represents the speed signal with its variations estimated by the model of the prime mover and generator and its average is the average of the measured speed signal as discussed in Chapter 3.

The generator speed is about 190 rad/s. By dividing the generator speed by the gear ratio the wind turbine rotor speed is 47.5 rad/s and the rotating frequency is equal to 7.56 Hz. Therefore, the frequency of 1st harmonic of the oscillatory torque is 7.56 Hz and the frequency of its 3rd harmonic is 22.68 Hz. The frequency spectra of the reference torque and generator speed are shown in Fig. 4-7(b) and (c) and Fig. 4-8(b), (c), and (d). Referring to Fig. 4-7(b) and (c), the components of the oscillatory torque are at 7.628 and

22.76 Hz. Referring to Fig. 4-8(b), (c), and (d) these frequencies are 7.503 and 22.63 Hz.

In both cases the frequencies are close to theoretical values with less than 1% error.
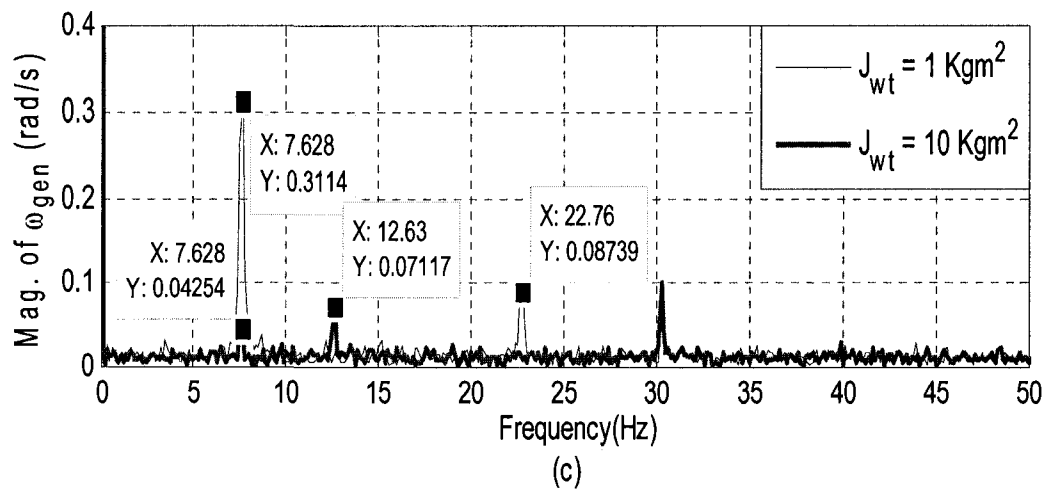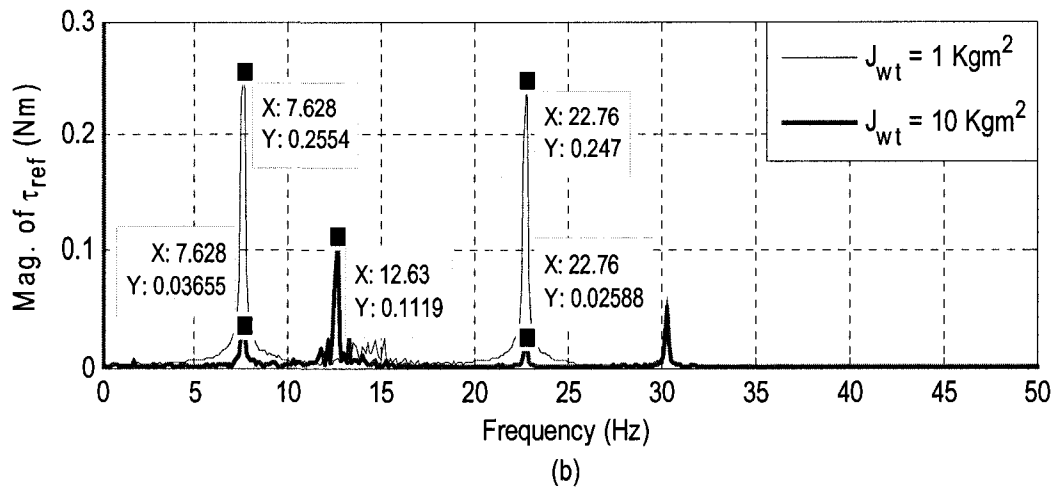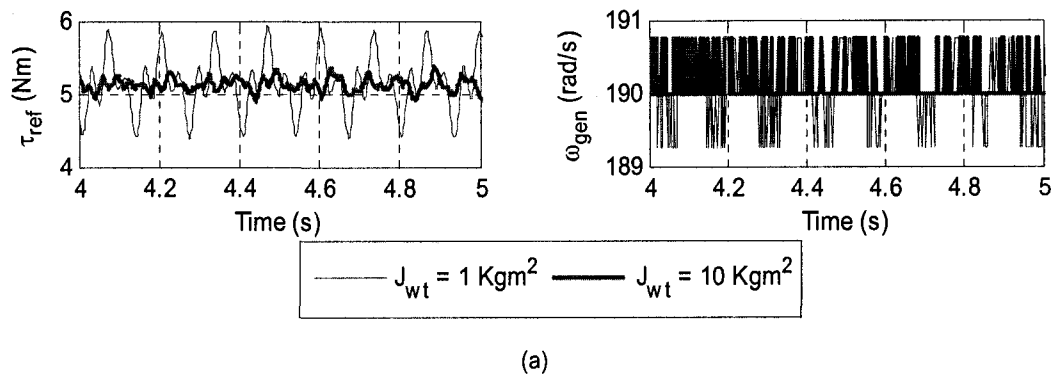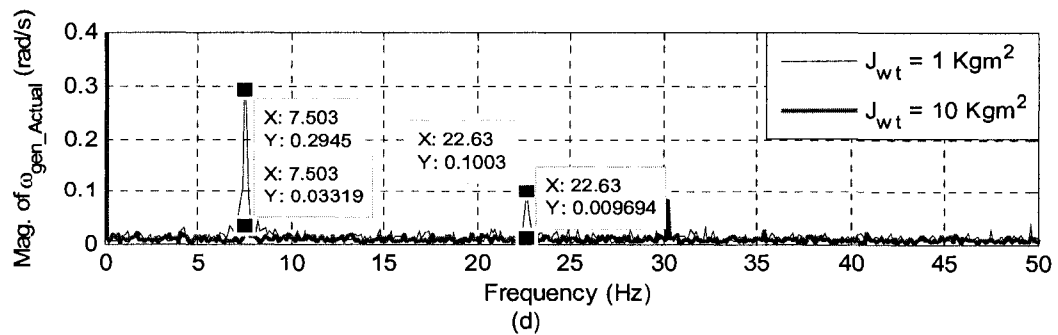

(a)

(b)

(c)

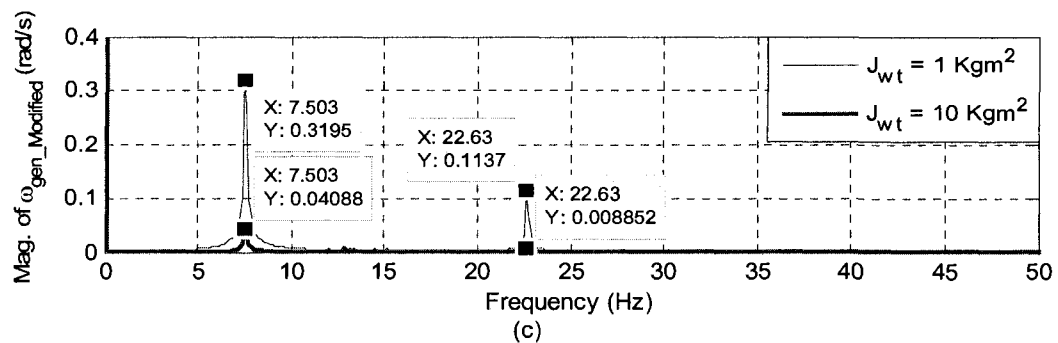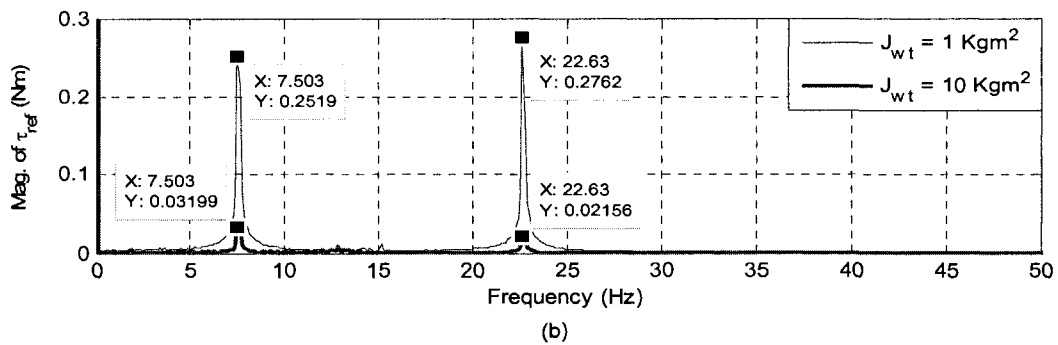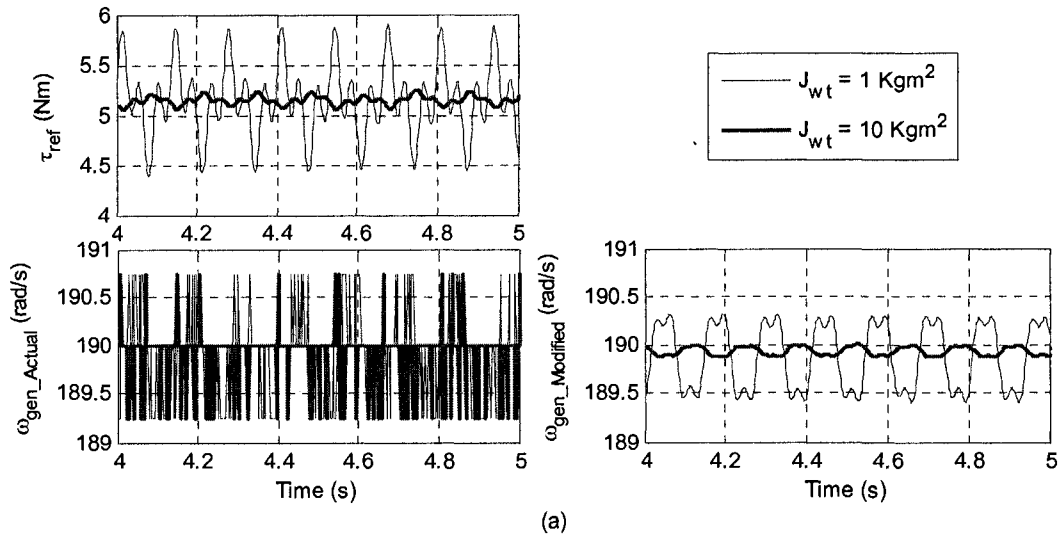Fig. 4-7 Unregulated WECS experimental results for case 1 by method-A

Fig. 4-8 Unregulated WECS experimental results for case 1 by method-B

There are some discrepancies between the magnitudes of the oscillatory torque components of method-A and method-B which are mainly due to generator speed signals which normally present non-zero values for all frequencies, for instance, about 0.02 rad/s as it can be seen on the generator speed frequency spectrum. This causes an error of 10% in some cases, since the values of variations on the generator speed are relatively very small and the values of noise or disturbance are to them. Thus, they contribute in creating the components of the reference torque which causes an error between the two methods.

According to equation 2-14, the system natural frequencies for J_{wt} equal to 1 and 10 kgm^2 are 14.1 and 12.65 Hz, respectively. Now, by referring to Fig. 4-7, additional components on the reference torque can be observed for both wind turbines with J_{wt} equal to 1 and 10 kgm^2. The frequencies of these components are close to the systems' natural frequencies. This usually happens because the generator speed signal presents non-zero values for the frequencies around the system's natural frequency which creates additional component on the reference torque.

These frequencies are highly attenuated by applying method-B as it can be seen in the frequency spectra of reference torque and the generator modified speed in Fig. 4-8. The reason is that the actually modified generator speed signal has been fed back to the model of the wind turbine which presents a more ideal speed signal than the actual measured generator speed signal.

Case 2) In this case the effect of the wind turbine with masses moment of inertias equal to 1 and 10 kgm^2 on suppressing the system responses variations due to the wind speed variations are investigated. The results for this case are shown in Fig. 4-9 (by

applying method-A) and Fig. 4-10 (by applying method-B). The wind speed profile for this case is $Vw = 7.87 + 0.2\ sin2\pi t + 0.2\ sin6\pi t + 0.2\ sin20\pi t$ m/s. It should be noted that the wind speed profile for wind turbines with J_{wt} equal to 1 and 10 kgm^2 are not in phase since the results for two cases are captured at different time. The results are taken in steady-state. The oscillatory torque components are set to zero, thus the variations on the system responses are due to wind speed harmonics only. The results show that the effect of variations on the reference torque and the generator speed are less for the case where the wind turbine has higher mass moment of inertia.

The relation between the generator speed, input (reference) torque, and generator torque (load torque plus the torque due to the generator losses) for the prime mover and the generator as one mass can be calculated (in frequency domain) by the well-known equation 4-3.

$$\Omega(j2\pi f) = \frac{T_{ref}(j2\pi f) - T_{gen}(j2\pi f)}{j2\pi f J_T + B_T} \qquad (4\text{-}3)$$

Where Ω is the generator speed in rad/s, T_{ref} is the applied torque to the generator in Nm, T_{gen} is the load torque plus the torque due to the generator losses in Nm, j is the complex number equal to $\sqrt{-1}$, f is the frequency of the applied torque in Hz, J_T and B_T are the sum of masses moment of inertias in kgm^2 and sum of friction constants in Nms/rad of the prime mover and the generator which are equal to 0.0174 and 0.00245, respectively. Thus, the magnitudes of the generator torques and speed ignoring the effect of B_T, which has high effect for the frequency range very close to zero, can be related as:

$$|\Omega(j2\pi f)| \approx \frac{|T_{ref}(j2\pi f) - T_{gen}(j2\pi f)|}{2\pi f J_T} \qquad (4\text{-}4)$$

Now, referring to Fig. 4-9(b) and (c) and Fig. 4-10(b), (c), and (d), by applying equation 4-4 it is possible to investigate whether the generator torque and speed responses do correspond to each other. In other words, it shows whether the prime mover current creates the expected variations on the generator speed. It should be noted that the frequency spectra presented in Fig. 4-9(b) and Fig. 4-10(b) represent the numerator of equation 4-4 ($| T_{ref} - T_{gen} |$). Referring to Fig. 4-9(b), for the case where J_{wt} is 1 kgm^2, the magnitudes of the generator speed harmonics for 1, 3, and 10 Hz are calculated (according to equation 4-4) as 1.2, 0.41, and 0.23 rad/s, respectively. The related values can be read from Fig. 4-9(c) which are 1.158, 0.3912, and 0.2233 rad/s. Referring to Fig. 4-10(b), for the case where J_{wt} is 1 kgm^2, the magnitudes of the generator speed harmonics for 1, 3, and 10 Hz are calculated as 1.21, 0.41, and 0.22 rad/s, The related values can be read from Fig. 4-9(d) which are 1.133, 0.396, and 0.2145 rad/s, respectively.

By comparing the calculated values and experimental results for generator speed signals, it shows a 6% error for the worst case. The errors are mainly because of the noise or disturbance on the generator speed signal and also the accuracy of the measuring devices. The additional reasons which cause error for method-B can be considered due to the estimated values of generator torque, the total prime mover and the generator mass moment of inertia and friction damping constant.

As far as the comparison between results of method-A and method-B are concerned, the worst case correspond to magnitudes of $\tau_{ref} - \tau_{gen}$ at 10 Hz in Fig. 4-9(b) and Fig.4-10(b) that have 0.018 Nm difference which is about 7% error. It should be noted that all mentioned percentage errors in this discussion are applicable just to the
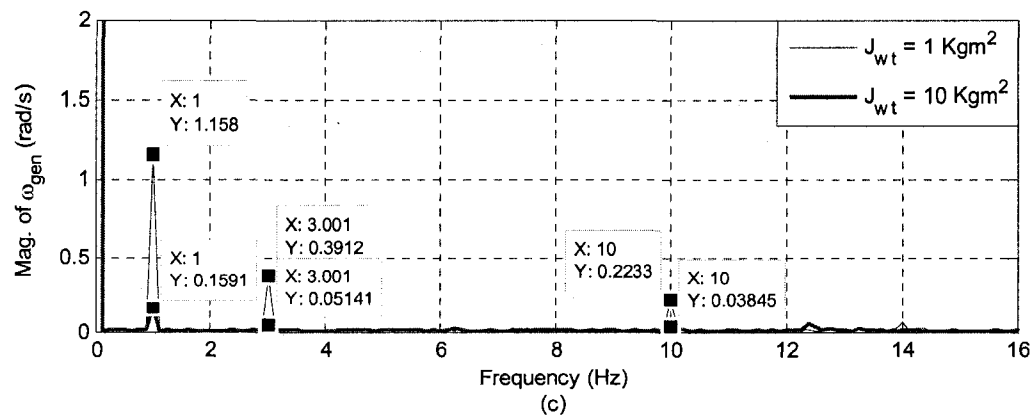
expected and measured variations on the torques and the generator speeds and not the averages (DC values) of torques and generator speeds.
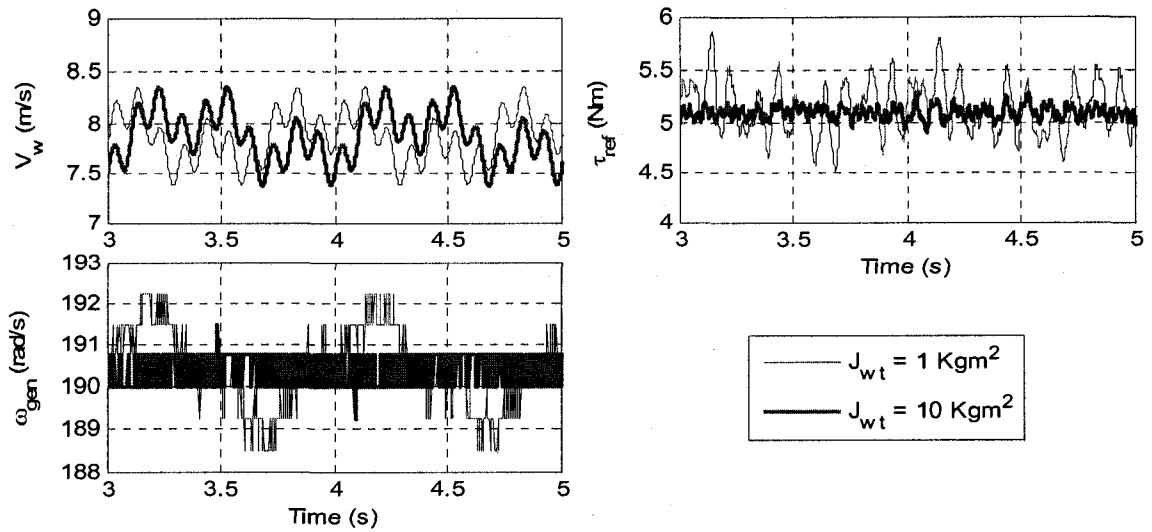
(a)
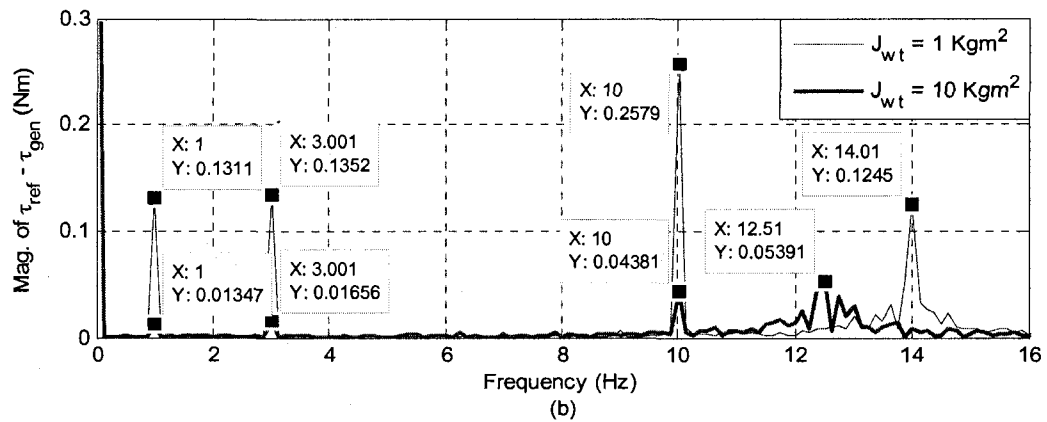
(b)

(c)

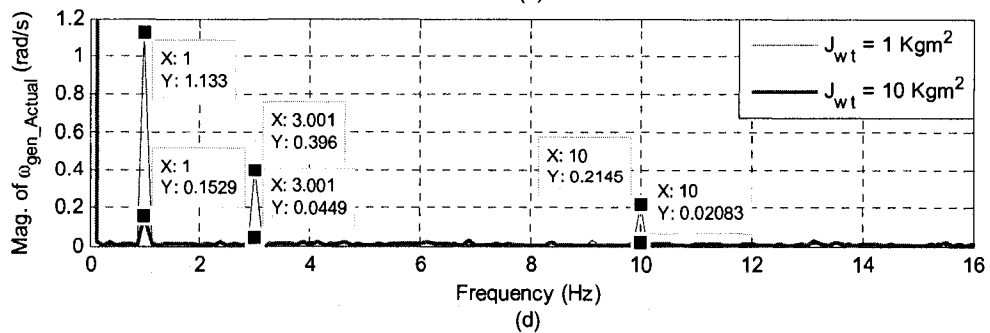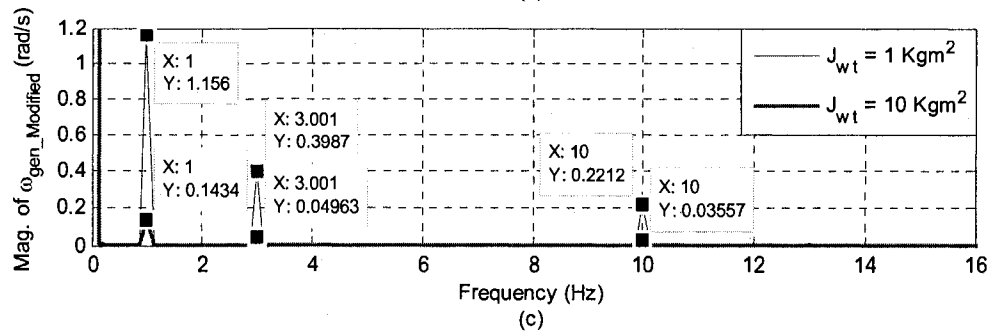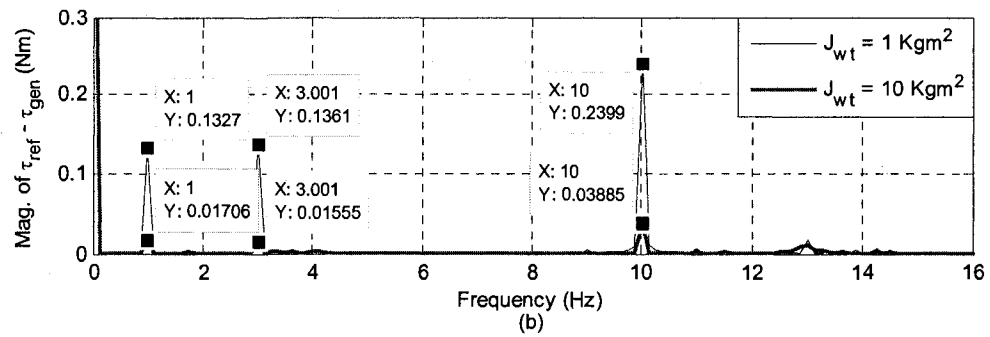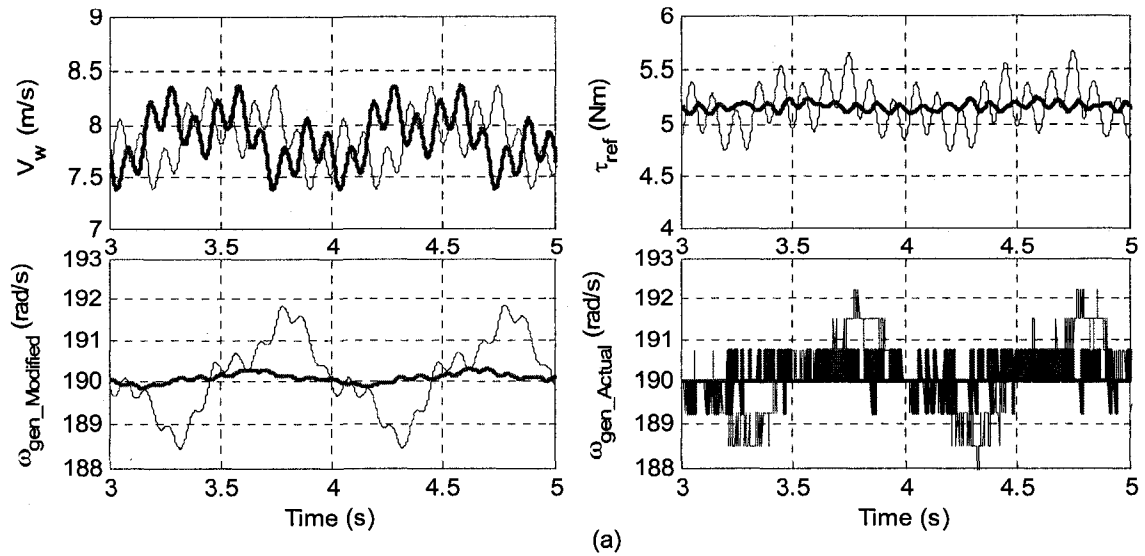Fig. 4-9 Unregulated WECS experimental results for case 2 by method-A

Fig. 4-10 Unregulated WECS experimental results for case 2 by method-B

Case 3) In this case the excitation of the system's natural frequency is investigated. The results for this case are shown in Fig. 4-11(a) and (b) (by applying method-A) and Fig. 4-11(c) (by applying method-B). The wind speed profile for these tests is $Vw = 7.87 + 0.4 \sin 26\pi t$ m/s. The natural frequency of the system is 13.04 Hz. The results in both figures are captured in steady-state condition except for Fig. 4-11(a) which is explained below. First, comparison between the two methods is discussed.

In Fig. 4-11(a) the implementation with method-A is shown. The shaft damping constant (B_{sh}), as given in Table 4-2, is set equal to 0.7307 Nms/rad. At the time when the 13 Hz harmonic is added to the wind speed, the reference torque started to grow unbounded, for this reason the 13 Hz component from the wind speed has been set to zero which caused a reduction in the reference torque to its steady-state value as shown in the figure. The same test by method-B was done as shown in Fig. 4-11(c) where B_{sh} is equal to 0.7307 Nms/rad. The variation on the reference torque is quite large but it is bounded and was not growing. It can be concluded that the effect of values of B_{sh} on implementation by method-A are not as effective as they should be (this matter is discussed in the tests presented in the following cases as well).

The results of Fig. 4-11(b) show the system responses by method-A where B_{sh} is set equal to 2 Nms/rad. As a result, the reference torque was bounded and the results are very close to the results by method-B with $B_{sh} = 0.7037$ Nms/rad. By these tests it can be concluded that since the frequency of the wind speed harmonic, 13 Hz, is very close to the system's natural frequency the variations on the reference torque is high. The actual and modified generator speed signals in the results by method-B are provided for comparison purpose which shows how close these two signals are.
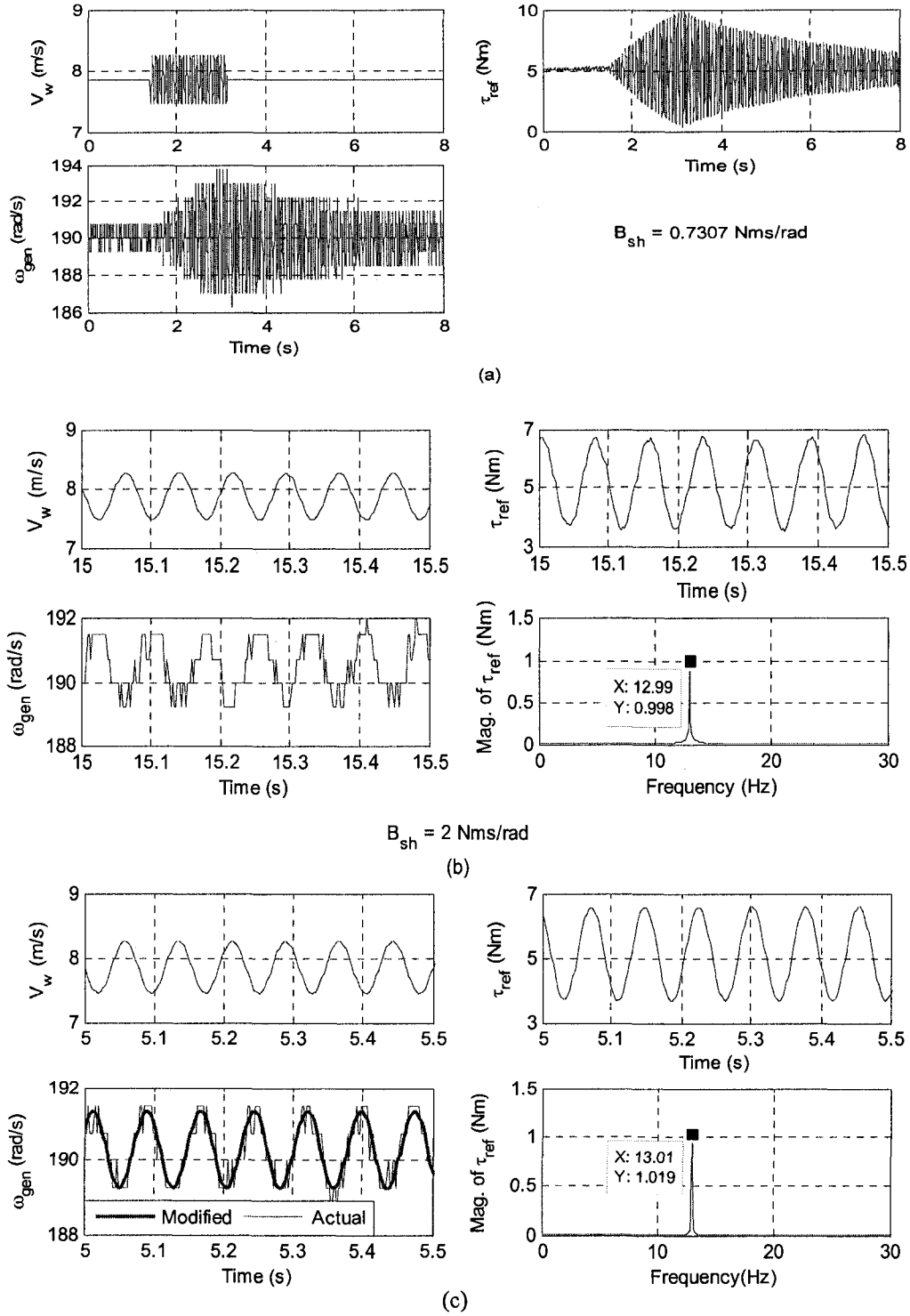
Fig. 4-11 Unregulated WECS experimental results for case 3; (a) By method-A, B_{sh} =

0.7307 Nms/rad; (b) By method-A, B_{sh} = 2 Nms/rad; (c) By method-B

112

Case 4) In this case it is investigated how the 3rd harmonic of the oscillatory can excite the system's natural frequency. The results for this case are shown in Fig. 4-12(a) (using method-A) and Fig. 4-12(b) (using method-B). In this case the shaft torsional spring constant (K_{sh}) is set equal to 4500 Nm/rad. Therefore, according to equations 2-14 and 2-18, the system's natural frequency and shaft damping constant (B_{sh}) are calculated as 21.15 Hz and 1.185 Nms/rad, respectively. As it was mentioned in the case 1, for rated generator speed the frequency of 3rd harmonic of the oscillatory torque is 22.68 Hz. Since this frequency is close to the system's natural frequency; as it can be seen from the Fig. 4-12 high variations on the reference torque should be expected due to the 3rd harmonic of the oscillatory torque. The frequency spectrum of the reference torque in Fig. 4-12(a) shows a component at 20.95 Hz which is very close to 21.15 Hz (system's natural frequency) but, this component is eliminated by applying method-B. It should be noted that the 20.95 Hz component should not be appeared on the reference torque response. The reason is that the reference torque variations are due to wind turbine oscillatory torque only. Thus the components with the frequencies about 7.5 Hz (1st harmonic) and 22.7 Hz (3rd harmonic) must exist.

It should be noted that the value of B_{sh} for the implementation by method-A was 3.2 Nms/rad; the minimum value which allowed the system to operate otherwise the reference torque would grow boundlessly. There was no such limitation for implementation by method-B. So, the results by method-B are provided for $B_{sh} = 1.185$ Nms/rad.

113
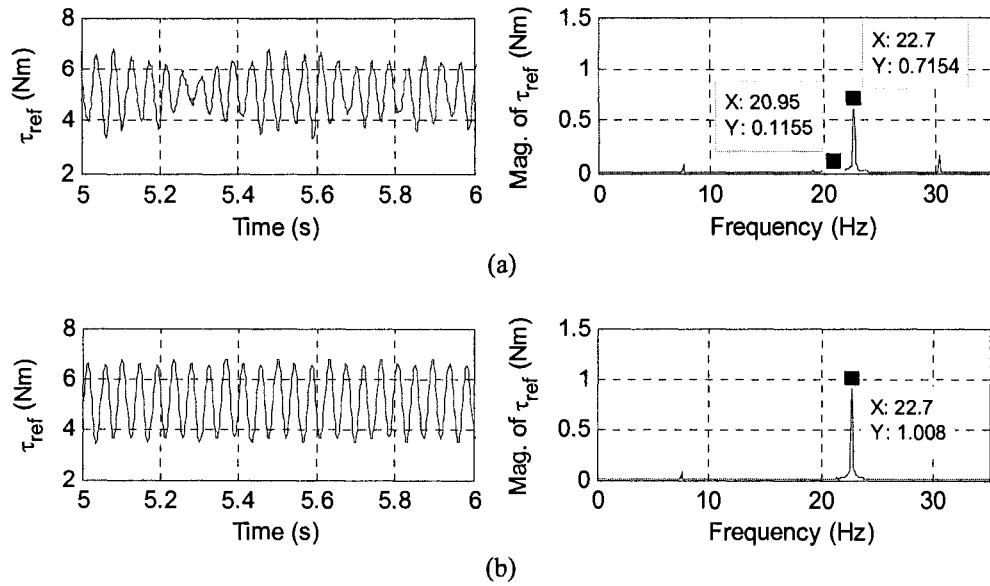
Fig. 4-12 Unregulated WECS experimental results for case 4; (a) By method-A; (b) By

method-B

Case 5) In this case the effects of wind speed step changes on the system

responses are investigated. The results for this case are shown in Fig. 4-13 (for $J_{wt} = 3$

kgm^2) and Fig. 4-14 (for $J_{wt} = 7$ kgm^2). Fig. 4-13(a) and Fig. 4-14(a) show the results by

method-A. Fig. 4-13(b) and Fig. 4-14(b) show the results by method-B. The load on the

generator is kept constant which is half rated load, 63 (Ω/phase), during these tests. The

components of the oscillatory torque are set to zero. Therefore, the variations on the

system responses are due to the wind speed step changes. The results are provided for the

wind turbines with the masses moment of inertias equal to 3 and 7 kgm^2. According to

equation 2-18 the values of B_{sh} are 0.7307 and 0.7491 Nms/rad, respectively. The

minimum value of B_{sh} which the system with method-A was operable at, was 0.9

Nms/rad. There was no such limitation on using method-B. Since this value is close to

114

the values calculated above, all the tests for method-A and method-B are done for B_{sh} = 0.9 Nms/rad.

The wind speed is kept constant at 7.87 m/s. Then, step changes of ±1 m/s are applied to the wind speed as shown in the figures. By comparing the results of Fig. 4-13 and Fig. 4-14, it can be clearly seen that the transient response of the system with the wind turbine with higher mass moment of inertia is slower. The other point is that with each step change in the wind speed the system's natural frequency will appear on the reference torque before it reaches its steady-state. These are shown in Fig. 4-13(a) and (b). The system's natural frequency when J_{wt} = 3 kgm^2 is 13.04 Hz. The calculated frequencies (based on the points marked on the zoom of the reference torques, bottom-right figures of Fig. 4-13(a) and (b)) for method-A is 12.97 Hz and for method-B is 13.07 Hz which are very close to the theoretical value with an error of less than 0.5%.

The generator phase voltage waveform is shown in Fig. 4-14(a). It can be seen that with each wind speed change, the generator voltage varies significantly (about 25% in this case) which shows the necessity of regulating the WECS.

The reference current and prime mover current waveforms are provided in each figure to show their transients. In Fig. 4-14(b) the modified and actual generator speed signals are indicated showing that the modified speed signal has the same transient response as the actual speed with much less noise or disturbance. It can be also seen that the implementation by method-B presents the same transient as the implementation by method-A does.

Fig. 4-13 Unregulated WECS experimental results for case 5 (J_{wt} = 3 kgm^2); (a) By method-A; (b) By method-B

116

Fig. 4-14 Unregulated WECS experimental results for case 5 (J_{wt} = 7 kgm^2); (a) By method-A; (b) By method-B

Case 6) In this case the effects of the load step changes on the system responses are investigated. The results for this case are shown in Fig. 4-15 (for J_{wt} = *3* kgm^2) and

117

Fig. 4-16(for J_{wt} = 7 kgm^2). Fig. 4-15(a) and Fig. 4-16(a) indicate the results by method-A. Fig. 4-15(b) and Fig. 4-16(b) indicate the results by method-B. The wind speed is kept constant at 7.87 m/s. The components of the oscillatory torque are set to zero. Therefore, the variations on the system responses are due to the load step changes. The results are provided for the wind turbines with the masses moment of inertias equal to 3 and 7 kgm^2. The shaft damping constant B_{sh} = 0.9 Nms/rad was used for all the tests in this case for the same reason explained in case-5.

The resistive load values before and after the load disturbances are shown on the reference torques related to each test. The systems' natural frequencies for the wind turbines with the masses moment of inertias 3 and 7 kgm^2 are 13.04 and 12.72 Hz, respectively. By referring to figures which are zooms of the reference torques, the natural frequencies for the systems with J_{wt} equal to 3 and 7 kgm^2 are 13 and 12.8 Hz, respectively, for the results by method-A. Those frequencies are calculated as 13.11 and 12.8 Hz, respectively, for the results by method-B. These values are very close to the theoretical values presenting an error of 0.6% in the worst case.

The results show that the transient response of the system with higher mass moment of inertia is slower. In the implementation by method-A, the shaft damping B_{sh} is not as effective as it should be, as it can be clearly seen from the results. In normal conditions before and after load disturbances (in its steady-state) there are still signs of excitation of the natural frequency. Also it takes much longer time for the reference torque to damp out in method-A than in method-B. The reason is because of the modified generator speed signals in method-B which have less noise or disturbance comparing to the generator speed signal in method-A. Referring to the results by method-B, it can be

118

seen that the smoother and less noisy reference torque is created as a result of using the generator actually modified speed signal.

(a)
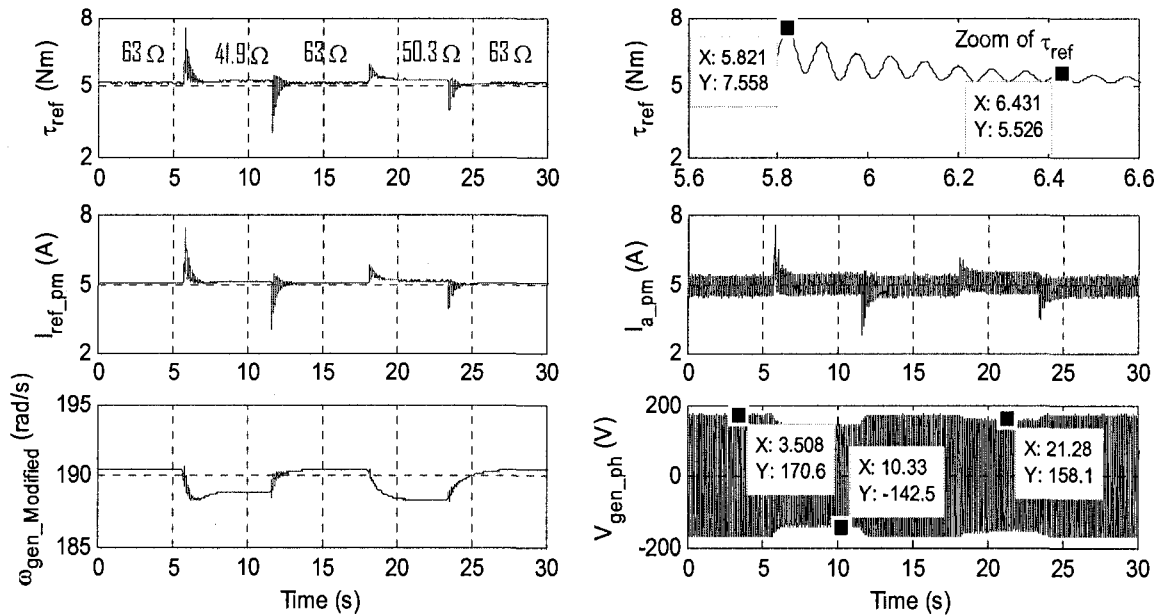
(b)

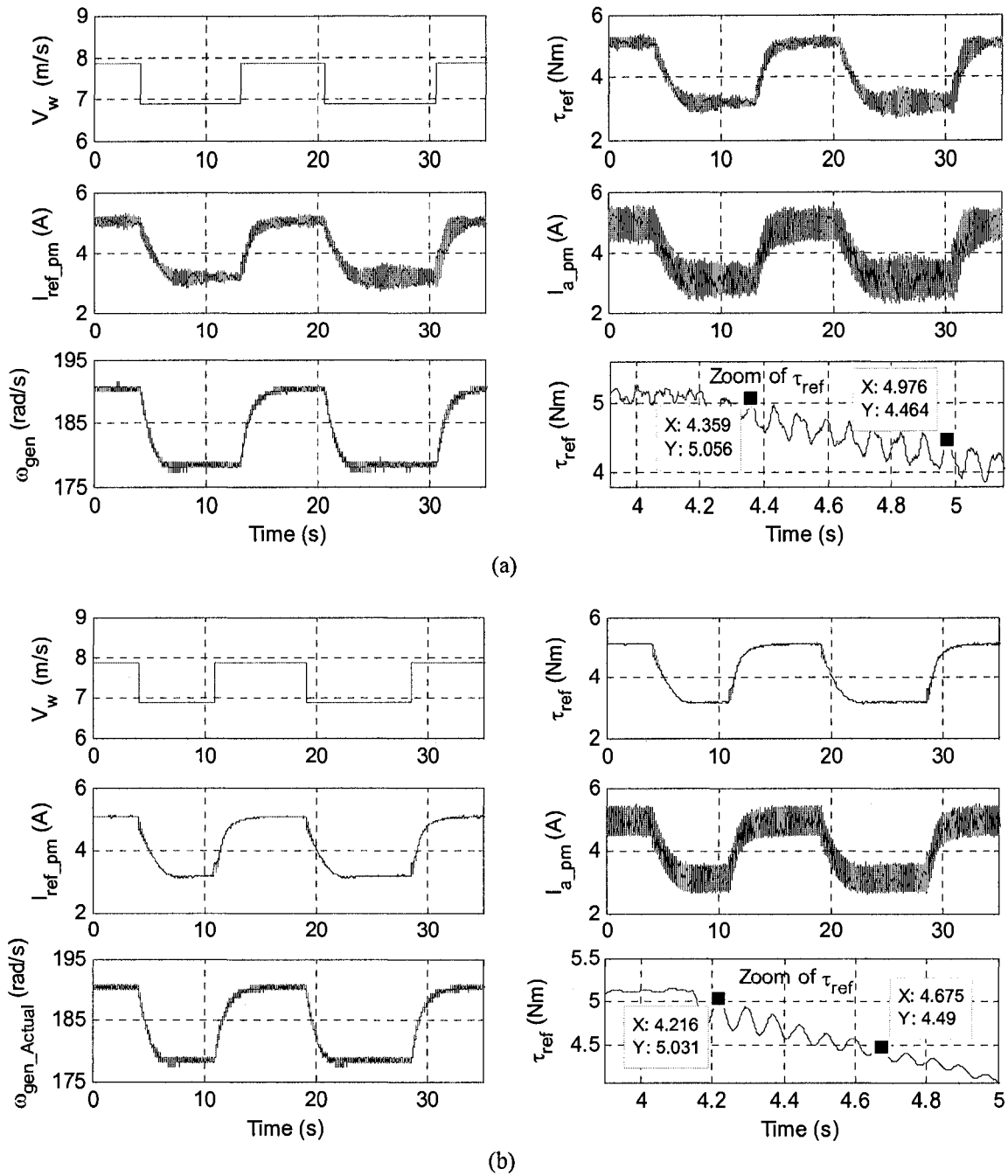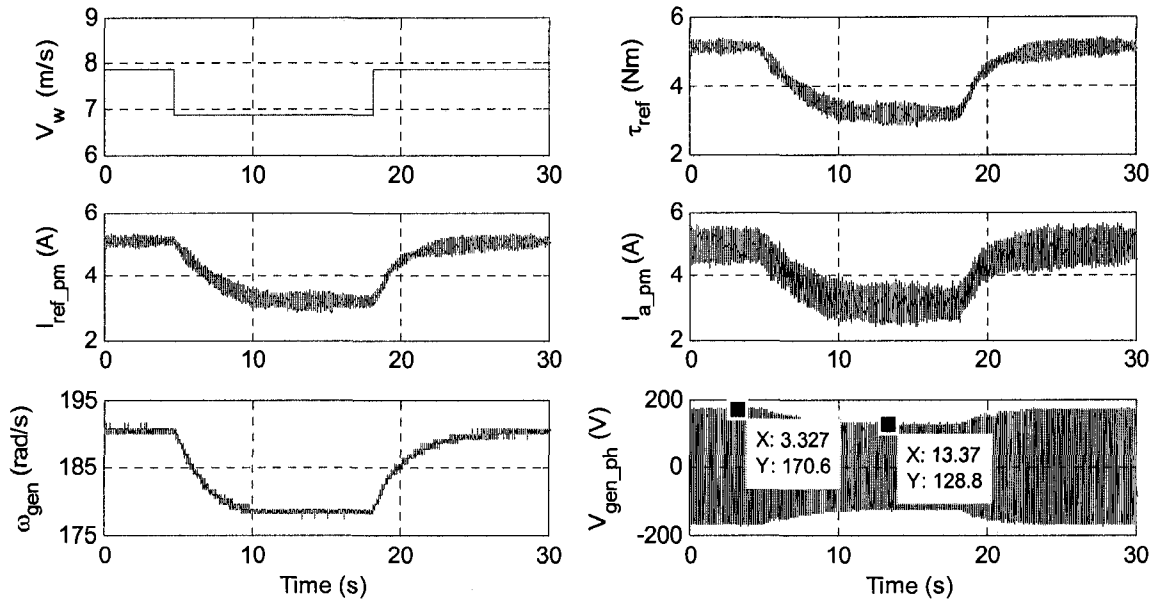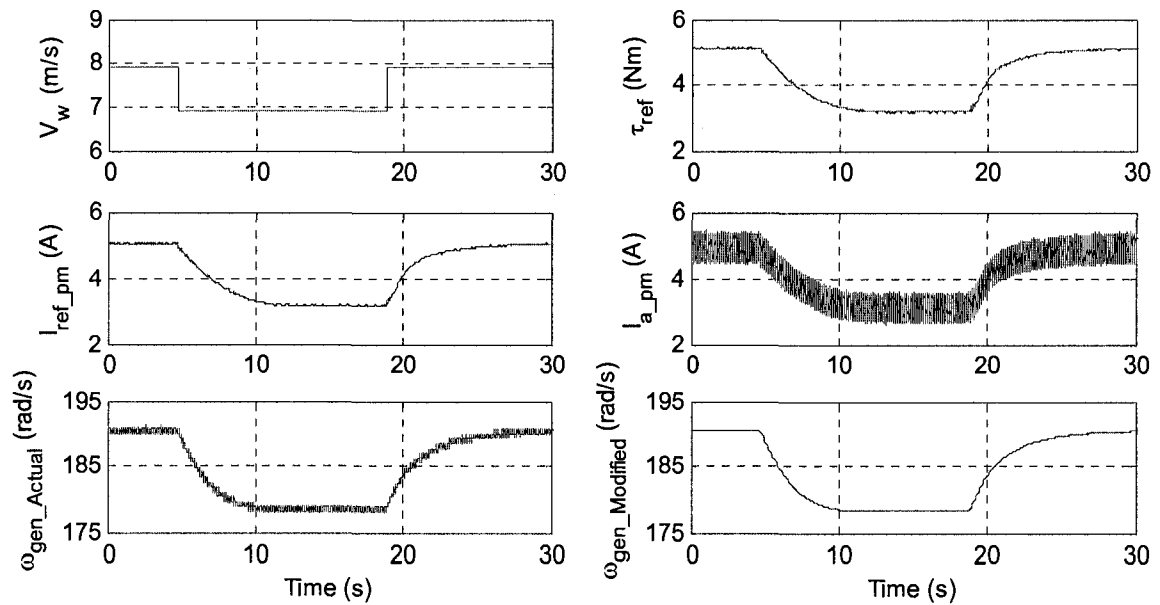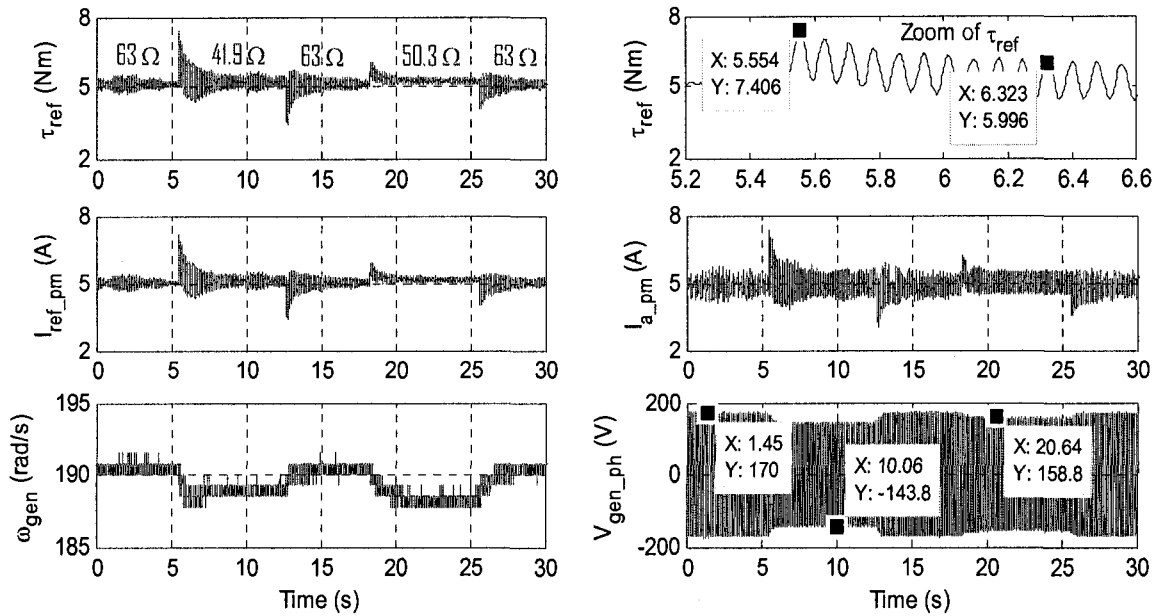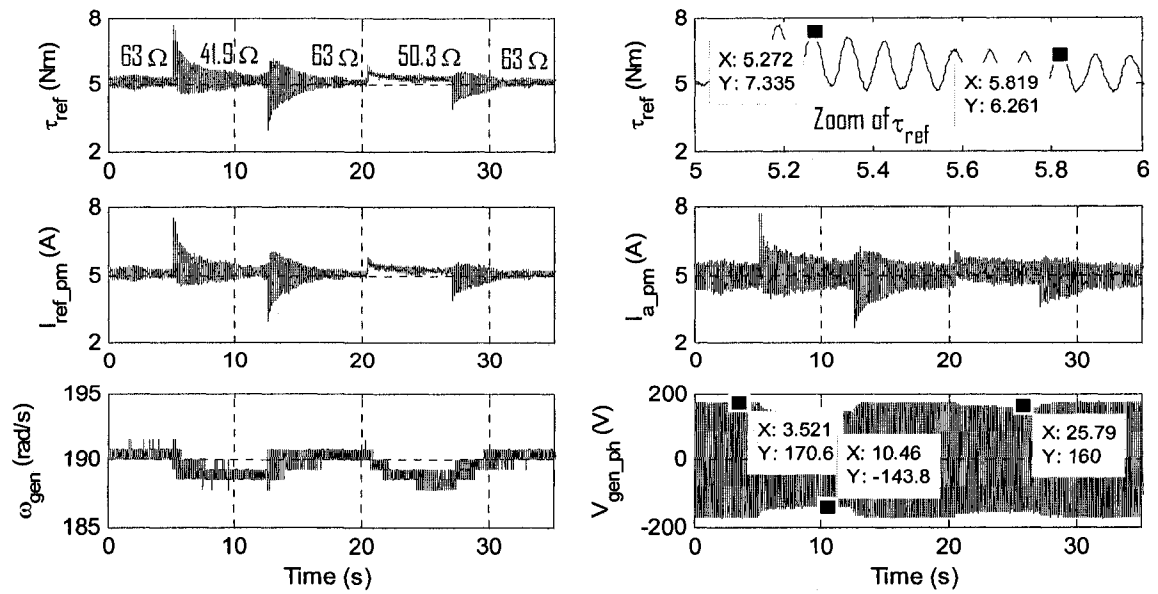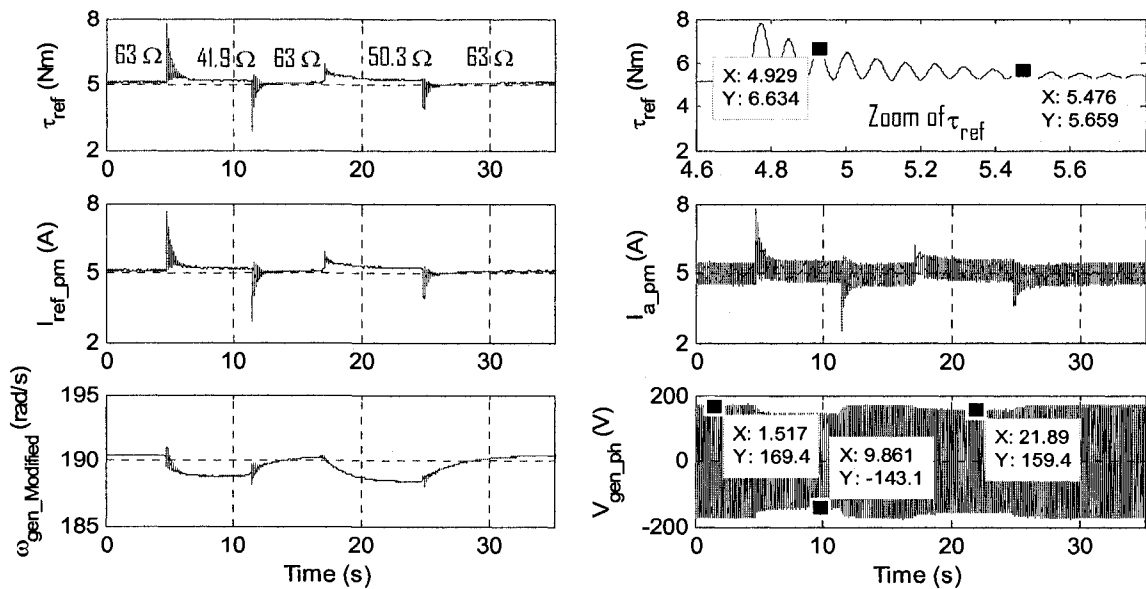**Fig. 4-15** Unregulated WECS experimental results for case 6 ($J_{wt} = 3$ kgm²); (a) By method-A; (b) By method-B

(a)

(b)

Fig. 4-16 Unregulated WECS experimental results for case 6 (J_{wt} = 7 kgm^2); (a) By

method-A; (b) By method-B

The phase voltages are also shown in the figures of each test and they show

variations on the generator voltage due to the load change. The voltage level reduction

for larger load change is about 16% and for lower load change is about 8%. The reference current and prime mover current are provided indicating their transient and steady-state responses.

4.4.2 REGULATED WECS

The results in this section are related to the experimental set-up shown in Fig. 4-2. This can be considered as a stand-alone application of a regulated WECS. The top part of Fig. 4-2, as mentioned before, was designed and implemented in [30]. The whole system has been tested under two major cases which show the transient and steady-state responses of the regulated WECS due to wind speed and load variations. The results are shown for the WTE implemented with method-A and method-B. In all results the oscillatory wind turbine torque is in effect.

There was a limitation on using method-A. The system response was unstable (reference torque was growing) for the shaft damping constant (B_{sh}) less than 2 Nms/rad. Therefore, all results for method-A are taken with B_{sh} equal to 2 Nms/rad. Since, there was no limitation for the implementation with method-B, the results for this method, are taken for the shaft damping constant (B_{sh}) equal to 0.7307 Nms/rad when $J_{wt} = 3$ kgm^2 and 0.7419 Nms/rad when $J_{wt} = 7$ kgm^2. These values are calculated according to equation 2-18.

Case 1) The effects of wind speed step changes are investigated in this case for the wind turbine with the mass moment of inertia 3 and 7 kgm^2. The results for this case are shown in Fig. 4-17 and Fig. 4-18. Fig. 4-17 indicates the results for the wind turbine

with the mass moment of inertia 3 kgm^2 and Fig. 2-18 indicates the results for the wind turbine with the mass moment of inertia 7 kgm^2. In each figure the results are provided for the implementation with method-A and method-B. Step changes of 1 m/s are applied on the wind speed of 7.9 and 6.9 m/s to observe the system responses due to these changes. As it can be seen from the results of both figures, as wind speed decreases the VSI supplies some portions of active power required for the fixed load, 63 Ω/phase, in order to maintain the generator speed close to its rated speed.

In other words, the generator sees smaller load even though the load connected to its output is kept unchanged. It should be noted that the generator speed when wind speed is equal to 6.9 m/s is slightly lower 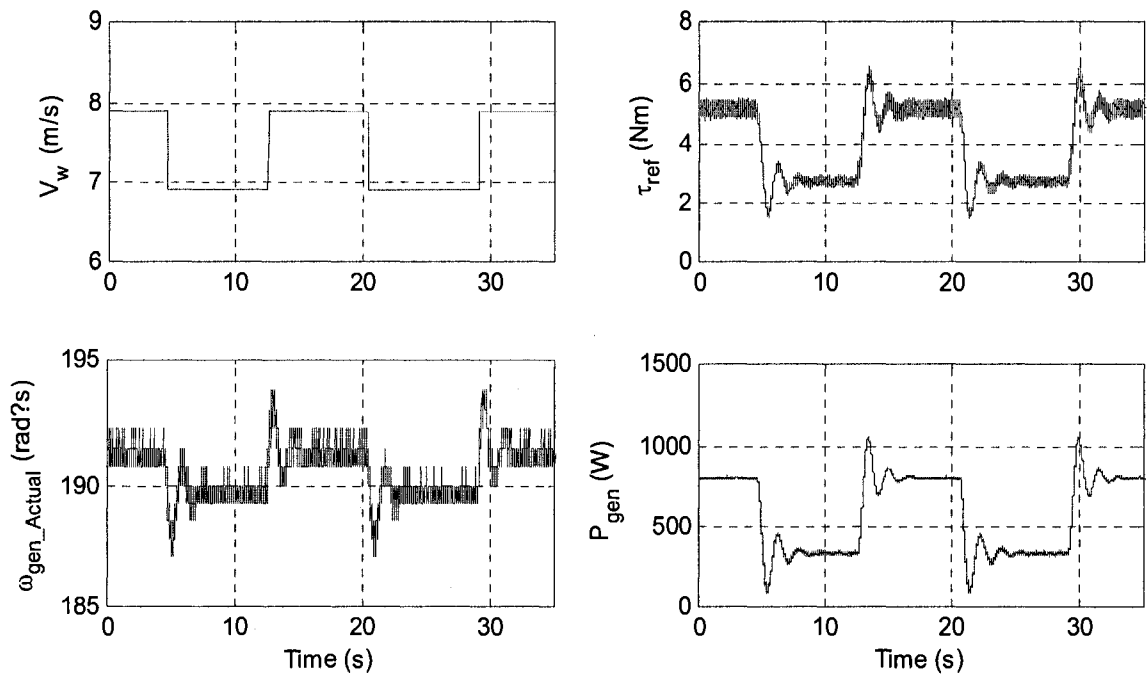than the time when wind speed is equal to 7.9 m/s. This is acceptable, because the aim is to regulate the frequency of the generated voltage and not the shaft speed. Recall that there is the slip factor for induction machines/generators. So as the generated power decreases, the shaft speed required for producing power/voltage with a given frequency decreases.

By comparing the results of the Fig. 4-17 and Fig. 4-18, it can be concluded that the responses for the wind turbine with mass moment of inertia J_{wt} = 3 kgm^2 has more oscillations to reach to its steady-state than the case where the wind turbine has the mass moment of inertia J_{wt} = 7 kgm^2. It can be also concluded that the implementations by method-A and method-B result in very close responses with the fact that there is no limitation on setting the value of the shaft damping (B_{sh}) for the implementation with method-B.
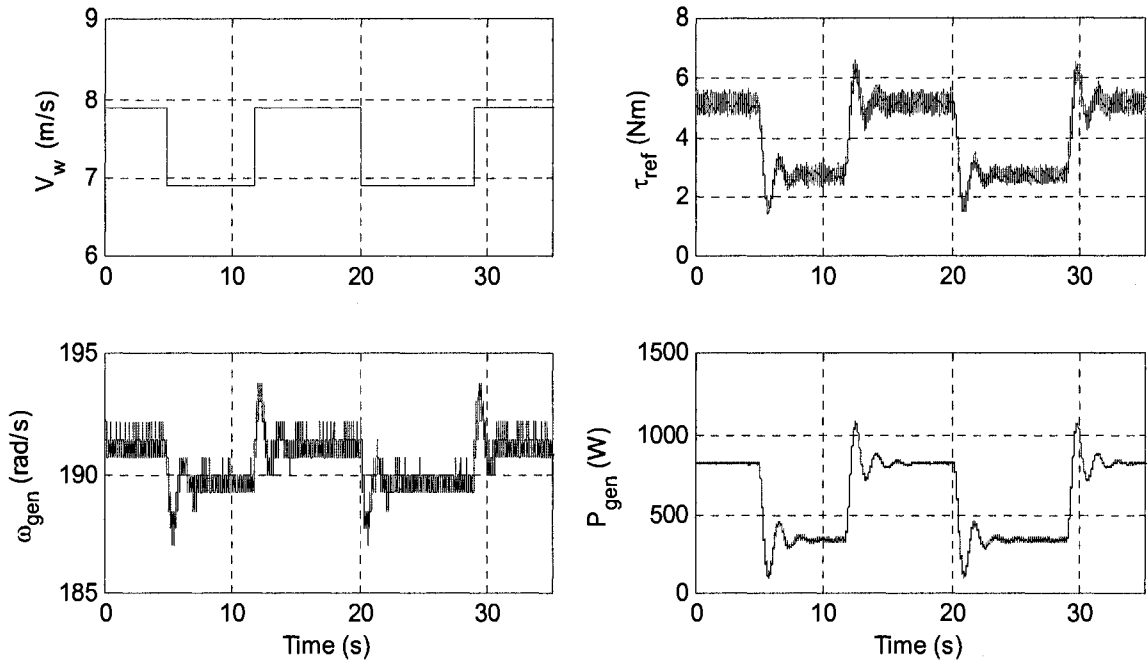
Fig. 4-17 Regulated WECS experimental results for case 1 ($J_{wt} = 3$ kgm^2); (a) By
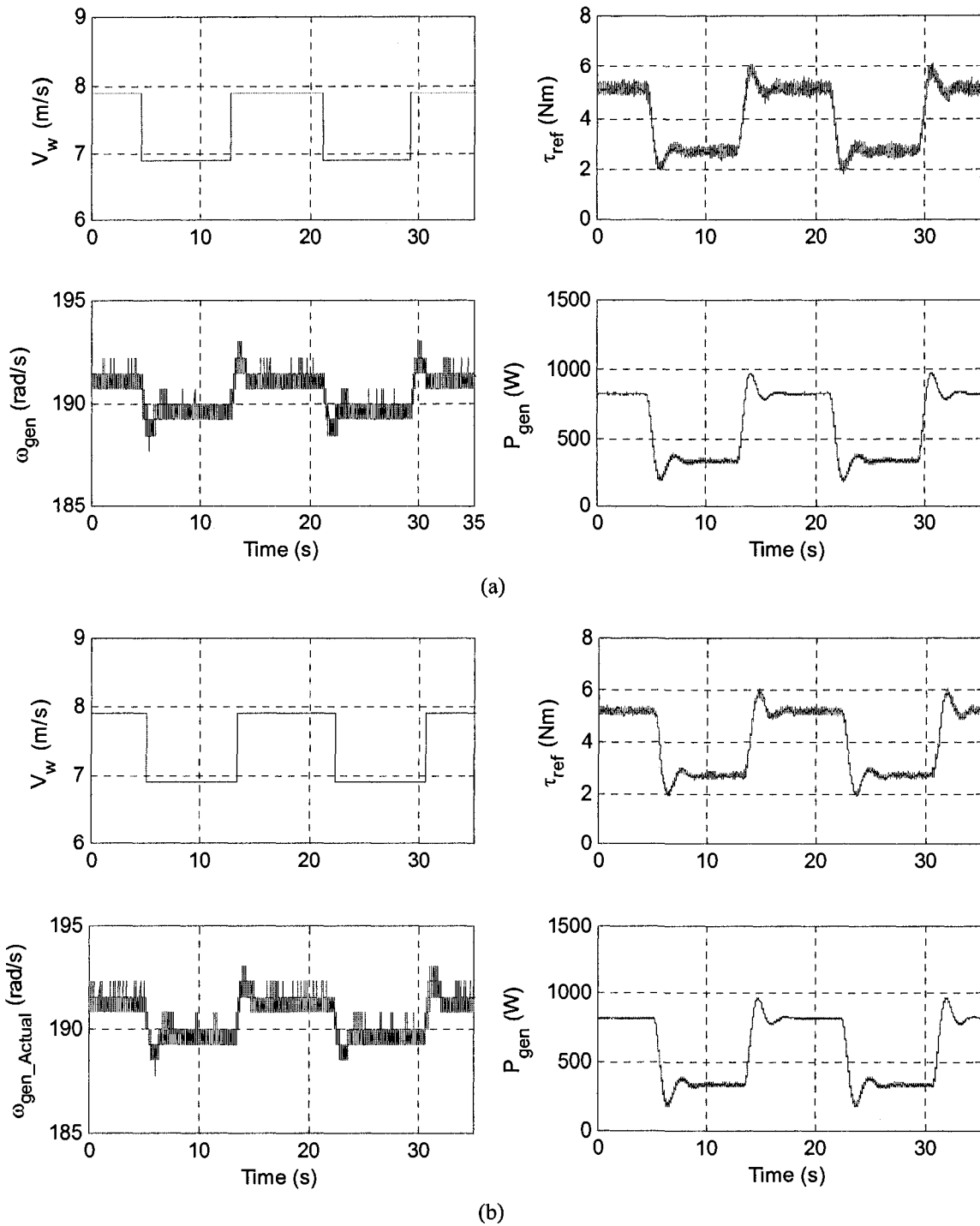
method-A; (b) By method-B

Fig. 4-18 Regulated WECS experimental results for case 1 (J_{wt} = 7 kgm^2); (a) By

method-A; (b) By method-B.

It is worth mentioning that the value of B_{sh} is mainly very effective on the system's natural frequency and frequencies close to it. By comparing the reference torque responses obtained by method-A and method-B, it can be seen that the response by method-A is noisier than the response by method-B even though the shaft damping was set to a higher value in method-A. The value of B_{sh} does not affect the transient time and general shape of the responses in transition from one state to another. But, in method-A the oscillations with the system's natural frequency around the average values in steady-state and transient are less damped even for larger value of B_{sh}.

Case 2) The effect of the load variations are investigated in this case for the wind turbines with the masses moment of inertias 3 and 7 kgm^2. The results for this case are shown in Fig. 4-19 and Fig. 4-20. The wind speed is kept constant at 7.9 m/s for these tests. Fig. 4-21 shows the results for the wind turbine with the mass moment of inertia 3 kgm^2 and Fig. 2-20 shows the results for the wind turbine with the mass moment of inertia 7 kgm^2. In each figure the results are provided for the implementation with method-A and method-B. The resistive loads have been changed as their values are shown on the reference torques responses of each figure before and after the load change. It should be noted that the values of the resistances are phase values.

The results show that since the wind speed is constant the VSI operates in such a way that the generator sees constant load which is 63 (Ω/phase). In other words, the reference torque, the generator speed, and the generator power remain the same in steady-state after each load change. The generator phase voltage is also provided and shows that it remains constant before and after each disturbance. The number of oscillations on the

125

reference torque and the variations on the generator speed are higher for the case where

the wind turbine mass moment of inertia is 3 kgm^2 than the case where it is 7 kgm^2.
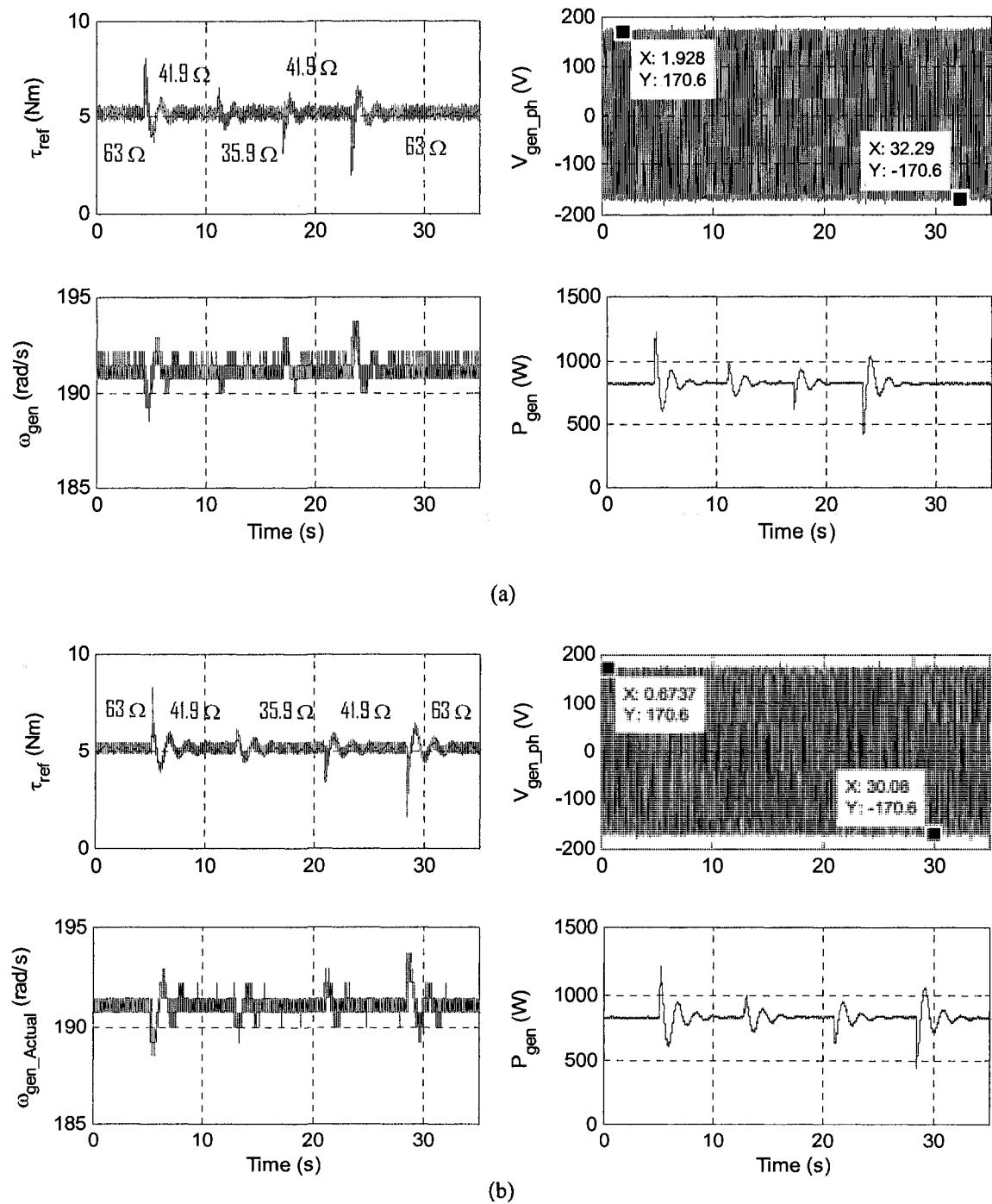

(a)

(b)

Fig. 4-19 Regulated WECS experimental results for case 2 (J_{wt} = 3 kgm^2); (a) By
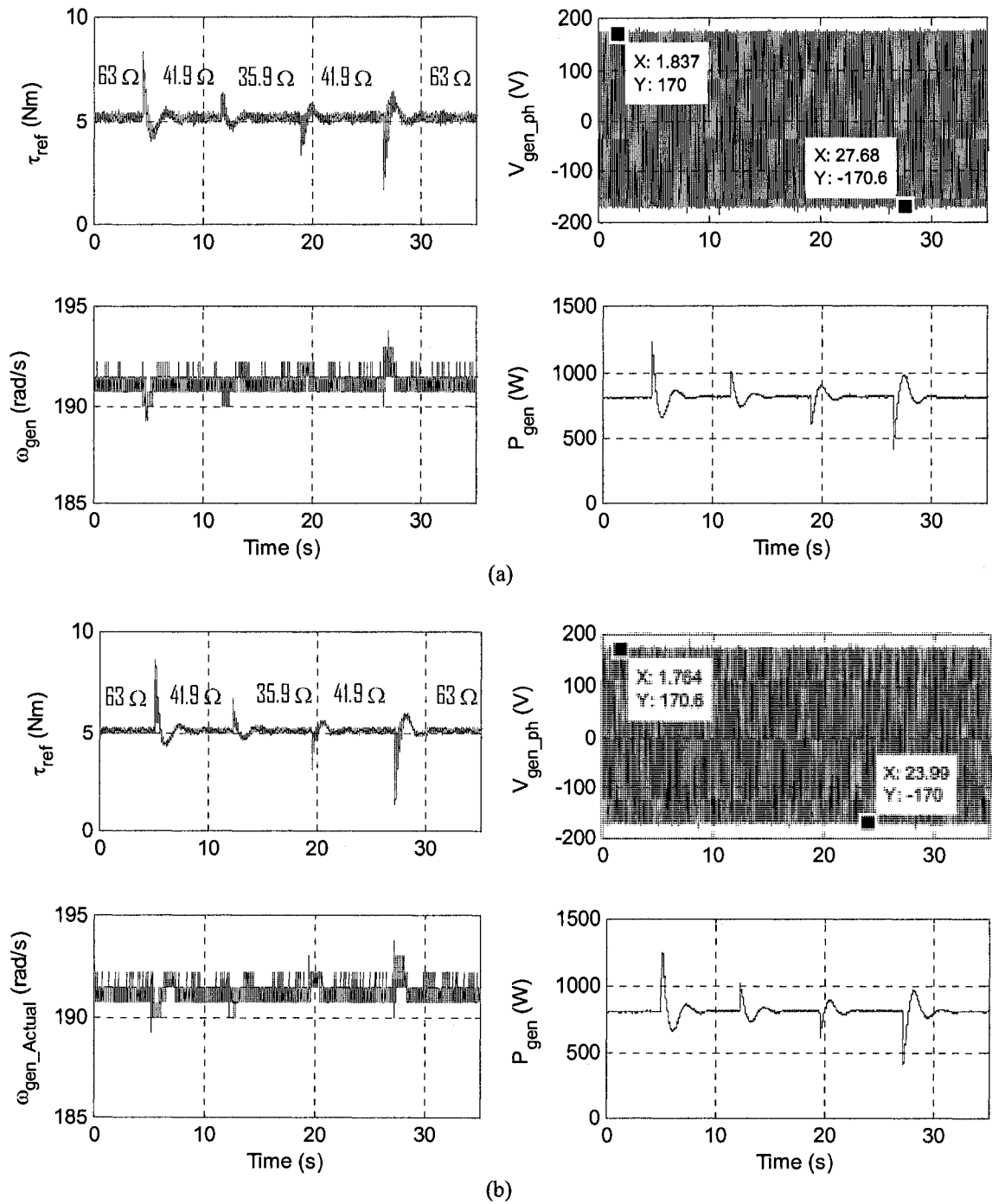
method-A; (b) By method-B

Fig. 4-20 Regulated WECS experimental results for case 2 ($J_{wt} = 7 \text{ kgm}^2$); (a) By method-A; (b) By method-B

4.5 CONCLUSIONS

The 2-hp WTE designed and implemented in Chapter 3 was used for emulating a stand-alone WECS by replacing the dynamometer with a self-excited induction generator. The new configuration provided the opportunity as a test bench to first, test the unregulated WECS and investigate the effect of wind speed variations, load variation, and system parameters on the generator behavior and produced electricity. Then, the designed WTE was used in a stand-alone regulated WECS which can be counted as one of real application of the designed WTE. The part of the system which was controlling and regulating the generator voltage and frequency was designed and implemented by Mr. Ghulam Dastagir who was M.A.Sc. Student in the Electrical Engineering Department.

The WTE has been implemented with two methods called method-A and method-B. They are both effective but have disadvantages. The main disadvantage of method-A is that in some cases it does not work (instability occurs) if the value of B_{sh} is set below a certain value. This minimum value changes from case to case. In other words, the value of B_{sh} cannot be varied as widely as it should for practical applications.

The main disadvantages of implementation by method-B is that the filter's corner frequencies might need to be changed for wind turbines with different natural frequencies; in order to attenuate those frequencies from generator speed signal. It also requires the estimation of the total mass moment of inertia friction constant of the prime mover and the generator and also the generator torque. To estimate the generator torque, the generator power needs to be measured which requires additional current and voltage sensors in comparison with method-A.

The main features of the designed and implemented WTE are:

> Capable of emulating the wind turbines with different mass moment of inertias, drive train with flexible shaft with different torsional spring constants, and damping constants, and ideal gear box with different gear ratios.

> Capable of emulating the oscillatory torque.

> Provides the capability of experimentally verifying the facts highlighted in conclusion of Chapter 2 as simulation results.

CHAPTER 5

CONCLUSIONS

5.1 SUMMARY

The increased level of penetration of wind power in the power generation systems has motivated a further analysis of the dynamic behavior of the wind energy conversion systems (WECS). A key element in a WECS test bench is a wind turbine emulator (WTE) which can be described as a controllable source of mechanical torque with the features of a wind turbine (rotor) and drive train. Different ways of implementing WTEs have been proposed in the literature. They can be categorized in terms of complexity of the wind turbine model, type of the electric machine as prime mover, number of feedback signals such as torque and speed signals, types of power electronics converters, and control strategies.

In this Thesis, a simplified model of a wind turbine consisting of the wind turbine mass moment of inertia and damping constant, a flexible low speed side shaft with damping constant, an ideal gear box, a rigid high speed side shaft, and the generator with the mass moment of inertia and damping constant. This simple configuration provides the opportunity for investigating the effects of four important factors on the system responses which are the mass moment of inertia, the system's natural frequency, the shaft damping constant, and the oscillatory torque.

A 2-hp WTE was designed and implemented to investigate whether the expected results can be achieved experimentally. In the first step, the WTE has been preliminary tested by using a dynamometer as mechanical load. Using the dynamometer eliminates

the requirement for having electrical generator and load, since it works as a variable mechanical load. The desired torque for the wind turbine emulator and dynamometer can be defined as a function in the MATLAB/Simulink model, for simulation studies and later for practical implementation using the dSPACE ds-1103 DSP development kit. The experimental set-up performed well and the experimental results presented good correlation with the simulation results.

The same 2-hp WTE with slight modifications (to be suitable for applying it to WECSs) was used for running a self-excited induction generator in the unregulated and also in the regulated stand-alone mode. The WTE was implemented by two methods of measured speed signals which are called method-A (using actual speed signal) and method-B (using a modified speed signal). Several tests were carried out by both methods. Implementation by method-A was limited by a minimum value of the shaft damping constant. There was no such limitation for implementation by method-B, but in this method, the transfer functions of the filters might need to be changed for different wind turbines. It was shown that the transient and steady-state responses for both methods agree with each other except for the cases where the system's natural frequency is excited; in these cases, for implementation by method-A, the shaft damping constants had to be set to higher values than the theoretical values to prevent system's instability.

In the end, it can be stated that the implemented WTE is effective (with some limitations) in providing the expected results on the high speed shaft responses due to four important characteristics of the wind turbine which are the mass moment of inertia, the system's natural frequency, the shaft damping constant, and the oscillatory torque. The implemented WTE, in its actual form, is suitable to be used in a test bench for

investigating the performances of different control strategies as part of WECS which might be proposed in the future.

5.2 SUGGESTIONS FOR FUTURE WORK

(1)   Improving the capability of the WTE by:

> Using an incremental encoder with higher number of pulses/revolution, in this case implementation by method-A should have less limitation on the value of the shaft damping constant.

> Using higher version of MATLAB/Simulink and dSPACE which will make the data transmission to be done at lower sampling time. In this case, the reactance of the inductor in series with the prime mover can be reduced which results in capability of emulating higher rate of change of prime mover torque.

> Using additional current and voltage sensors for each phase of the generator. In this case, it is possible to measure the power of the generator for unbalanced loads, which is necessary for implementation of the system by method-B.

(2)   Development of the hysteresis current controller(s) in such a way to be able to use the generator or the dynamometer for the start up of the wind turbine and enforcement of the prime mover to act as load (wind turbine rotor resistance against rotation) in this situation. Since it is mentioned in the literature that in some WECSs the generator is also used for start-up of the wind turbine.

(3) Testing the WTE in a grid connected configuration. This provides the opportunity to investigate the excitation of the system's natural frequency (equation 2-15), since excitation of this mode occurs on a condition that the generator speed is constant.

REFERENCES

[1] National Renewable Energy Laboratory (NREL), "http://www.nrel.gov/".

[2] Wind Service Holland, Member of "World Wind Energy Association", "http://home.wxs.nl/~windsh/wsh.html".

[3] E. Hau, "Wind Turbines: Fundamentals, Technologies, Application, Economics", Springer, 2nd (English) edition, 2006.

[4] A. D. Napoli, F. Crescimbini, and G. Noia, "A Microprocessor Controlled D. C. Drive of Wind Turbines", European Wind Energy Conference and Exhibition (EWEC 89), pp. 687-691.

[5] T. Ackermann, "Wind Power in Power Systems", John Wiley and Sons Ltd., 2005

[6] L. A. C. Lopes, J. Lhuilier, A. Mukherjee, and M. F. Khokhar, "A Wind Turbine Emulator that Represents the Dynamics of the Wind Turbine Rotor and Drive Train", Proceedings of 36th Annual IEEE Power Electronics Specialists Conference (PESC'05), June 2005, pp. 2092-97.

[7] M. Monfared, H. M. Kojabadi, and H. Rastegar, "Static and dynamic wind turbine simulator using a converter controlled dc motor", Elsevier Ltd., Renewable Energy 33 (2008) 906-913, June 2007.

[8] B. Rabelo, W. Hofmann, M. Glück, "Emulation of the Static and Dynamic Behaviour of a Wind-turbine with a DC-Machine Drive", Proceedings of 35th Annual IEEE Power Electronics Specialists Conference (PESC'04), June 2004, pp. 2107-12.

[10] S. H. Song, B. C. Jeong, J. H. Oh, G. Venkataramanan, H. I. Lee, and J. J. Kim, "Emulation of Output Characteristics of Rotor Blades Using a Hardware-In-Loop Wind

Turbine Simulator", Proceedings of 20th Annual IEEE Applied Power Electronics Conference and Exposition (APEC'05), March 2005, Vol. 3, pp. 1791-96.

[11] P. E. Battaiotto, R. J. Mantz, and P. F. Puleston , "A Wind Turbine Emulator Based on A Dual DSP Processor System", Control Eng. Practice, 1996, Vol. 4, No. 9, pp.1261-66.

[12] R. Cardenas, R. Peña, G. M. Asher, and J. C. Clare, "Experimental emulation of wind turbines and flywheels for wind energy applications", European Power Electronics and Applications Conference, EPE2001, Graz, Austria, August 2001, pp. 1-10.

[13] D. Dolan, "Real-Time Wind Turbine Emulator Suitable for Power Quality and Dynamic Control Study", A M.A.Sc. Thesis, University of Toronto, 2005.

[14] H. M. Kojabadi, L. Chang, and T. Boutot, "Development of a Novel Wind Turbine Simulator for Wind Energy Conversion Systems Using an Inverter-Controlled Induction Motor", IEEE Transactions on Energy Conversion, September 2004, Vol. 19, No. 3, pp. 547-552.

[15] R. Teodorescu, F. Iov, and F. Blaabjerg, "Flexible development and test system for 11 kW wind turbine", Proceedings of 34th IEEE Power Electronics Specialist Conference (PESC03), June 2003, Vol. 1, pp. 67-72.

[16] Bergey Windpower Co., "http://bergey.com/".

[17] N. Baines and T. Way, "Development of Prognostic/Health Management (PHM) Technologies for Wind Turbine: Final Report", Avenca Limited, November 2006.

[18] R. T. Stefani, B. Shahian, C. J. Savant, and G. Hostetter, "Design of Feedback Control Systems", Oxford University Press, 4th edition, 2002.

[19] G. L. Johnson, "Wind Energy Systems", Prentice-Hall Inc., 1985

[20] Z. Lubosny, "Wind Turbine Operation in Electric Power Systems/Advanced Modeling", Springer, 2003.

[21] H. H. Lin, R. L. Huston, "Dynamic Loads in Parallel Shaft Transmissions, I-Modeling and Analysis", NASA Technical Memorandum 100180 and AVSCOM Technical Memorandum 87-C-2, December 1987.

[22] O. V. Thorsen and M. Dalva, " Combined Electrical and Mechanical Model of Electric Submersible Pumps", IEEE Transactions on Industry Applications, March/April 2001, Vol. 37, No. 2, pp. 541-547.

[23] P. Novak, I. Jovik, B. Schmidtbauer, "Modeling and Identification of Drive-System Dynamics in a Variable-Speed Wind Turbine", Proceedings of 3rd IEEE Conference on Control Applications, August 1994, Vol. 1, pp. 233-238.

[24] N. Mohan, T. M. Undeland, and W. P. Robbins, "Power electronics : converters, applications, and design", John Wiley & Sons Inc., 3th edition, 2003.

[25] B. C. Kuo and F. Golnaraghi, "Automatic Control Systems", John Wiley & Sons Inc., 8th edition, 2003.

[26] Electro-Craft Corporation, USA, (Engineering Handbook), "DC Motors, Speed Control, Servo Systems", Pergamon Press, 3rd edition, 1977.

[27] A. A. Aquino Lugo, "Gray Box Modeling of Electric Drives Using Radial Basis Functions: An Experimental Case", A M.A.Sc. Thesis, University of Puerto Rico, 2006

[28] R. C. Dorf and R. H. Bishop, "Modern Control Systems", Pearson Education, 10th edition, 2005.

[29] dSpace HelpDesk, dSPACE GmbH, May 1999.

[30] G. Dastagir, "Voltage and Frequency Regulation of A Stand-Alone Self-Excited Induction Generator with An Unregulated Prime Mover", A M.A.Sc Thesis, Concordia University, Montreal, 2008

[31] M. G. Simões and F. A. Farret, "Renewable Energy Systems: Design and Analysis with Induction Generators", CRC Press LLC., 2004.

APPENDICES

APPENDIX A: RELATION BETWEEN THE WIND SPEED AND OPERATING POINT ON THE WIND TURBINE CHARACTERISTIC

In this part it will be shown that, how the operating point can be related to the wind speed, based on the equations introduced in Chapter 2. It can be understood easier in the form of a question that is, for a given system parameters and specifications at what wind speed the prime mover can generate 1500 W at the rotational speed of 188.5 rad/s (1800 RPM). Assuming that the rotor radius is 1.7 m, the air density is 1.224 kg/m^3, the gear ratio is 4, the rotor friction constant is 0.1 Nms/rad, and $C_t(\lambda)$ is expressed by equation 2-8.

In this case, the prime mover torque is equal to $\tau_{pm} = P/\omega_{pm} = 1500/188.5 = 7.96$ Nm. On the other hand, the rotor speed is equal to $\omega_{wt} = \omega_{pm}/4 = 188.5/4 = 47.12$ rad/s. Now, the wind turbine must overcome the torque due to rotor losses and the high speed side torque (the prime mover torque) considering the gear ratio. Thus, it can be written:

$$\tau_{wt} = B_{wt}\omega_{wt} + 4\tau_{pm} = 4.71 + 31.84 = 36.55 \quad \text{Nm} \tag{A-1}$$

By equating equations 2-9 and A-1:

$$1/2\rho\pi R^3 C_t(\lambda)V_w^2 = 36.55 \Rightarrow C_t(\lambda)V_w^2 = 3.8 \tag{A-2}$$

By combining equations 2-4, 2-8, and A-2, they can be reduced to one equation and one unknown. The resulting equation is solved for V_w (the only unknown), by using Maple software, and it is calculated $V_w = 8.84$ m/s. By using equation 2-4 and calculated wind speed, the related tip speed ratio will be equal to 9.12. It should be noted that the tip speed ratio at which the maximum power occurs, is 8.

APPENDIX B: ELECTRONICS CIRCUIT FOR SWITCHES GATING SIGNALS

Fig. B-1 shows the circuit which provides the proper gating signals for the switches in the prime mover converter leg. It provides sufficient current, required for operating the drive circuit of the switches. It also creates the required dead time between the gating signals for the switches, preventing short circuit. It should be noted that this circuit was designed and built based on the suggestions provided by Mr. Yongzheng Zhang, who was M.A.Sc. Student in the Electrical Engineering Department. The same circuit was used for creating the dynamometer converter leg gating signals.
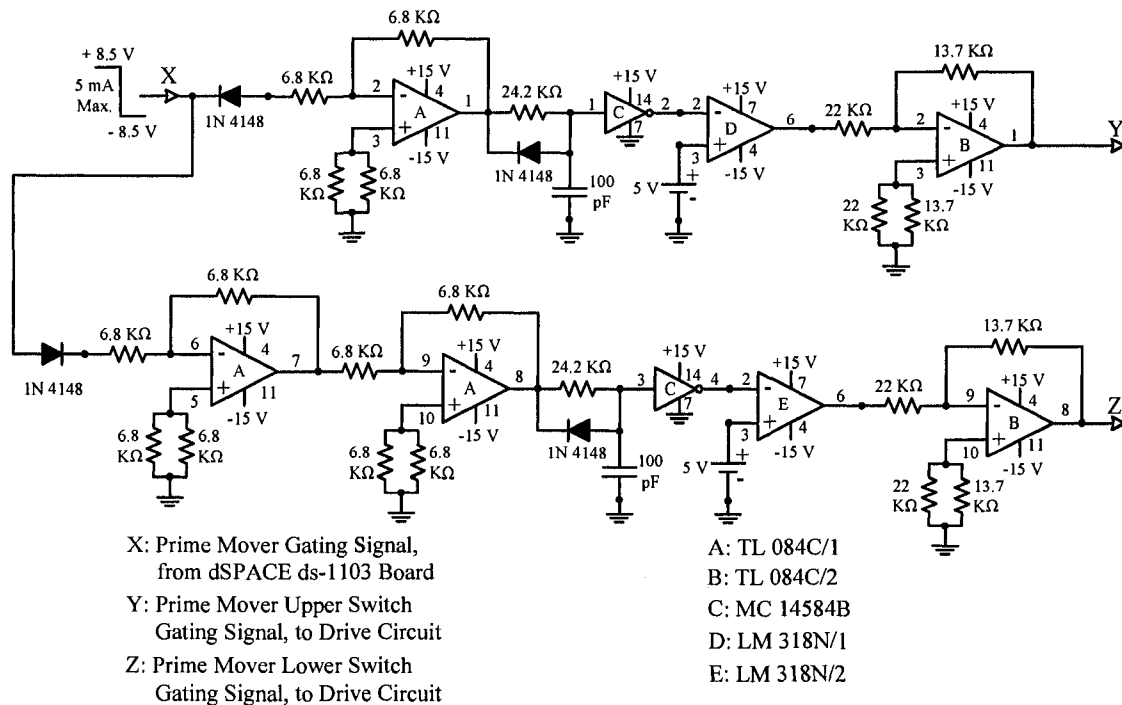

X: Prime Mover Gating Signal,
 from dSPACE ds-1103 Board
Y: Prime Mover Upper Switch
 Gating Signal, to Drive Circuit
Z: Prime Mover Lower Switch
 Gating Signal, to Drive Circuit

A: TL 084C/1
B: TL 084C/2
C: MC 14584B
D: LM 318N/1
E: LM 318N/2

Fig. B-1 Electronic circuit for creating gating signals for the switches